Master Thesis

Investigation of Parameters Determining the Accuracy of Gas-Initially-In-Place Calculation from Well Test Interpretation

Written by:
Gudrun Lemmerer, BSc.
0935234

Advisors:
Univ.-Prof. Dipl.-Ing. Dr.mont. Herbert Hofstätter
Dipl.-Ing. Dr.mont. Markus Kästenbauer
Dipl.-Ing. Abbas Zamani

Irdning, 21.02.2016

EIDESSTATTLICHE ERKLÄRUNG

Ich erkläre an Eides statt, dass ich die vorliegende Diplomarbeit selbständig und ohne fremde Hilfe verfasst, andere als die angegebenen Quellen und Hilfsmittel nicht benutzt und die den benutzten Quellen wörtlich und inhaltlich entnommenen Stellen als solche erkenntlich gemacht habe.

AFFIDAVIT

I hereby declare that the content of this work is my own composition and has not been submitted previously for any higher degree. All extracts have been distinguished using quoted references and all information sources have been acknowledged.

Danksagung / Acknowledgement

First of all, I want to thank everyone at RAG, Rohoel-Aufsuchungs AG, for the opportunity to work on this thesis. The support in terms of software environment, finance and help is beyond everything that a student could ask for. Many thanks, to DI Michael Krassnitzer and DI Alan Reingruber, who accepted me as a member of the reservoir management team.

I want to tell many thanks to my supervisor, Markus Kästenbauer, who not only acted as the main source of inspiration, but became a great mentor and friend over the years. Thank you for your patience and perseverance!

I would like to thank my petroleum engineering professors at the Montanuniversitaet: Our professor for drilling engineering, Univ.-Prof. Dipl.-Ing. Dr.mont. Gerhard Thonhauser, and our professor for production engineering Univ.-Prof. Dipl.-Ing. Dr.mont. Herbert Hofstätter. Dipl.-Ing. Abbas Zamani, thank you for your support and help. I would like to thank Dipl.-Ing. Dr.mont Rudolf Fruhwirth, who provided his software cVision® for free to do investigations, and also took the time to introduce me to his software.

Last but not least I want to mention the great effort and support coming from my parents, who always believe in me, stand by me in rough times and accept my decisions. Birgit, my sister, always gives great advice. Jakob, thank you for everything!

Kurzfassung

Die Druckaufbaumessung ist ein integraler Bestandteil bei der Bewertung neuer Gaslagerstätten. Sie wird dazu verwendet, Eigenschaften der Lagerstätte zu eruieren, und dient auch dazu, etwaige Lagerstättengrenzen und eine potentielle, rasche Druckabsenkung, die auf eine limitierte Lagerstätte hinweist, frühzeitig zu erkennen.

In dieser Arbeit wird deswegen die Methode von rein analytischen Auswertungen genauer beleuchtet. Ein Hauptaugenmerk liegt dabei auf der „Nicht-Eindeutigkeit“ (non-uniqueness) einer Druckaufbaukurve: unterschiedliche Bedingungen können dieselbe Kurve liefern, was eine aussagekräftige Analyse erschwert. Um die Vorhersagegenauigkeit der Bohrlochtests einzuschätzen, sind alle verfügbaren Druckaufbaumessungen aus der RAG Rohöl-Aufsuchungs AG - Konzession in der oberösterreichisch-salzburgischen Molassezone digitalisiert worden, wodurch insgesamt rund 600 Messungen analysiert werden können. Die momentan angewandte Methodik zur Einschätzung des durchschnittlichen Lagerstättendrucks ist umstritten. Die Aussage der gesammelten Daten dazu ist aber eindeutig: Die Analyse von Open-Hole und Cased-Hole Tests zeigt eine große Fehleinschätzung des gewinnbaren Gasvolumens.

Die Möglichkeit der numerischen Modellierung der Tests wird vorgestellt und evaluiert. Die Standard-Auswertungssoftware eignet sich gut, um die gewonnenen Erkenntnisse aus den Bohrlochtests zu modellieren, und sie mit dem umfangreichen Wissen der Geologen interdisziplinär zu verbinden. Die dynamische 2D- oder 3D-Simulation der Tests mit einem handelsüblichen Simulationsprogramm erlaubt, verschiedene geologische Gegebenheiten auszuwerten, und zeigt dabei eindeutig, dass die Eruierung des durchschnittlichen Lagerstättendrucks bei Lagerstättengrenzen ein äußerst unsicheres Unterfangen ist, und sowohl eine deutliche Unterschätzung der Reserven, wie auch eine leichte Überschätzung bedeuten kann. Dabei kann im Vorhinein ohne eine ungefähre Einschätzung der Erstreckung einer Lagerstätte keine Aussage darüber getroffen werden, welcher Fall eintreten wird. Die Einschätzung der Reserven anhand von solchen Tests mit der Materialbilanzmethode ist daher mit großen Unsicherheiten versehen.

Sowohl die gesammelten Archivdaten, als auch die Simulationsergebnisse werden verwendet, um ein neuronales Netz zu füttern. Bei den Archivdaten stellt sich heraus, dass nur das Filtern bzw. Einschränken des Datensatzes, wie das Ausschließen von Lagerstätten, die weniger als 5 Mio. Sm^3 Gas produziert haben, oder die Unterteilung in verschiedenen Formationen, einen numerischen Zusammenhang zeigt. Diese Datengruppen können als geologisch ähnliche Formationen interpretiert werden, die sich sowohl während des Testes, als auch in der Produktionsphase ähnlich verhalten. Erste Versuche, Simulationsergebnisse zu einem neuronalen Netz zusammenzutragen, um die Aussagekraft späterer Tests dadurch im Vorhinein zu verbessern, zeigen, dass dies stark an das vorherrschende Wissen über geologische Bedingungen geknüpft ist und daher nur in wenigen Situationen Anwendung findet.

Abstract

Well testing is a very important part in the evaluation of gas discoveries. It is used to define the characteristics of a reservoir, to find boundaries and see a potential pressure depletion, which could verify the existence of a limited reservoir at an early stage.

This thesis evaluates the analytical test interpretation methods. An important point is the non-uniqueness of a well test interpretation. The same pressure curve can be the result of very different conditions, leading to difficulties in the interpretation. In order to find out about the exactness of the estimation of producible volumes from an early well test, data of all performed pressure build-up tests from the RAG Rohoel-Aufsuchungs AG - concession in the Molasse in Upper Austria and Salzburg is digitized, and therefore around 600 tests can be analyzed. The used method of deriving the average drainage pressure is highly controversial. The analysis of the archived data shows that in both cases, for open-hole and cased-hole tests, gas volumes are often estimated inexactly.

The possibility to build numerical models of the tests is presented and evaluated. The standard well testing software can be used to model the acquired insights and to converge it interdisciplinarily with the extensive knowledge of the geologist. Dynamic 2D- and 3D-simulation of the tests with a commercial simulation software allows to analyze different geologic environments and to show clearly that the determination of average pressures in reservoirs with boundaries is very risky, and can lead to a severe underestimation, but also a slight overestimation of the reserves. Without a rough estimation of the lateral extension beforehand, a prediction of the proper case is not possible. Therefore, the estimation of reserves in these environments with the material balance method is erroneous.

The compiled well test interpretation data and the results from the simulations are used to feed a neural network. With real-world data it is only possible to find numerical relations under certain preconditions, like the exclusion of samples with a lower production than 5 MMscm or the differentiation between formations. These reservoirs can be defined as geologically similar formations, which perform likewise during the test and during production. First trials to feed a neural network with simulation results and use this method to improve the prediction accuracy show that the capability of predicting gas initially in place strongly depends on the predefined knowledge about geological conditions. This method is, therefore, only partly applicable to real-world problems.

Table of Content

Page

List of Tables

Page

List of Figures

Page

Abbreviations

CHT	cased-hole test
cP	centipoise
DST	drill-stem test
ETR	early time region
EU	European Union
GIIP	gas initially in place
hr	hour
HS	Hall Formation
IM	imbricated Molasse
LTR	late time region
MB	material balance
MBE	material balance equation
MBH	Matthews-Brons-Hazebroek
mD	milliDarcy
MMscm	Million standard cubic meters
MTR	middle time region
NN	neural network
OHT	open-hole test
OPS	Upper Puchkirchen Formation
p.a.	per year
PRMS	petroleum resources management systems
PTA	pressure transient analysis
PV	pore volume
PVT	pressure-volume-temperature
RAG	Rohoel-Aufsuchungs AG
RC	reservoir compartmentalization
Rm^3	reservoir cubic meters
Sm^3	standard cubic meters
UPS	Lower Puchkirchen Formation
WT	well testing
WTI	well test interpretation

Acronyms

$\bar{p}$	average pressure in the drainage area	[bara] or [psia]
μ	viscosity	[Pa*s]
A	areal extent of the reservoir	[m²] of [ft²]
B_g	formation volume factor for gas (reservoir volume/volume at standard conditions)	$\left[\frac{Rm^3}{Sm^3}\right]$
B_{gi}	gas formation volume factor	$\left[\frac{Rm^3}{Sm^3}\right]$
B_o	formation volume factor for oil	$\left[\frac{Rm^3}{Sm^3}\right]$ or $\left[\frac{RB}{STB}\right]$
C_A	shape factor	[-]
c_t	total compressibility	[psi^{-1}]
G	GIIP at standard conditions	[MMscm]
G_{disc}	discovered gas initially in place	[MMscm]
G_{est}	first estimate of GIIP at standard conditions	[MMscm]
G_{fc}	cumulative forecasted gas of a specific horizon until abandonment	[MMscm]
G_{model}	gas initially in place in the model	[MMscm]
G_P	cumulative gas produced in standard conditions	[MMscm]
$G_{p1,2}$	cumulative gas production at time of respective pressure measurement	[MMscm]
G_{p1+2}	total produced gas in the production periods	[MMscm]
G_{prod}	cumulative produced gas of a specific horizon until 01.05.2015 (i.e. end of historic data)	[MMscm]
h	reservoir height	[m] or [ft]
i	subscript for initial conditions	-
k	permeability	[mD]
m	slope (Horner plot)	$\left[\frac{psi}{log_{10}-cycle}\right]$
$m(\bar{p})$	pseudo-pressure at average drainage area pressure	$\left[\frac{psi^2}{cP}\right]$
m(p)	real-gas potential	$\left[\frac{psi^2}{cP}\right]$
$m(p)_i$	real-gas potential at initial conditions	$\left[\frac{psi^2}{cP}\right]$
$m(p)_{ws}$	real-gas potential in the wellbore at shut-in	$\left[\frac{psi^2}{cP}\right]$

m(p*)	pseudo-pressure at the extrapolated pressure	$\left[\frac{psi^2}{cP}\right]$
n	number of moles of gas	[mol]
p	pressure	[bara] or [psia]
p*	extrapolated pressure in Horner at $\frac{t+\Delta t}{\Delta t} = 1$	[bara] or [psia]
$p^*_{1,2}$	extrapolated und depth-converted pressures (from total vertical depth (TVD) at measurement to perforation mid-point TVD) of the two shut-in periods	[bara]
p_{bp}	backpressure from surface lines	[bara]
p_{pc}	pseudo-critical pressure	[bara]
p_{pr}	pseudo-reduced pressure	[-]
p_{sc}	pressure at standard condition: 1.01325 bar	[bar]
PV	pore volume	[m³]
p_{wf}	well-flowing pressure	[bara] or [psia]
p_{ws}	shut-in pressure at the wellbore	[bara] or [psi]
q	flow rate	$\left[\frac{m^3}{day}\right]$ or $\left[\frac{STB}{day}\right]$
q_g	gas flow rate	$\left[\frac{Mscf}{day}\right]$
R	gas constant: 8.314	$\left[\frac{J}{mol * K}\right]$
r_{inv}	radius of investigation	[ft]
r_w	wellbore radius	[ft]
S	Skin factor	[-]
S_{wi}	initial water saturation	[-]
T	temperature	[K]
t	time	[hr]
t_p	total duration of production	[hr]
T_{pc}	pseudo-critical temperature	[K]
t_{pDA}	MBH dimensionless time	[-]
T_{pr}	pseudo-reduced temperature	[-]
T_{sc}	temperature at standard condition: 273.15	[K]
UR	cumulative production of a specific horizon	[MMscm]
UR_{est}	estimated ultimate recovery	[MMscm]
UR_{rel}	relative ultimate recovery	[-]
$UR_{rel,log}$	logarithm of the base 10 from the relative ultimate recovery	[-]
V	volume	[m³]
Z	real gas deviation factor	[-]

$Z_{1,2}$	real gas deviation factor at the respective pressures	[-]
Δt	time since shut-in	[days]
Φ	porosity	[-]

Unit conversion tables

1 psi	*	$1.45*10^{-4}$	=	1 Pa
1 STB	*	6.2898	=	1 m^3
1 cP	*	1000	=	1 Pa*s
1 mD	*	$1.01*10^{15}$	=	1 m^2
1 ft	*	3.2808	=	1 m
1 Mcf (=1000 ft^3)	*	0.0353	=	1 m^3
1 psi	*	14.5038	=	1 bar
1 Pa	*	10^5	=	1 bar

1 Introduction

Fossil fuels with their incomparable advantage of short-term energy supply have been used since the industrial revolution to energize the economy. Ever since, supply and demand have been rising as the purposes for consumption developed from mere lighting and heating to transportation and electricity generation [1, p. 1].

However, the European Union (EU) aims on a gradual transition in energy supply to drastically reduce carbon emissions. Different measures are taken, like the increase of the percentage of renewables in the energy supply, or the transition from coal and oil to gas power plants. With 32.5% of renewable energy from total energy consumption, Austria ranges in the Top 5 EU countries concerning the integration of renewables [2, 3]. But, missing storage opportunities and poor applicability in the transportation sector result in the fact that more than 50% of the energy supply is provided by hydrocarbons to ensure stable and secure supply conditions. Therefore, gas as an energy source and underground gas storage play an important part of energy security today and in the future (i.e. the concept of power-to-gas) [4]. The economic value and potential of this natural resource will keep on being important in the near future.

Another aim of the EU is to further increase energy efficiency. To be able to achieve this goal in the oil and gas industry, it is of upmost importance to explore, develop and produce global hydrocarbon reserves effectively and sustainably. Naturally, this task is more easily performable for gas reservoirs than for oil accumulations, because due to the extremely high compressibility of natural gas, around 85% of the available resources in a gas reservoir can be produced through expansion drive [5, p. 36/3].

The Austrian based international oil and gas company RAG (Rohoel-Aufsuchungs AG) is successfully producing their Austrian fields in Salzburg, Upper and Lower Austria since the late 60’s, starting to create a local market for gas as a reliable, cheap and clean natural resource. The majority of RAG gas reservoirs have been found in the Molasse basin in Salzburg and Upper Austria. The company has had many great discoveries over the decades and it continues to explore the potential of the region. Molasse gas reservoirs vary substantially in their size, from very small reservoirs to large accumulations, but normally the net pay is of sub-seismic thickness due to the prevailing environment of deposition and tectonic processes. Hence, the size and dissemination of a reservoir can hardly be assessed by seismic alone. The method of well testing is, therefore, used to assist in the evaluation of potential reserves.

Dynamic in-situ reservoir conditions are of utmost importance in all phases of a field development plan. Good reservoir information is the most important expenditure in any oil and gas project. Well testing (WT), or pressure transient measurement, is a very important part of this information gathering process and of the disciplines reservoir and production engineering [6, p. 1]. The scope and extent of WT differs in terms of the usage of the gained information and the definition of the aims. The findings of a well test interpretation (WTI), or

pressure transient analysis (PTA), can be used for reservoir evaluation, determination of features and extent of the hydrocarbon accumulation and later on for a sustainable reserves management [7, p. 1].

When drilling and finding a new reservoir, WT serves as the most valuable source of reservoir information. At this point, the focus lies on evaluation of the reservoir itself, optional feature description and the determination of the reservoir's extent. The objective of utmost importance is to define whether a well can be rated successful in terms of the reservoir's quality, productivity and size.

The challenges to analyse a pressure measurement are quite complex and sensitive to beforehand assumptions. As the analysis outcomes are directly related to the estimation of potential and reserves, an interdisciplinary approach, taking into consideration geological knowledge is important. "It is the duty and responsibility of industry managers to encourage full coordination of geologists, geophysicists and petroleum engineers to advance petroleum exploration, development and production" [8, p. 754].

Therefore, possible improvements in the area of reservoir evaluation and the description of various features, as well as the first guess of the reservoir's extent for RAG gas reservoirs need to be evaluated. The integration of simplified numerical modelling into the usual analytical PTA techniques has been performed by several authors [9, 10, 11, 12, 13, 14, 15, 16, 17]. Using Artificial Intelligence in conjunction with PTA has also been performed over the last two decades [18, 19, 20, 21]. Another aim is the combination of outcomes of an extended data analysis with numerical modelling and with artificial intelligence methods in order to test the method for reserves identification in newly drilled gas reservoirs.

2 Fundamentals

2.1 Reserves estimation in dry gas reservoirs

“Proved reserves are those quantities of petroleum, which (…) can be estimated with reasonable certainty to be commercially recoverable, from a given date forward, from known reservoirs” [22, p. 30] . These reserves can be quantified by the analysis of data from geoscience and engineering and can be correlated with economic conditions, operational methods and governmental regulations. [22, p. 30].

Reserves of petroleum systems can be estimated either through analogies, based on geological estimations or are adapted from the actual production. Volumetric estimations in the pre-drilling phase and during discovery are highly uncertain, but naturally the range of uncertainty decreases during the lifecycle of a reservoir and through the usage of several estimation techniques (Figure 1). Production performance based methods, which include material balance (MB), decline curve and numerical simulation should be exercised after a certain period of continuous production, which will highlight a reduction in reservoir pressures, and, therefore, reveal a depletion of reserves [22, p. 21]. Figure 1 demonstrates the development of uncertainty and highlights the fact that early estimates can be very pessimistic compared to the final recovery [23].

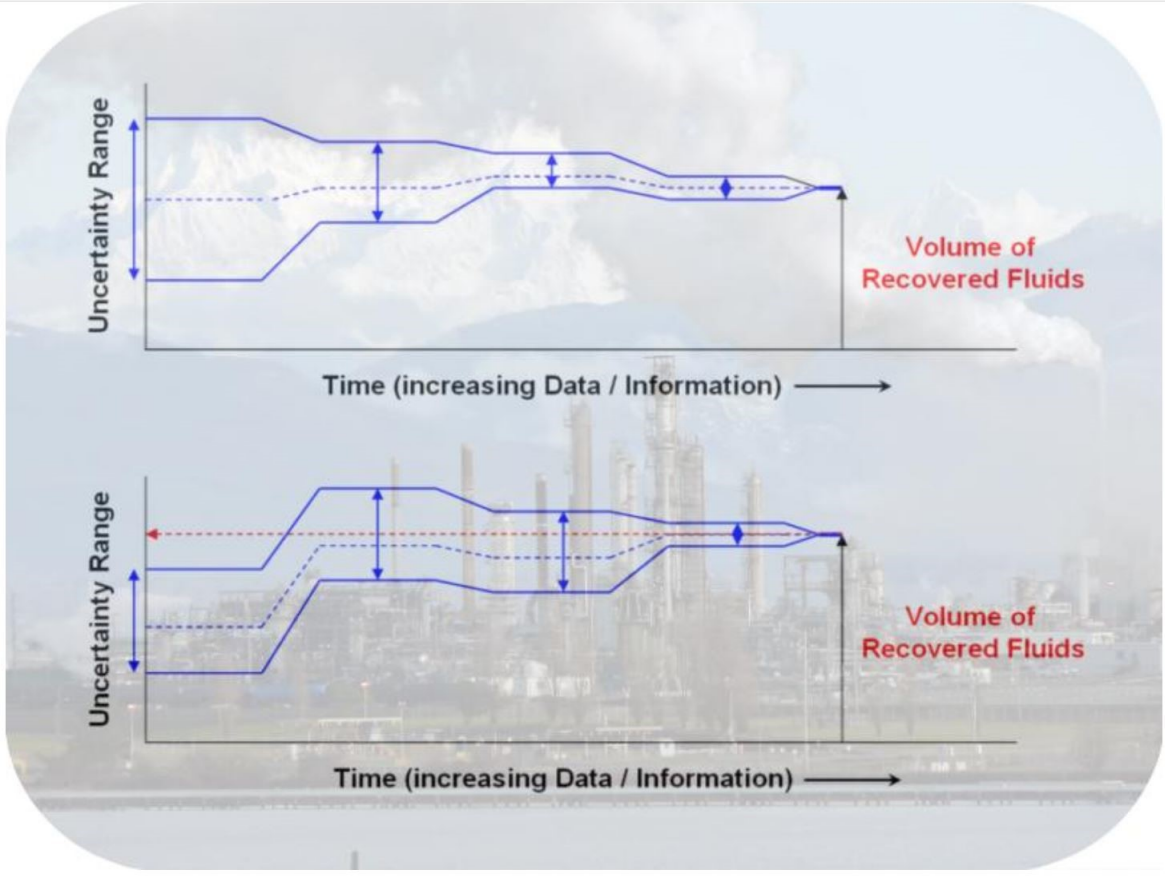

Figure 1: Change in the estimation of reserves through time [23].

2.1.1 Material balance equation for dry gas reservoirs

The material balance equation (MBE) is based on the concept that the pressure depletion of a reservoir reflects the total energy in the system. The fundamental equation is a simple mass balance, keeping track of the volumes flowing into, out of and staying in a reservoir [24, p. 737]. This can be visualized, when imagining a picture-perfect porous system, with a high permeability, which drains a certain percentage of its content. As the system is perfectly homogeneous the response in terms of reduced pressure can be seen everywhere in the reservoir within a reasonable amount of time. The basic aims for MB in gas reservoir engineering are the estimation of gas initially in place (GIIP) and the determination of the basic drive mechanism. Two different methods are available for these tasks: the p/Z plot and the Havlena-Odeh method. A first trend can be seen in the p/Z plot after a very short production period, but it is sensitive and error-prone. The Havlena-Odeh method is very exact, but a high amount of production data is required [25, p. 473]. The focus in this thesis lies on the p/Z plot.

For volumetric gas reservoirs the material balance equation is rather simple. The fundamental assumption is setting into relation the reservoir volume at the initial state with the remaining gas after depletion in **eq**. 1 [26, p. 157].

$$G\left(B_{gi}\right) = \left(G - G_p\right)B_g \tag{1}$$

G…GIIP at standard conditions (p_{sc}=1.01325 bara, T_{sc}=0°C) [MMscm]

B_g…formation volume factor for gas (reservoir volume/volume at standard conditions) $\left[\frac{Rm^3}{Sm^3}\right]$

G_P… cumulative gas produced in standard conditions [MMscm]

i…initial conditions

The pressure-volume-temperature (PVT) properties of real gas are related to each other in a very simple equation of state, in **eq.** 2

$$pV = ZnRT \tag{2}$$

p…pressure [bara]

V… volume [m³]

T… temperature [°K]

n... number of moles of gas [mol]

R… gas constant: 8.314 $\left[\frac{J}{mol*K}\right]$

Combination of **eq.** 1 and **eq.** 2 with the external assumption of an isothermal reservoir results into **eq.** 3:

$$\frac{p}{Z} = \frac{p_i}{Z_i}\left[1 - \frac{G_p}{G}\right] \tag{3}$$

Z… real-gas deviation factor at the respective pressure [-]

Equation 3 is reformulated and several reservoir pressures with their respective cumulative production are plotted in a Cartesian plot. A linear trendline through these points is used to cross the abscissa at the estimated GIIP (Figure 2) [27, p. 10].

However, certain conditions have an influence on the pressure behavior, which is directly reflected in the p/Z-plot [22, p. 21]:

- **Full/partial water drive:** Almost no pressure depletion for full water drive, similar behavior for partial. A sudden influx of water results in a total production which is significantly lower (depending on the relative strength of the aquifer) than could be expected from the “apparent gas in place”- trend.
- **Reservoirs with abnormal pressures:** The pressure behavior in the beginning reflects a higher GIIP, but the curve bends downwards due to various processes, like pore collapse and formation compaction [28, p. 1528], or (shale) water influx [29, p. 132]. A serious overestimation of initially gas in place and reserves can be the result of such a situation.
- **Low permeability wells:** The reservoir pressure builds very slowly after shutting in the well, the average pressures are therefore hard to estimate and the values are not representative [30, p. 50].
- **Connected/compartmentalized reservoirs:** The cumulative production will exceed the initial estimate, reflecting the effect of additional gas (Figure 3). This effect is discussed separately in the following section.

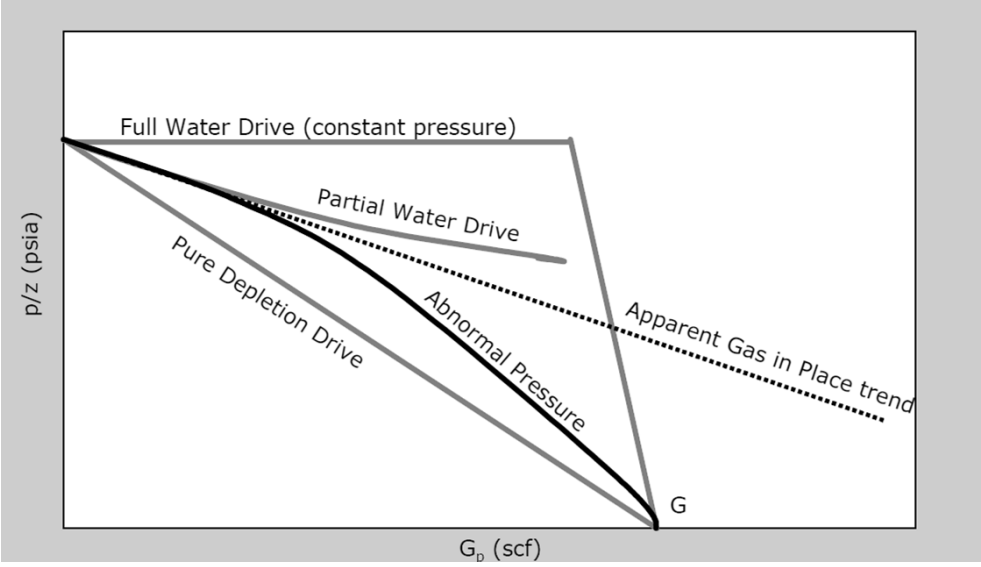

Figure 2: p/Z plot for various different reservoir drives [27, p. 10]

The usage of material balance is definitely satisfying for a homogenous depletion drive reservoir. Nevertheless, a linear shape can also be misinterpreted as depletion drive gas reservoir, resulting in a wrong assumption on the drive mechanism and, therefore, seriously over- or underestimation of GIIP [25, p. 473]. The problem is that the differentiation between a real and an apparent straight line is not straight forward and could be mixed up until an advanced stage of reservoir depletion [25, p. 487]. It is generally recommended to produce at least 5% of the GIIP before relying on the apparent pressure trend in a p/Z-plot, because of the variety of influencing parameters that can distort the pressure trend [30, p. 51].

2.1.2 Reservoir compartmentalization and layered reservoirs

The reservoir compartmentalization (RC) theory describes petroleum accumulations, which are split into various pressure segments separated by boundaries, through which the reservoir fluids will not flow freely over production time scales. The differentiation hereby is between sealing and pseudo-sealing boundaries, whereas the latter may not support large pressure differentials due to production and start leaking [31, pp. 1, 18].

The application of RC theory is used in cases of faulting and depositional heterogeneity [31, p. 25]. Generally speaking, the compartments are separate units with a barrier in between, allowing flow from one unit to the other at a certain pressure difference, depending on the transmissibility of the barrier. Sub-seismic reservoirs could, therefore, behave like small tanks in the early testing and production phase, in the long-term, the pressure development and production performance can change [32, p. 1]. Cases where wells with a rapid pressure decline were closed, and after several years showed a complete build up to initial pressures verify this theory and confirm the ability of a reservoir to recover [33, p. 3]. The reservoir's architecture as well as the p/Z plot behavior in cases of RC is illustrated in Figure 3 [34, p. 2].

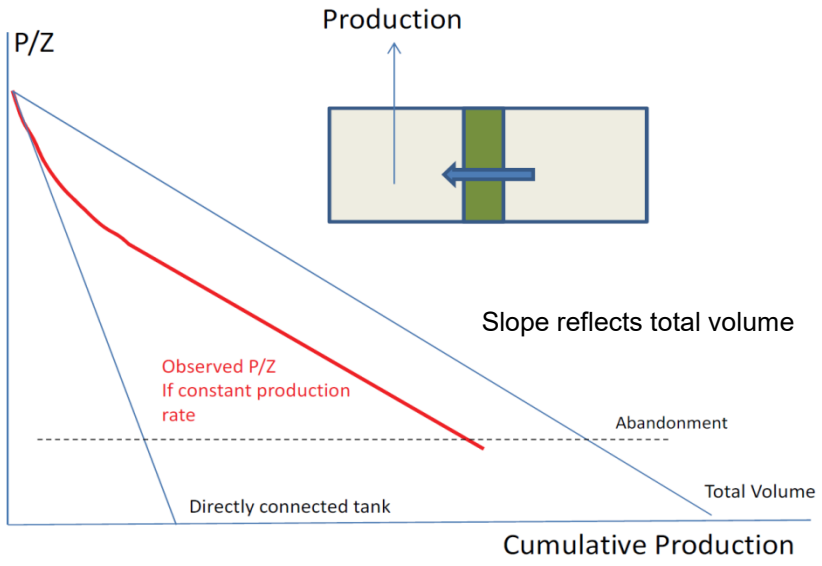

Figure 3: p/Z plot of a connected reservoir [34, p. 2]

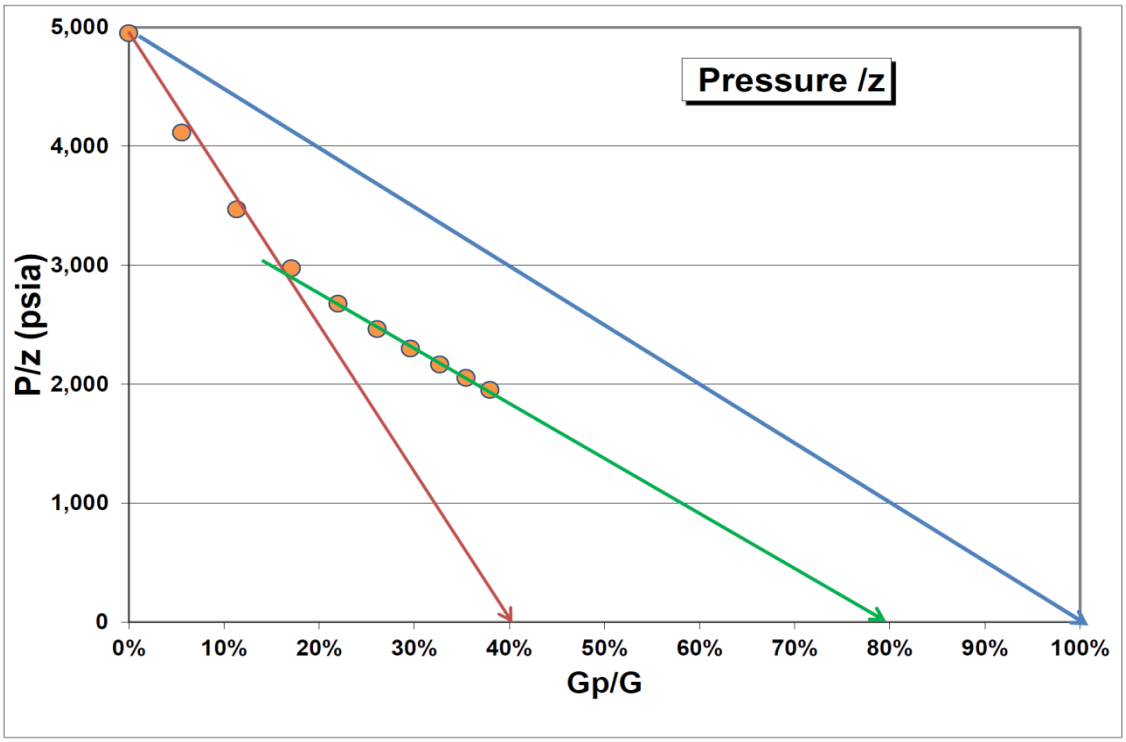

Figure 4: p/Z for a layered reservoir [35, p. 2]

Figure 3 demonstrates graphically, what is found in several studies as well: In compartmentalized reservoirs, initially determined reserves can be exceeded in the years of production by a high percentage. In one study, a re-evaluation of pressure data resulted in an increase in reserves of 10-40% [33, p. 1].

A very similar behavior can be found in layered reservoir with one layer being much more permeable than the second layer. A p/Z plot behavior in cases of layering is illustrated in Figure 4. For this example, a layered reservoir was simulated and a shut-in is performed every year for a time span of 4 days. The first pressure trend indicated 40% of the total reserves (red line), the second pressure trend (green line) is related to gas being produced from the tight layer and showed 80% of total GIIP, still underestimating the reserves. The "real" pressure behavior of the reservoir is the blue line. Both, the red and the green line, are apparently straight on the p/Z plot – but indicate a wrong GIIP [35, p. 3].

Issues in GIIP estimation through p/Z plot can occur, if erroneous data is inserted in the calculation, especially at an early production stage [36, p. 16]. Sources for errors can be numerous: Missing conversion of pressures at measured depth to pressures at reservoir depths or the usage of a wrong fluid gradient.

Unfortunately, most of the before-mentioned issues arise due to the usage of insufficiently stabilized pressures as substitutes for average reservoir pressures, although final stabilization could take several months (depending on the permeability of the drainage area). This method can lower the reserves estimates and forecasts significantly [37, p. 2]. The problems associated with average pressure estimation are discussed in detail in section 2.2.3.

2.2 Gas well testing: Evaluation, features and extent

2.2.1 Overview

General objectives for WT in the early life of a reservoir are the confirmation of mobile hydrocarbons in the reservoir, as well as obtaining valuable information on production behavior, dynamic properties and geology. The first well test in a zone of formerly undetermined potential usually is a drill-stem-test (DST) focused on the evaluation of the reservoir fluid, production capability and initial reservoir pressure. A DST, or open-hole-test (OHT), is executed without the prerequisite of production equipment and supports the investigation on commerciality of the discovery [26, p. 145]. An extended test, or cased-hole-test (CHT), is used for detail refinement in the geological description, as the radius of investigated volume becomes larger with time, and allows the detection of pressure depletion and heterogeneities (Table 1) [38, p. 3]

Table 1: Objectives for early pressure measurements.

Objectives of WT	
Short Test (OHT)	**Extended Test (CHT)**
Production capability	Long-term production capacity
Initial reservoir pressure	Damage
Damage	Effective permeability
Effective permeability	Reservoir shape and boundaries
Near-well boundaries	Pressure depletion
	Heterogeneities

2.2.2 Open-hole-test and cased-hole-test

Open-hole-test

In the early beginnings of this discipline, WT was performed as a production test against atmospheric pressure, measuring this open-flow capacity with a pitot tube. This method was not only wasteful, and damaging the well, but also the results were not very useful [30, p. 109]. Since about 80 years, instead of this wasteful method, a DST is performed instead.

In RAG the definition of an OHT is synonymous to a DST. Using the drilling equipment (drill pipes) and special testing equipment, a temporary completion allows for the reservoir to be produced and shut in while measuring the pressures and rates. This operation is executed with a drilling rig in place, which limits the total duration considering the cost perspective. A usual test sequence is illustrated in Figure 5 [39, p. 333]. After running in the equipment, a short clean-up and first flow-period is performed, followed by a short build-up (to measure the initial reservoir pressure), a second, longer flow-period (around 4 hours) and a final build-up period (around 6 hours).

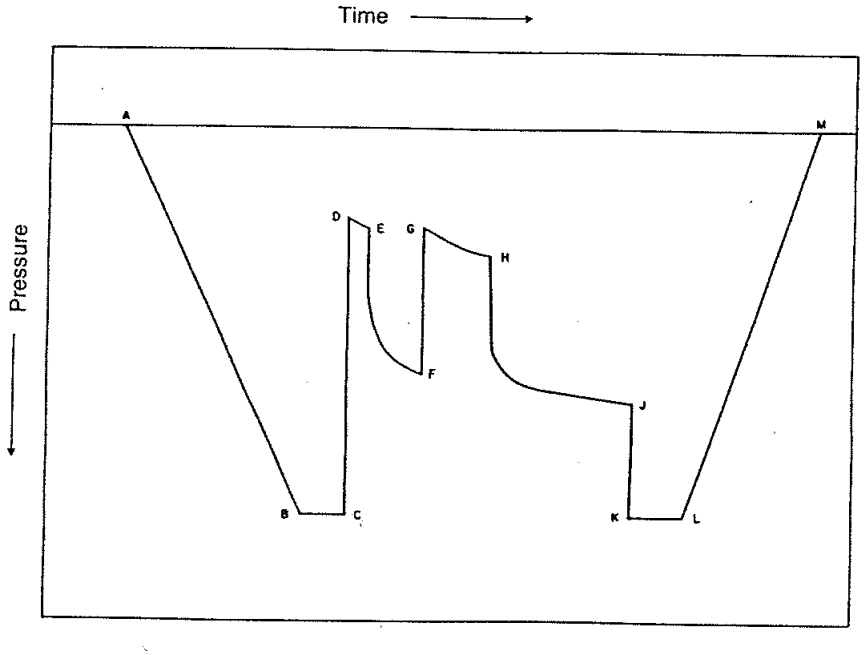

Figure 5: Ideal OHT sequence without scale [39, p. 333]

OHT operations

The formation to be tested is isolated with packers from the mud column in the annulus and directly connected with the drill string as a flow line (Figure 6). The testing string is filled with a gas cushion (formerly water) to control differential pressures across the packers, prevent borehole collapse across an unconsolidated formation [40, p. 2], indicate fluid production and calculate rates for oil tests and weak gas reservoirs. Therefore, three different pressures are important in a DST: Hydrostatic pressure of the mud column, cushion pressure and formation pressure. The testing equipment allows the drillers to shut-in and open valves through movement of the drill string, connecting to and disconnecting the drillstring from the reservoir. Pressure gauges measure the drawdown and build-up of sandface pressures. The produced gas is usually flared through a meter [26, p. 148]. After the testing procedures are successfully finalized, the pressure is equalized and after a phase of reverse circulation, the drill string is finally pulled out [6, p. 92].

Potential limits and hazards in an OHT are [26, p. 148]:

- Insufficient packer seat leads to a break in of the drilling fluid during operations. Also, testing equipment is limited to certain wellbore sizes.
- The possibility of stuck pipe is increased, which could lead to a loss of the equipment and well.
- Within an operation, only one reservoir unit can be tested at once: Several tests may become necessary, which could raise the costs significantly.

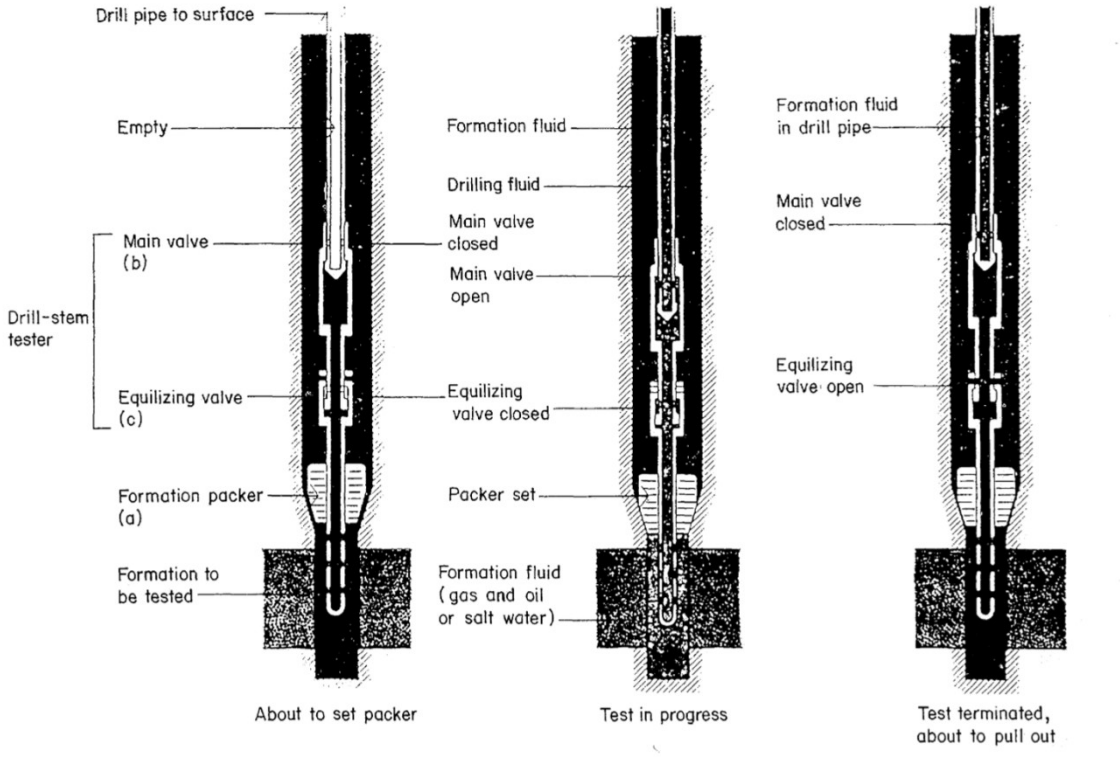

Figure 6: OHT assembly [26, p. 146]

- Gas hydrates can form at high pressures and low temperatures. It is mandatory to keep the well stream temperature high – heating [41, p. 723].

In RAG, these hazards are taken very seriously, which is the reason for elevated security policies during OHT operations. Generally speaking, tests in cased-hole environment could eliminate many of the before mentioned problems. But it is certainly a fact that good knowledge of the geological setting through the comparison with analogies as well as a good preparation of the testing operations result in a very low risk – in the last years, despite a high number of executed open-hole tests no incident worth mentioning has happened.

According to Howard, an OHT is highly erroneous due to the short time, but can be used as an indication if further testing is required [5, p. 30/15]

Cased-hole-test

A CHT is performed, as the name suggests, in a cased-hole environment. Of course, also a DST could be performed in such an environment, but in RAG a CHT is a production test with following extended shut-in.

A CHT may be necessary in the following situations:

- The persisting environment does not allow for an OHT to be performed, due to the risks of stuck pipe, wellbore instability, and others.

- Several layers have not yet been tested, or an OHT was not necessary, because there was no doubt that the well was going to be cased and produced. In these cases clarification may be needed in terms of extent, rate and reservoir properties.
- The obtained information of the OHT is not sufficient.

After a well is cased and the formation under inspection is perforated, a tubing string and pressure gauges are installed. After lowering the pressure gauges the well is produced for a certain duration – in remote areas without a gas network, this time is limited to about 8 hours. Afterwards, the well is shut in to allow for the pressures to build up for about 2 weeks.

CHTs do not infer hazards to the drilling personal, and are preferred in terms of safety. Of course, a CHT is able to deliver much more information about the reservoir than an OHT but the invested capital is higher for a cased well than at the stage of an OHT. On the other hand, an OHT allows for testing of layers, which due to particular reasons will not be perforated in the short-term future. This way, reserves can be booked after a successful test and the decision can be made whether or not to drill further production wells on these targets.

2.2.3 Pressure transient analysis for gas wells

Infinite acting radial flow (IARF) and Horner plot

PTA focuses on measuring and analyzing pressure changes as a function of time. Several features, discussed in section 2.2.1, can be found using the following equations, which are all provided in oilfield units, as this is the most applicable form in the industry.

The radial flow equation in an infinite reservoir for slightly compressible fluids (oil) gives a total pressure drop as described in **eq.** 4 [42, p. 49]:

$$p_i - p_{wf} = 162.6\frac{q\mu B_o}{kh}\left[log_{10}\frac{kt}{\Phi\mu c_t {r_w}^2} - 3.23 + 0.87S\right] \quad (4)$$

$p_{i,wf}$… initial/well-flowing pressure [psi]

q… flow-rate [STB/day]

μ… viscosity [cP]

k… permeability[mD]

h… reservoir height [ft]

Φ… porosity [-]

c_t…total compressibility [psi^{-1}]

r_w… wellbore radius [ft]

B_o… formation volume factor for oil [RB/STB]

t… time [hr]

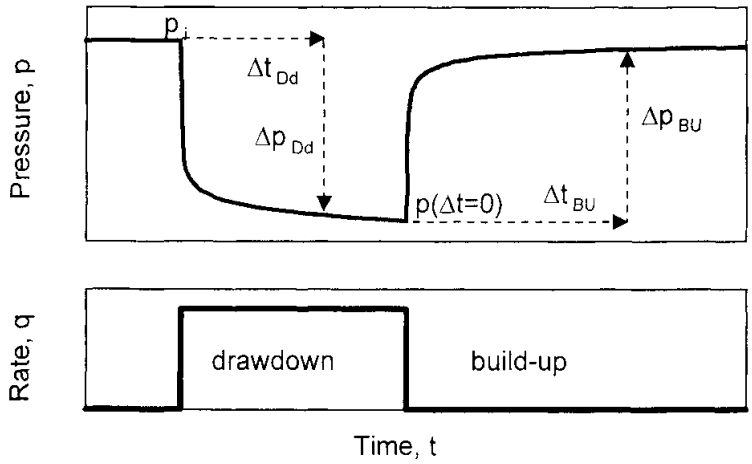

Figure 7: Illustration of drawdown and build-up [38, p. 1]

S… Skin factor [-]

Principally, any change in pressure during a test, drawdown or build-up, can be chosen for analysis (Figure 7). Nevertheless, a build-up is less error-prone, because the rate is fixed as zero during the whole period.

The analytical equation for pressure build-up is found with the method of superposition, superposing the pressure drop at the well due to a positive rate (rate at shut-in) with the same negative rate, the sum equaling to zero rate. The resulting pressure drop at a time Δt is given in **eq.** 5 [42, p. 18]:

$$p_{ws} = p_i - 162.6\frac{q\mu B_o}{kh}\left[log_{10}\frac{t_p + \Delta t}{\Delta t}\right] \tag{5}$$

p_{ws}… shut-in pressure at the wellbore [psi]

t_p… total duration of production [hr]

Δt… time since shut-in [hr]

Typically, **eq.** 5 is plotted in a Horner plot (Figure 8) with the Horner time on the abscissa and pressure $p_{ws,\Delta t}$ at the ordinate [43, p. 503]. The constant rate production yields a straight line. Using the slope of the plotted line, m, within one log-cycle, the product kh can be calculated with **eq.** 6 [42, p. 49]:

$$kh = \frac{162.6q\mu B_o}{m} \tag{6}$$

m…slope [psi/(log_{10}-cycle)]

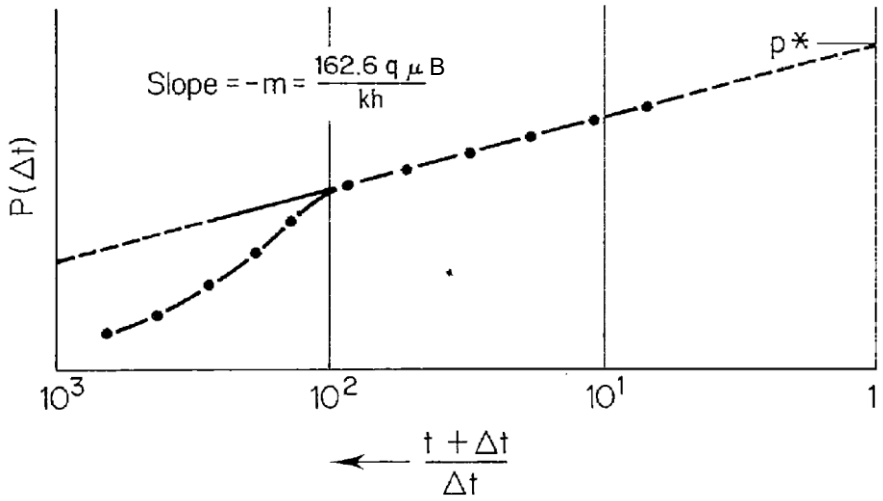

Figure 8: Horner plot [26, p. 140]

As gas is a highly compressible fluid, these equations have to be slightly changed. Pressure is substituted with real-gas potential in **eq.** 7 (in field units), introduced by Al-Hussainy, Ramey and Crawford accounting for changes in pressure, viscosity and compressibility simultaneously [44, p. 624]. The underlying assumption is an isothermal flow condition.

$$m(p) = 2\int_{p_m}^{p} \frac{pdp}{\mu(p)z(p)} \tag{7}$$

m(p)…real-gas potential or pseudo-pressure [psi²/cP]

Using the real-gas potential, **eq.** 5 and **eq.** 6 change to **eq.** 8 and **eq.** 9 [30, p. 168f., 38, p. 310]

$$m(p)_{ws} = m(p)_i - 1{,}637\frac{q_g T}{kh}\left[log_{10}\frac{t_p + \Delta t}{\Delta t}\right] \tag{8}$$

$m(p)_{i,ws}$…real-gas potential initial/at shut-in pressure in the wellbore [psi²/cP]
q_g… gas flow rate [Mscf/day]

$$kh = 1{,}637\frac{q_g T}{m} \tag{9}$$

The skin factor can be calculated using the real-gas potential at one hour after shut-in, $m(p)_{1hr}$, and at the last real-gas potential before shut-in, $m(p)_{wf}$ for calculation in **eq.** 10 [38, p. 310]

$$S = 1.151\left[\frac{m(p)_{1\,hr} - m(p)_{wf}}{m} - \log_{10}\left(\frac{k}{\Phi\mu c_t {r_w}^2}\right) + 3.23\right] \tag{10}$$

Another important parameter that is derived from the Horner plot is the extrapolated pressure, p*, which is used as the average drainage region pressure, $\bar{p}$, illustrated in Figure

8. To arrive at this value, the last slope of the plot is extrapolated linearly. The cross section of the ordinate at $\frac{t_p+\Delta t}{\Delta t} = 1$ gives the desired pseudo-pressure m(p*), which is converted to p* (Figure 8) [45, p. 113].

Regions, effects and derivative plot

Three different time intervals after shut-in yield certain responses [46, p. 555]. The early-time region (ETR) is dominated through inner boundaries (skin, wellbore storage) followed by the middle time region (MTR), a period showing reservoir behavior (homogeneous with infinite-acting radial flow (IARF) or heterogeneous). In the late time region (LTR), outer boundary effects are visible on the pressure response [45, p. 73]. The identification of these periods is considered as one of the most important tasks in WT [45, p. 79].

As the theory for IARF prerequisites a homogeneous reservoir, every deviation in terms of permeability, porosity, thickness, etc. changes the pressure behavior. A very good illustration of different flow behavior can be achieved with the so-called derivative plot (Figure 9 [47]). Along with the pressure, the derivative, p', which illustrates the changes of the slope of the pressure data, is plotted and analyzed on a log-log scale plot. As suggested by Lee, the best mix of pressure analysis techniques includes the log-log plot with the derivative, and the Horner plot [48].

The derivative is very sensitive to pressure changes (Figure 9) [45, p. 79]. There are several boundary effects that could cause the deviation of the horizontal part of the derivative, because different flow regimes develop, including faults (impermeable or permeable), reservoir boundaries, change in mobility or permeability (shale-out), channels and other geological features. It is concluded that the detected heterogeneities can only be understood, if longer tests are performed to create the complete pressure response [45, p. 114]

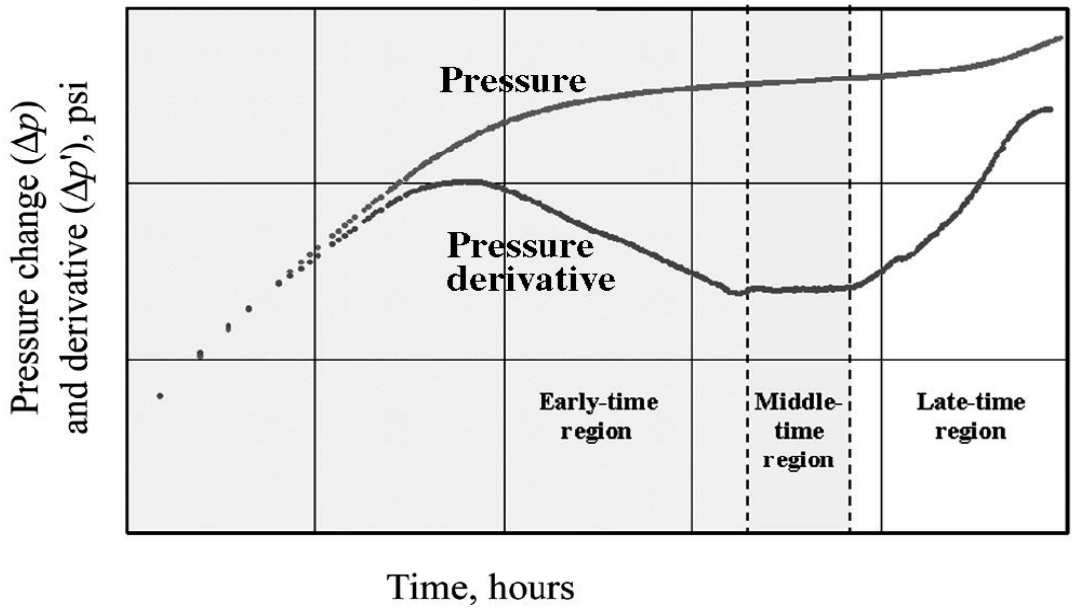

Figure 9: Derivative behavior [47].

Faults and other flow barriers

The presence of faults and flow barriers significantly changes the pressure response, mathematically described by the principle of superposition using an image well. With one flow barrier, the slope on the Horner becomes 2m, instead of m [45, p. 113]. Without going into the mathematical details, the main behaviors of the Horner plot and log-log plot for radial flow, radial flow plus a sealing boundary, and a closed boundary reservoir are shown in Figure 10, Figure 11 and Figure 12. Downwards turning derivatives could either show depletion, water breakthrough or, which is interesting, an improvement of the reservoir a certain distance from the wellbore. In these cases, the difference in the initial and the final shut-in pressure will help distinguish if depletion occurs or not [49, p. 3].

Linear flow (channel) exhibits a special behavior (Figure 13), which is even more pronounced in a three-sided channel. On a Horner plot linear channel flow exhibits an exponential behavior. Pressure extrapolation, as described in the previous section, is inadvisable in this case [38, p. 217].

It has to be kept in mind, though, that the pure knowledge about a flow barrier does not give an exact description of this feature, a fact which is discussed in the following section.

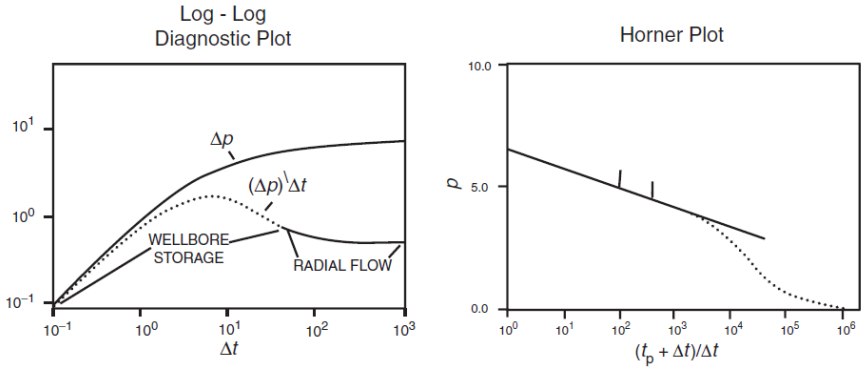

Figure 10: Infinite acting radial flow system [50, p. 1281].

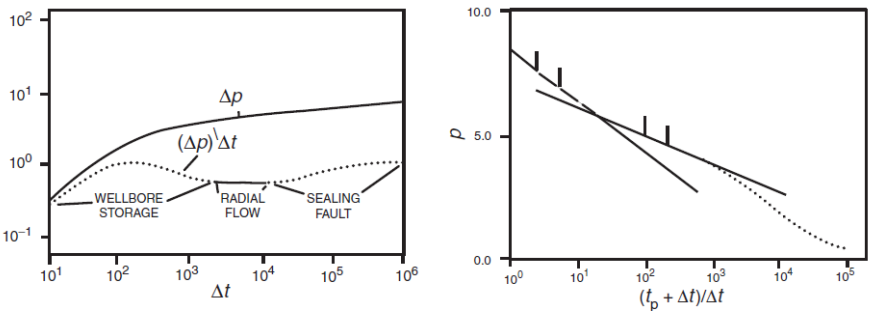

Figure 11: One sealing fault [50, p. 1281].

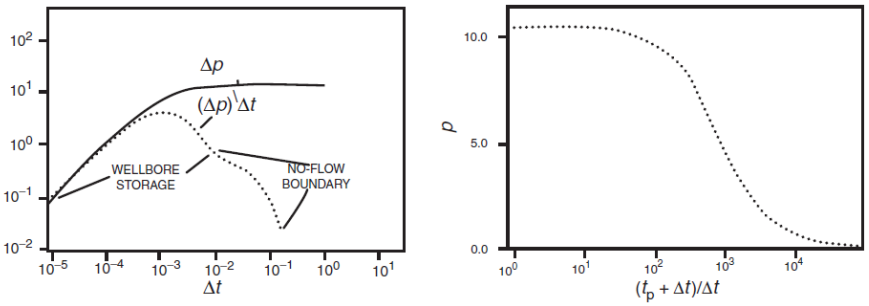

Figure 12: Closed system [50, p. 1281].

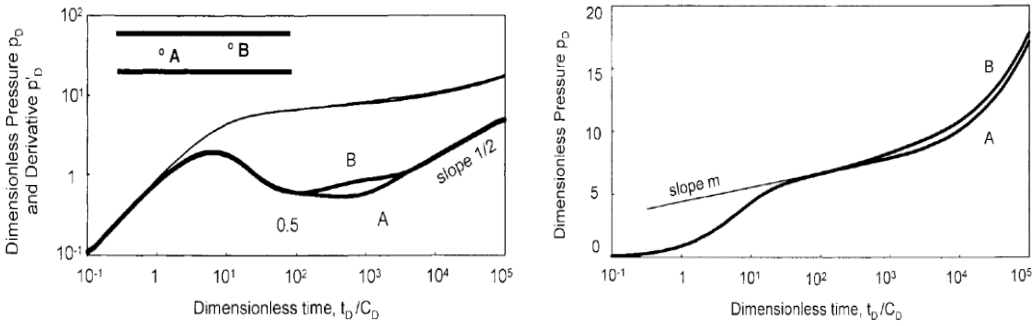

Figure 13: Channel system [38, p. 210/211]

Modelling challenges of PTA

The results of a well test analysis depend on the quality of the measured data, and on the reservoir model selection. The accuracy of measured data can be reviewed and the test can be repeated. A wrong model selection, on the other hand, has more complex consequences [51, p. 2].

It is an advantage to being able to consider geological peculiarities, and arrive at a certain proof for their existence. But, the same well test outcome can be matched with many different models. The term for this phenomenon is “non-uniqueness” and has a direct influence on the quality of an analysis [52, p. 335].

Non-uniqueness roots in the circumstance that the origin of similar pressure behaviours can be of very different nature, even the assumption of a certain flow regime can be misleading. For instance, various boundary effects, which all have a similar influence on the LTR of the derivative, can be caused by a (sealing) fault, a shale-out, a sudden change in mobility or even by transient inter-porosity flow in a dual-porosity system.

A closed-system behaviour as shown in Figure 12 can not only be caused by a singular mechanism: The reason can be a closed reservoir or a constant pressure boundary (gas-cap, aquifer,…) [45, p. 114]. A linear flow is not only exhibited by a channel, but could also be proof for a change in permeability, which would suggest the possibility for the reservoir to be recharged by the less permeable zone. Another author suggests that the slope in the LTR

of the well lest can be caused by the mobility change in an edge water drive reservoir [53, p. 252]. In the case of a strongly upward-turning derivative, the use of MB is highly inadvisable [54, p. 59]. According to Pridie [49, p. 4], for upward turning derivative profiles, reserves cannot be determined at all and, therefore, the focus should lie on the production rates.

The general problem of non-uniqueness is especially valid during the exploration phase with literally no secondary information [51, p. 2]. The reduction in geological uncertainty can be very low [14, p. 3]. Therefore, force-fitting certain geological features, which are meant to catch a distinctive behaviour on the derivative, can lead to wrong assumptions. Generally speaking, WT interpretation techniques seduce the user to decouple from geological principles, leading to rather unrealistic perceptions due to the freeness that non-uniqueness provides. The best way to avoid this is an in-depth investigation of framework conditions, an integral analysis of all available data and an interdisciplinary approach [11, p. 4] [51, p. 5]. Input from the geologist in form of well logs, geophysical maps, core data and outcrop studies can assist a lot in the decision-making process during the WTI [45, p. 114]. This can become a win-win situation for either, geologist and reservoir engineer [55, p. 1].

2.2.4 Average pressure calculation alternatives

The determination of average reservoir pressures from a build-up through pressure extrapolation as explained in the previous section is complemented by other methods. The three most well-known methods are the Matthews-Brons-Hazebroek (MBH) [56], the Ramey-Cobb [57] and the Dietz method [58] and are explained in short to show their opportunities and restrictions.

MBH method

This method is developed to estimate the average drainage area pressure from build-up tests for reservoirs with specific bounded shapes. The calculation procedure is the following:

1. Horner plot – IARF straight line is extrapolated to m(p*) at $\frac{t_p+\Delta t}{\Delta t} = 1$, the slope m is evaluated.
2. The dimensionless producing time is evaluated with **eq**. 11 (in field-units)

$$t_{pDA} = \left[\frac{0.0002637k}{\Phi \mu c_t A}\right] t_p \tag{11}$$

   t_{pDA}… dimensionless time [-]
   A… drainage area [ft²]

3. Consult Figure 54, Figure 55, Figure 56 and Figure 57 in the Appendix for the curve depicting the assumed reservoir shape and read the value for p_{DMBH}, in order to calculate the average drainage area pseudo-pressure, m($\bar{p}$), with **eq**. 12 (again, using field units):

$$m(\bar{p}) = m(p^*) - \left(\frac{m}{2.303}\right) p_{DMBH} \tag{12}$$

m(p*)…pseudo-pressure at the extrapolated pressure [psi²/cP]

$m(\bar{p})$, …pseudo-pressure at average drainage area pressure [psi²/cP]

Ramey-Cobb method

The method of Ramey and Cobb requires the same input data: Drainage area shape, size and well location, but only the Horner plot is involved in the evaluation.

1. Evaluation of t_{pDA} from **eq.** 11, and comparison to $(t_{DA})_{pss}$ from the fifth column in Table 10 in the Appendix.
2. If $t_{pDA} < (t_{DA})_{pss}$, $m(\bar{p})$, can be read from the Horner plot at $\left(\frac{t_p+\Delta t}{\Delta t}\right) = exp(4\pi t_{pDA})$
3. If $t_{pDA} > (t_{DA})_{pss}$, the value for C_A is found in Table 10 and $m(\bar{p})$ is read from the Horner plot at $\left(\frac{t_p+\Delta t}{\Delta t}\right) = C_A t_{pDA}$

C_A… shape factor, see Table 10.

Dietz method

This method is applicable, if pseudo-steady-state (pressure drop at the boundary is constant) is reached. From the Miller-Dyes-Hutchinson plot, which is another form of a semi-log plot with p_{ws} vs. log(Δt), $\bar{p}$ can then be directly evaluated at shut-in time $(\Delta t)_{\bar{p}}$, defined by **eq.** 13 (in oil-field units):

$$(\Delta t)_{\bar{p}} = \frac{\Phi \mu c_t A}{0.0002637 C_A k} \tag{13}$$

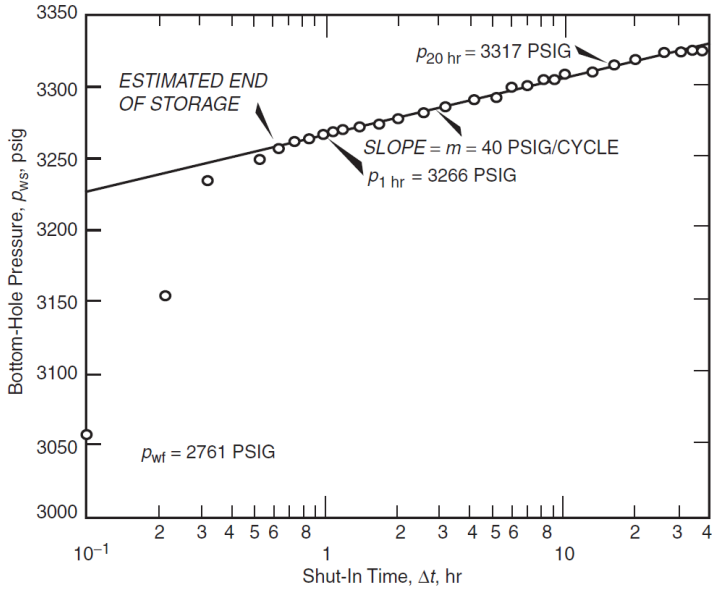

Figure 14: Miller-Dyes-Hutchinson plot [45, p. 1/58, 6, p. 51]

2.3 Geological background: Gas reservoirs in the Molasse basin

The Upper-Austrian Molasse basin is a part of the North Alpine Foreland basin extending from Switzerland via Bavaria to the Carpathian foredeep [59, p. 64]. The asymmetrical Oligo-Miocene Molasse basin is bounded by the Alps in the south and the European foreland (Bohemian massif) in the North. It started to form onto the fundament of crystalline approximately from late Eocene onwards, because of a collision between the Apulian plate and the North European craton [60, p. 130]. Through a successive downwards bending a steep to shallow slope developed, which was successively filled with shallowing upwards clastics during the middle Oligocene [61, p. 102] [62, pp. 1-3].

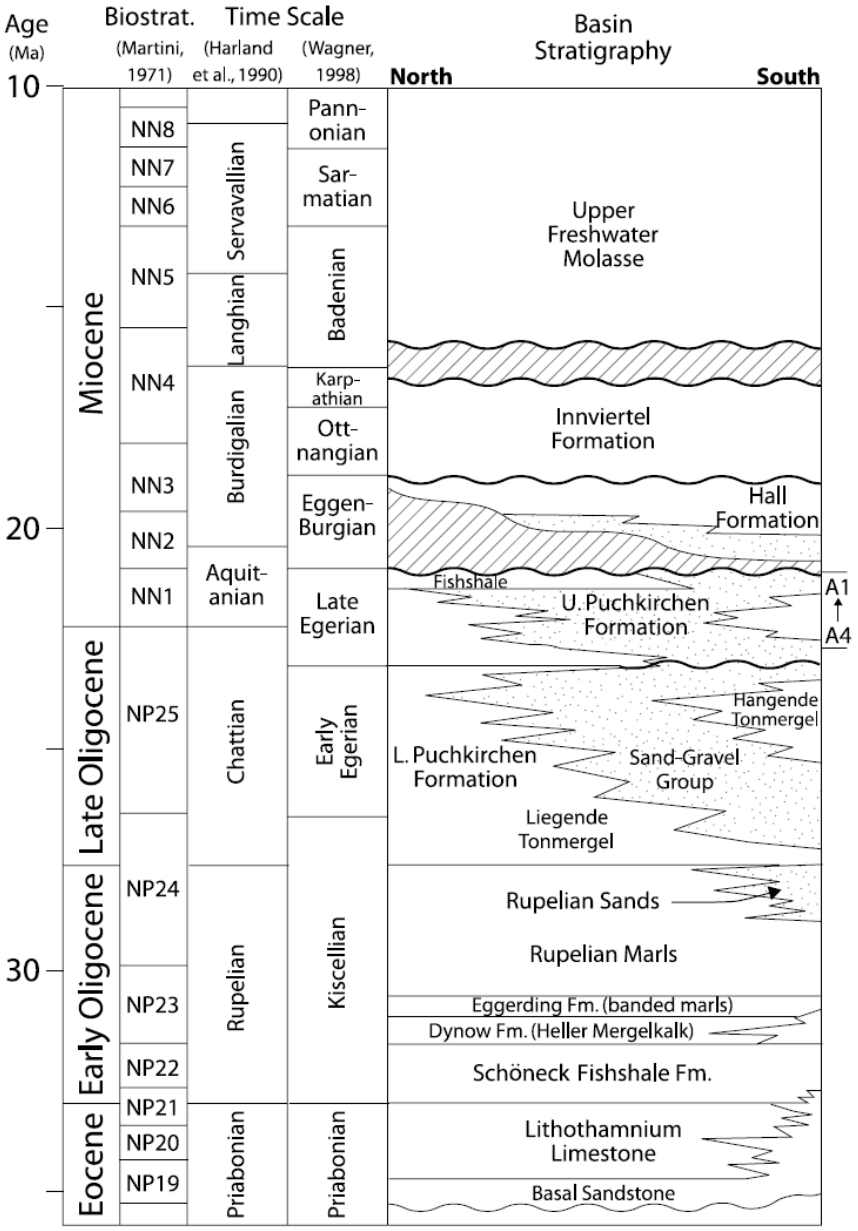

Figure 15: Geological succession of the Molasse [63, 64, p. 738]

In the Kiscellian, the early Oligocene, the Molasse basin developed to become a deep-marine basin. During this time the area north of the Alps was completely isolated from the rest of the sea. In the south, under anoxic conditions, hydrocarbon source rocks were deposited. In the late Kiscellian, the connection to the open sea was redeveloped [61, p. 101].

In the following epochs of Egerian and Eggenburgian (Figure 15), the Puchkirchen basin developed, comprising of Rupelian Sands, overlaid by the Lower Puchkirchen Formation (UPS), the Upper Puchkirchen Formation (OPS), and Hall Formation (HS) [59, p. 66]. The majority of the tested RAG reservoirs were found within UPS, OPS and HS, which therefore form the main formations for gas reservoirs in Upper Austria (Figure 18).

The UPS is divided into mudstones, conglomerates and sandstones, and is separated from the OPS through an erosional unconformity. The lower HS overlies the OPS and the deposits are very similar to the Puchkirchen Formation. The upper HS has a different lithology and is not part of the Puchkirchen basin, but also relevant for gas production [59, p. 66].

The main characteristics of the Puchkirchen basin are successions of gravity flow deposits – turbidity currents, debris flows, submarine slides and slumps. The deposits were fed by intramontane streams and the resulting conglomerate consists of mature, well-rounded components, deposited in a west-east directing channel-belt north to the Alpine thrust front (Figure 16) [59, p. 66].

Reservoir targets in the Molasse

Main targets for gas reservoirs are channel systems (Figure 16), because they reach up to a height of several meters of fine- to medium-grained sandstone beds. The low-sinuous, narrow channels are often laterally extending. Nevertheless, the complexity of these

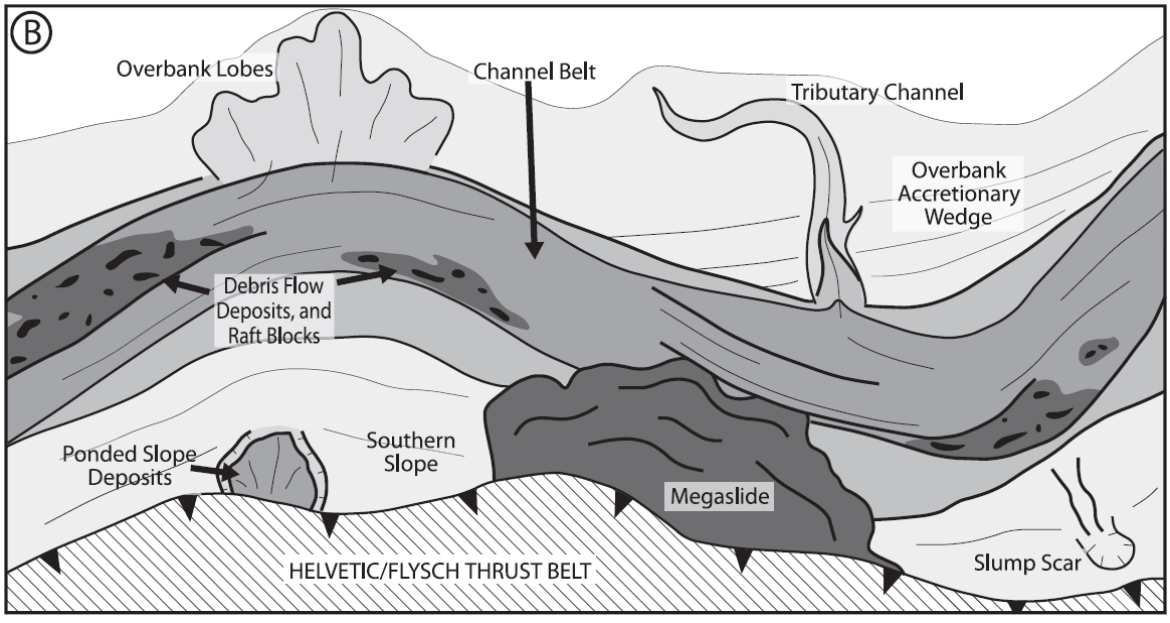

Figure 16: The Puchkirchen channel belt [64, p. 739]

reservoirs is relatively high due to an interlayering of various lithofacies (sandstone, sand matrix, conglomerates, mud-matrix) and erosional incisions within the channels. The logical consequence is a reduction in vertical permeability and a tendency to reservoir compartmentalization.

The tributary channels are side-arms of the axial channel belt and are filled with fine-to medium grained sandstone with horizontal permeabilities between 5-50 mD and low vertical permeabilities. The reservoir quality is not consistent, because a transition to tight-sands as well as lateral thinning and pinch-out in direction of the axial belt is possible.

The overbank accretionary wedges (Figure 16), consisting of mudstones and thin-bedded sandstones, are associated with the axial channel belt deposits. The proximity to the connected channel may allow the connected gas to flow into the main reservoir. The overbank lobes are laterally continuous medium to fine-grained reservoirs with high permeabilities and a reliable seal.

Slope fan plays are exclusively positioned directly north to the Alpine thrust front detached from the main axial channel system. They consist of thick sandstone beds with a high net-to-gross (N/G) ratio and are relatively rare.

Also, in the southern part of the Molasse basin another reservoir species, the imbricated Molasse (IM), is found, which is composed of tectonically shifted Molasse sediments. These reservoirs are highly compartmentalized and thick-bedded, and due to the tectonic activities often found overpressured.

2.4 Artificial intelligence: Neural networks

“Some argue there is a substantial amount of oil to be found by applying new analysis techniques to data already on the shelf.” [65, p. 50]

Since the mid-80’s artificial intelligence and predictive analytics (AIPA) is applied in the petroleum industry, rising because more experts in the field are available and case studies are published, which work as a paragon [66, p. 1]. The applications of AIPA methods range from production control and optimization, forecasting, stimulation (candidate selection) and WT to many other areas. But still, the oil industry has significantly less activities in AI than other comparable industries [67, p. 547]

AIPA is a general term including various families in the fields of artificial intelligence (AI) as well as data analysis, automation and advanced visualization. According to a survey conducted to assess the knowledge on AI methods in the petroleum industry [67, p. 547], the best-known technique is data mining followed by neural networks (NN), an AI technique. The category of AI involves NN, fuzzy logic and evolutionary computation.

Generally speaking, AI proposes new analytic tools trying to rebuild the essentials of life. Not only are these programs able to learn a specific behavior, but also they are capable of handling new situations [68, p. 64]. In this respect, problems which were previously difficult to solve are now implemented in these sophisticated tools and hybrids of them [69, p. 40]. For example, in integrated reservoir modelling using AI, the reservoir and well behavior guide the model rather than the current understanding of physics and geology, which drive conventional simulation models. Hyperdimensional, complex data is well suited for analysis by machine learning, which is a key element of today’s applications of AI [65, p. 54].

2.4.1 Neural networks

The perceptron, a binary linear classifier able to categorize linearly separable inputs as one or another class, was invented in 1957 [70, p. 277]. After a long dry-period Hopfield revived the NN research in 1980’s, since then the development flourishes [68, p. 65].

Basically, a NN consists of various layers, interconnected by simple processing elements, which are called neurons and whose functionality is loosely based on the brain neuron. The

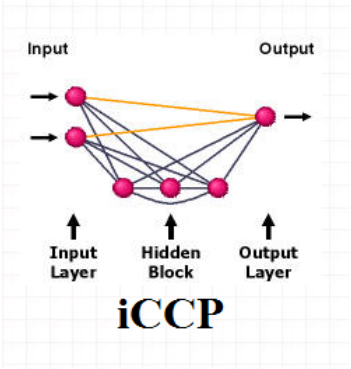

Figure 17: Neural network architecture [72].

input data is processed via a non-linear activation function using inter-unit connection strengths (weights), which are adapted to a training-dataset in order to achieve a desired output. A NN is more reliable to mirror non-linear behavior than regression methods and very able to discover hidden patterns, as it can handle noise [66, p. 93].

There are two different types of NN: Unsupervised NNs are mainly for clustering and classification reasons (well logs and lithology identification) without providing a measurement of correctness. Supervised NN are used, if input data and output data is presented and the output data can be matched [68, p. 67]. The architecture of the NN, which is used in this thesis, is shown in Figure 17. This special NN is an improved completely connected perceptron (iCCP), implemented in the cVision® tool. It has the advantage that there are only a total of three layers, making the choice of the correct number of hidden layers obsolete.

A dataset, which is provided to the NN, is split into three separate groups: 60% are used for training, to modify the weights of the neurons until convergence. In the training set, the outputs are used to calibrate the NN. Validation and testing datasets each make up 20% of the network. Those groups are not used for training, but to check the network. Testing datasets have not been seen by the network during training at all.

With backpropagation, the outputs of the NN are compared to the provided outputs. The errors are iteratively propagated backwards and split on the weights. The weight and the input can, therefore, be illustrated like vectors, pointing in the same direction, if they converge to a correct output [68, p. 67]. However, overtraining of a NN has to be carefully avoided. It happens, if a polynomial is fit perfectly to presented data: If a NN is overtrained, it perfectly mirrors the training dataset, but loses its ability to exhibit general answers.

3 Data management and statistics

Usually, OHTs and CHTs are planned and protocolled in terms of operations, and analyzed in terms of pressure behavior. RAG data concerning gas well tests has been gathered since the early 1960's. However, a database including the analysis outcomes and determined parameters did not exist before this thesis. Therefore, the first goal was to set up a database.

3.1 Data gathering and availability

During the period of 1963 and 1972 data was not yet organized in such form that the interpretation as well as the raw data are available today. Therefore, these tests could not be considered in the evaluation.

Between 1972 and the early 1980's data evaluation, especially extrapolated pressures – relevant for the GIIP calculations – and boundaries are mostly unavailable. Therefore, pressure data was manually inserted into files, which were then interpreted with Saphir®.

In the period of 1980 to early 2000, the data availability was very fluctuating. Some pressure recordings have been preserved and were newly interpreted, whereas many of the interpretations were available in the well folders and could therefore be used directly.

In the years from the late 90's onwards, for most gas well tests excessive interpretations are available, on the one hand as Saphir® files, on the other hand in written form, describing findings and features.

Due to the digital revolution and several innovations, protocols and analyses changed significantly over the years. The following parts usually exist:

→ Operations protocol with general information
→ Downhole pressure recordings:
  - Analogue pressure gauges (until early 90's): Pressure is scratched on metal foil. Depending on purpose and usefulness (i.e. data quality), points along the whole recording have been read and converted into pressure data for PTA or just last/highest pressure point has been taken. All foils are still available, but skill of using the conversion tables is essentially lost. From about mid 80's on, pressure build ups have been routinely digitized for interpretation, but apparently without saving this raw data on electronic storage media.
  - Since late 90's: Digital recordings, provided as ASCII files.

→ PTA (methods described in Section 2.2.3).
  - Until late 70's: In-house hand-written calculations and analysis.
  - Late 70's to early 80's: Basic printed calculations, attributes from Horner plot.
  - 80's and 90's: PTA performed by external consultants, attributes from Horner plot.
  - Since late 90's: In-house Saphir® analysis, introducing the derivative analysis.

3.2 Data processing

In total, data for around 600 tests and of these 476 successful gas OHTs and CHTs have been collected. Figure 18 shows the amount of successfully performed OHT and CHT, as well as their distribution in terms of different formations. The formations are: Imbricated Molasse (IM), Hall Formation (HS), Upper Puchkirchen Formation (OPS), Lower Puchkirchen Formation (UPS), and the rest is Flysch, Upper Cretaceaous, Upper Eocene (OTHER).

A detailed yearly bar chart is shown in Figure 19. It is visible that a change has occurred in the late 1990's and early 2000's, where fewer tests in total and almost no OHTs were performed. From 2005 onwards, OHT's are revived, but CHTs still make up a high percentage of total tests.

As explained in Section 2.1, GIIP calculations with MB are usually used in mature reservoirs with distinct depletion. This means that a certain percentage should have been recovered in order to make sure the measurements are reliable. Nevertheless, the depletion between the extrapolated pressures (p*) of shut-in period one and two from OHT and CHT in RAG are used for an initial guess in reserves. The pressure depletion in a test is used to affirm a high enough quantity of reserves to be economical enough for casing, in CHT they assist in the decision to build surface lines. Some error in GIIP determination is knowingly accepted because at such an early time even a vague estimation is valuable for derisking investiment decisions. The issues of pressure extrapolation have also been discussed in section 2.2.3.

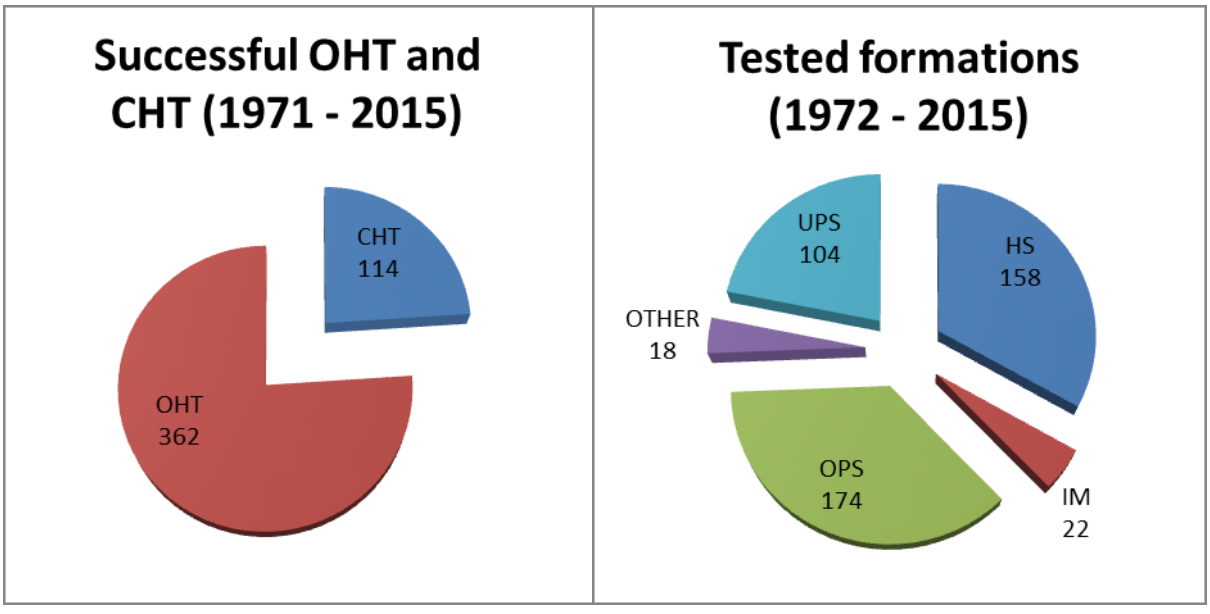

Figure 18: Analyzed OHT and CHT(left) (b) Tested formations (right)

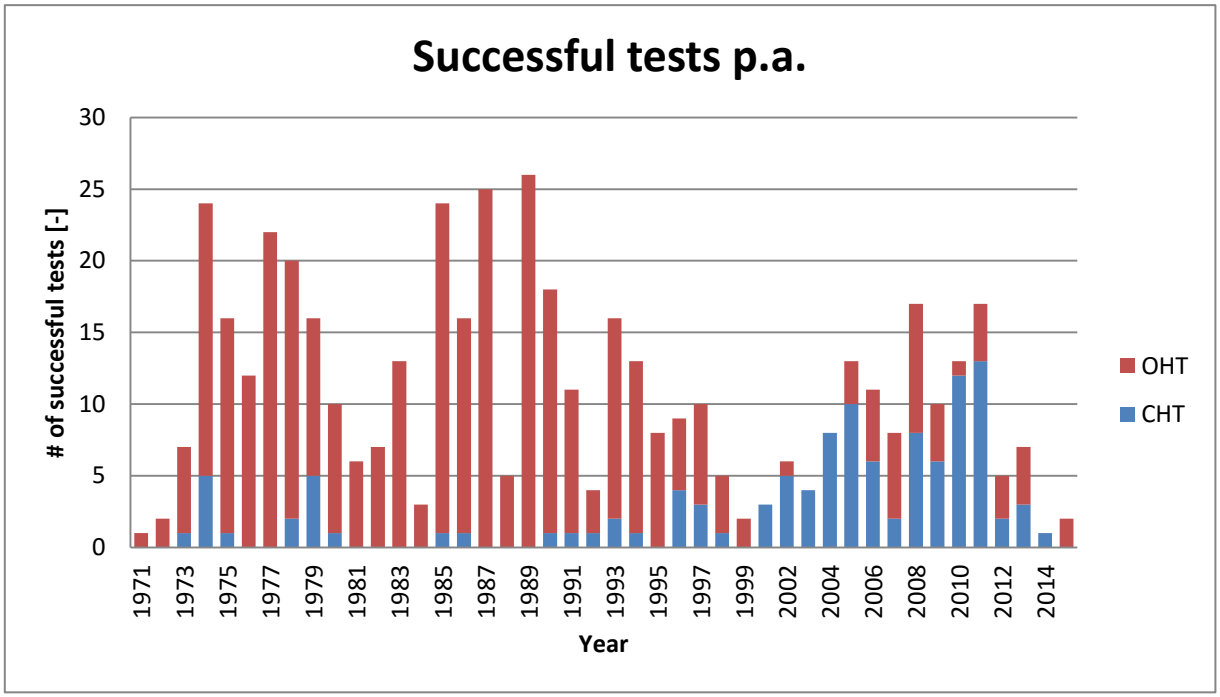

Figure 19: Yearly performed tests.

GIIP and Ultimate Recovery (UR) Estimation

Equation 3 in section 2.1 explain the calculation method and visual plot to estimate GIIP from depletion. Equation 3 is slightly reformulated for the usage of this calculation method with OHTs and CHTs to **eq.** 14:

$$G_{est} = \frac{\left(G_{p1} * \frac{p_2^*}{Z_2} - G_{p2} * \frac{p_1^*}{Z_1}\right)}{\left(\frac{p_2^*}{Z_2} - \frac{p_1^*}{Z_1}\right)} \tag{14}$$

G_{est}… estimate of GIIP at standard conditions [MMscm]

$p^*_{1,2}$… extrapolated and depth-converted pressures (from true vertical depth (TVD) at measurement to perforation mid-point TVD) in the shut-in periods [bara]

$Z_{1,2}$… real gas deviation factor at the respective pressures [-]

$G_{p1,2}$…cumulative gas production at time of respective pressure measurement [MMscm]

The ultimate recovery from a gas reservoir depends on the abandonment pressure of the reservoir, which itself is determined by the operating pressure of the surface gas transmission network [25, p. 489]. If available these pressures are used for the calculation of UR in **eq.** 15. If not, it is assumed that 85% of the calculated gas volume is producible [5, p. 36/3].

$$UR_{est} = \frac{\left(\frac{p_2^*}{Z_2} - \frac{p_{bp}}{Z_{bp}}\right) * \left(G - G_{p1+2}\right)}{\frac{p_2^*}{Z_2}} + G_{p1+2} \quad (15)$$

$$G_{p1+2} = G_{p1} + G_{p2}$$

UR_{est}… estimated ultimate recovery [MMscm]

p_{bp}… backpressure from surface lines [bara]

Z_{bp}… real gas deviation factor at backpressure [-]

G_{p1+2}… total produced gas in the production periods [MMscm]

Cumulative production

In order to compare apples with apples, in our case UR_{est} with a respective counterpart, the final production from a specific horizon has to include the total historic production and future production (forecast), specified in **eq.** 16.

$$UR = G_{prod} + G_{fc} \quad (16)$$

UR…cumulative production of a specific horizon [MMscm]

G_{prod}… cumulative produced gas of a specific horizon until 01.05.2015 (i.e. end of historic data) [MMscm]

G_{fc}…reserves (data according to the current production forecast) [MMscm]

Ratio of UR to UR_{est}

Equation 17 gives the ratio between the ultimate recovery to the first estimated value after OHT or CHT. If this ratio is above 1, more gas was produced than estimated, if the value is below 1, less gas was produced than estimated.

$$UR_{rel} = \frac{UR}{UR_{est}} \quad (17)$$

UR_{rel}… relative ultimate recovery [-]

For averaging purposes, i.e. per year, or per test method, a simple mathematical transformation is performed in **eq.** 18:

$$UR_{rel,log} = log_{10}(UR_{rel}) \quad (18)$$

$UR_{rel,log}$… logarithm of the base 10 from the relative Ultimate Recovery [-]

Values above 0 indicate a higher production than first estimate, i.e. 1 is equivalent to a 10-times higher UR than UR_{est}, below 0 is a lower UR than UR_{est}, e.i. -1 indicated 1/10 of UR_{est} is actually producible.

Of course, this ratio is valid only for those reservoirs, where the tested interval is consistent with the final perforation interval. This fact is examined for each test and included in the dataset (for all details see Appendix A), as well as considered in the statistics.

Boundaries and radius of investigation (R_{inv})

One of the greatest advantages of the derivative analysis is that boundaries exhibit a certain behavior and are, therefore, more easily quantified. The origin of the boundaries can vary and is discussed in detail in section 2.2.3. Table 2 gives a summary of the detected boundaries for various formations. For example, there are 84 tests in formation HS: 70 of those 84 tests can see one boundary, 54 detect two boundaries, 38 detect three boundaries, 11 are able to see four boundaries and six tests indicate a radial boundary. It has to be mentioned that only those tests are considered in this statistic, for which a Saphir® file exists (either done by a reservoir engineer or by the author). In total, 257 Saphir® files are available, 149 are analyzed by RAG reservoir engineers. Another 108 analyses have been done by the author, by manually typing in the pressure-gauge information to be able to analyze them in Saphir®. There are still 219 candidates left, where no digital information on the pressure behavior is available yet.

Table 2: Recognizable boundaries in the test analysis for each formation.

Formation	#	Boundary 1	Boundary 2	Boundary 3	Boundary 4	Radius
HS	84	70	54	38	11	6
IM	17	11	11	7	3	2
OPS	91	75	55	39	15	4
OTHER	12	8	8	6	5	3
UPS	53	43	35	21	4	4
Total	476	**207**	**163**	**111**	**38**	**19**

Radius of investigation is also calculated by Saphir® for the tests, and is evaluated for the others using **eq.** 19 (again in oil-field units). [6, p. 19]. The importance of this value is high, because it is especially needed in the NN applications in section 3.4.

$$r_{inv} = 0.029\sqrt{\frac{kt_{si}}{\mu\Phi c_t}} \tag{19}$$

r_{inv}…radius of investigation [ft]

Φ…porosity of the reservoir [-]

t_{si}…duration of shut-in [hr]

The internal calculation procedure of Saphir® for the parameters involved in the radius of investigation formula is not completely transparent and numerically complicated, therefore, **eq.** 19 [71, p. 4] is used and adapted to the Saphir® values by a multiplication with 0.915, accounting for any differences between the two approaches. For reasons of simplification, rock and water compressibility is ignored in the total compressibility, because gas compressibility is some orders of magnitude larger. Figure 20 shows the comparison of calculated and Saphir®-generated radii of investigation. The correlation coefficient of 0.9819 is very exact and the straightforward multiplication can, therefore, be used to obtain comparable values from both datasets.

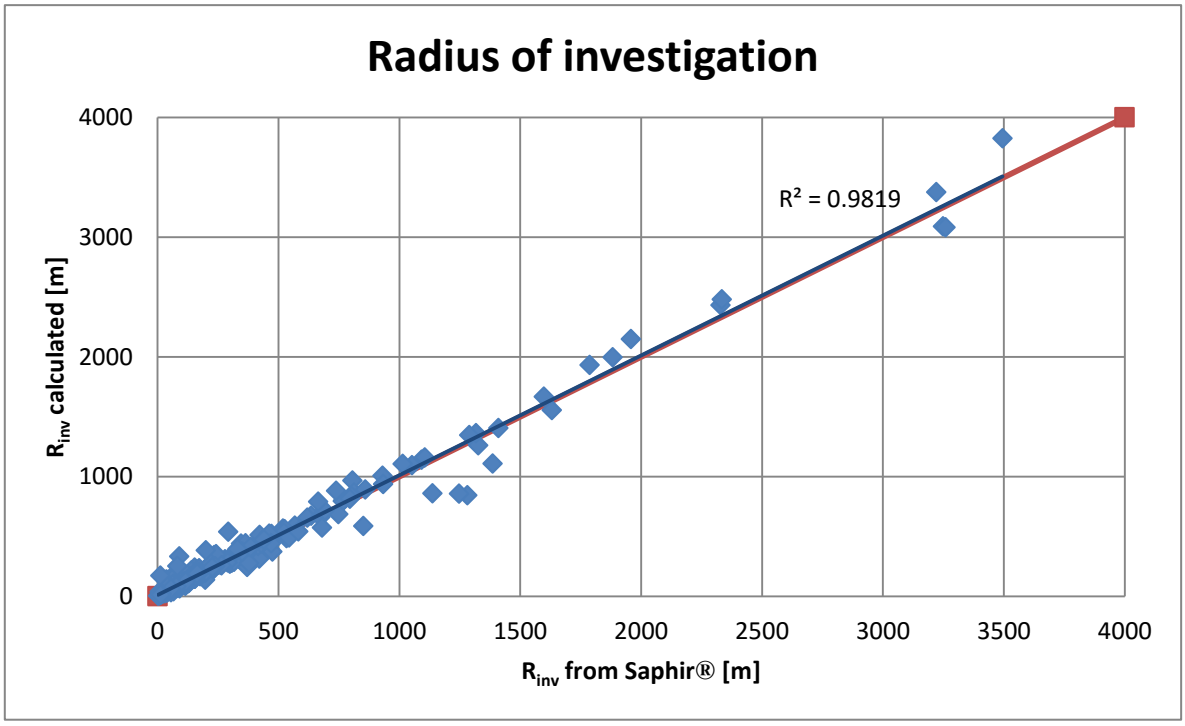

Figure 20: R_{inv} calculated by Saphir® versus the calculated R_{inv}.

3.3 Statistics and discussion

As described in section 3.1, the availability as well as the structure in data changed a lot over the years. The discrepancies arising due to this fact are often negligible, but some have impacts on the results and investigations, and are therefore discussed in section 3.3.1. Furthermore, sections 3.3.1 to 3.3.3 take a closer look at the data. Trends and features are discussed.

Figure 21 shows all performed tests as their ratio of UR to UR_{est}. This figure essentially shows two data clouds: The first cloud involves tests until 2000, the second involves the tests performed after 2000. Until 2000, the test data shows a trend of volumetric underestimation. After 2000, the data is less scattered and rather balanced in terms of over- and underestimation. One reason for this is the fact that gas from tighter regions connected to a reservoir will only be produced after a certain amount of pressure depletion – resembling the "reservoir compartmentalization" effect, which is explained in section 2.1.2. Therefore, the UR of older tests may include this "late-gas", whereas the UR from newer tests may not. Besides this fact, other reasons can be valid, discussed on the following pages.

3.3.1 Gas initially in place underestimation

Additionally some operational differences over the years have a high impact on the reserves estimation potential of the tests: The change in test procedure is reviewed in terms of underestimation of reserves. Overall, the structure of an OHT is kept constant: first flow and shut-in period followed by a second flow and shut-in period. Ideally, it is possible to recover

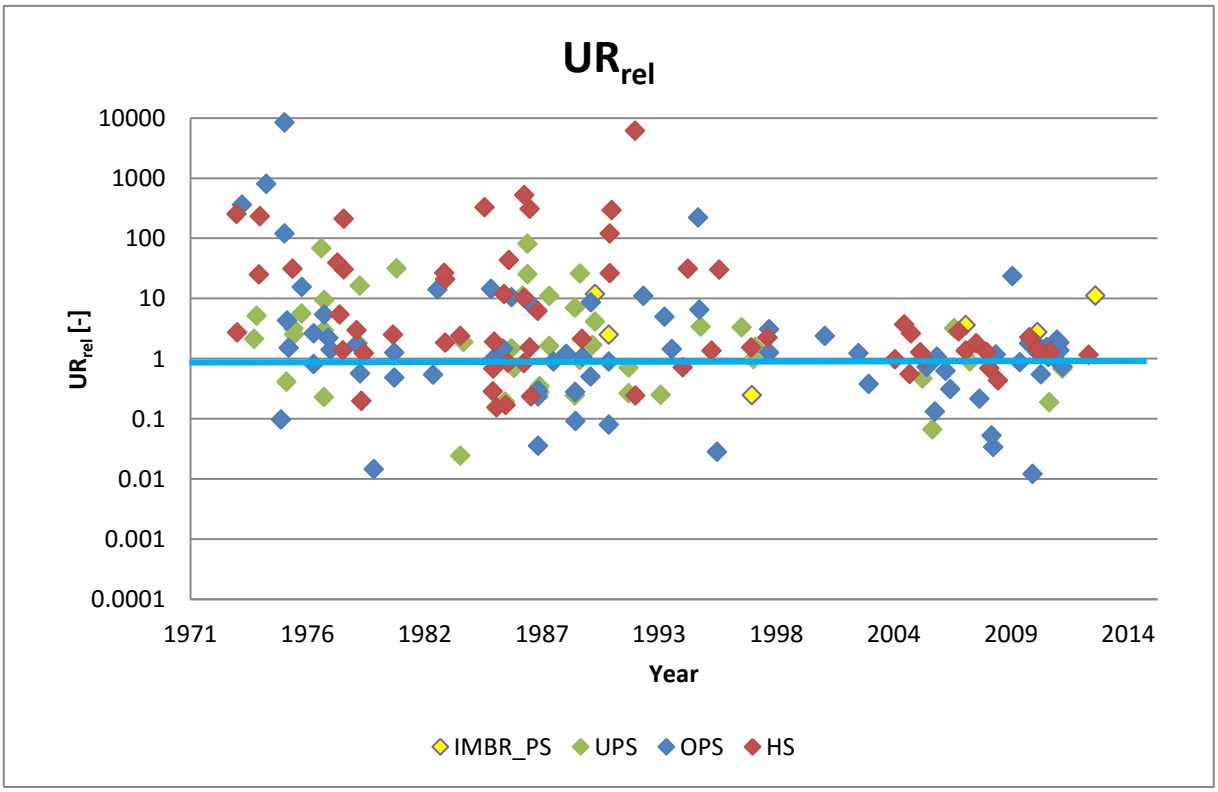

Figure 21: Ratio of ultimate recovery to estimated ultimate recovery.

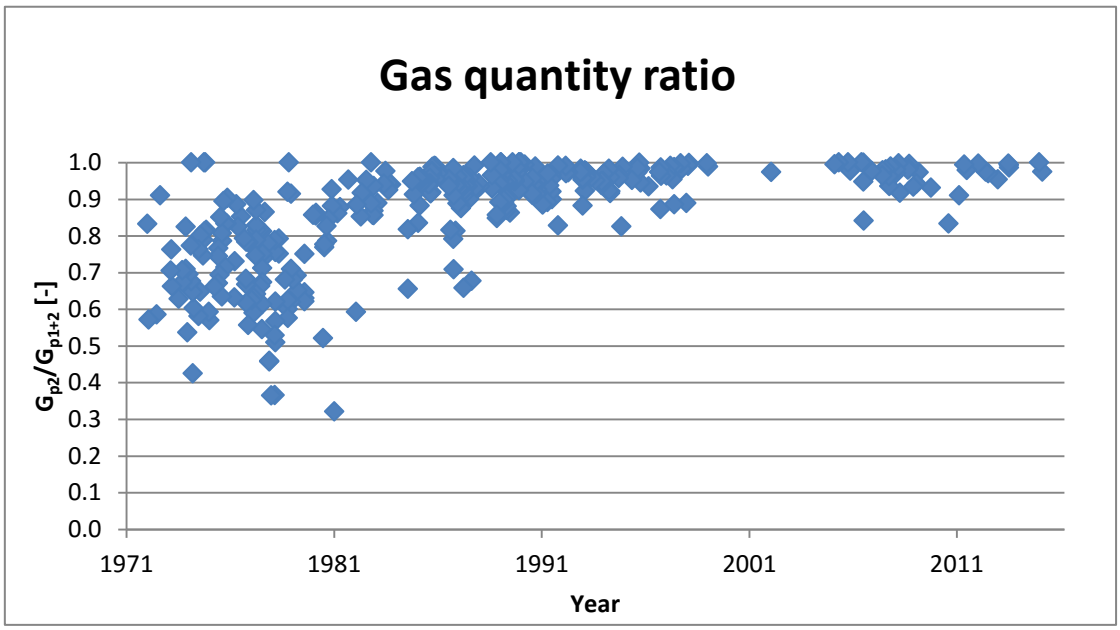

Figure 22: Produced gas at 2nd flow period to totally produced gas during the test.

two different (extrapolated) pressures with a significant production, and, therefore, depletion, in the second flow period. To achieve valuable results, the first flow period has to be kept short, as initial pressure conditions are meant to be discovered.

In reality these rules have not been followed consequently in the first decades of OHT performance. Figure 22 shows the ratio of produced gas during the second flow period to total production during the test. Adhering to the above stated rules means a ratio approximating 1. Of course, this fact has many consequences on the comparison of the tests. First of all, a high percentage of tests does not show any depletion, p^*_2 is higher than p^*_1, and does not allow for GIIP calculation. Other tests show a very high depletion due to incorrect pressure extrapolation.

Another perspective on the dataset is shown in Figure 23. The yearly average of the parameter $UR_{rel,\ log}$ is plot, which presents the dataset annually, being a great demonstration of the two features explained. On the one hand, operational issues lead to severe underestimation in reserves, on the other hand “late gas” leads to a general increase in UR. First and foremost, many huge reservoirs in channel systems have been discovered in these early years, where a first estimation of UR is simply unable to reflect the total reservoir size. These reasons lead to a higher average value of $UR_{rel,log}$ for the early decades.

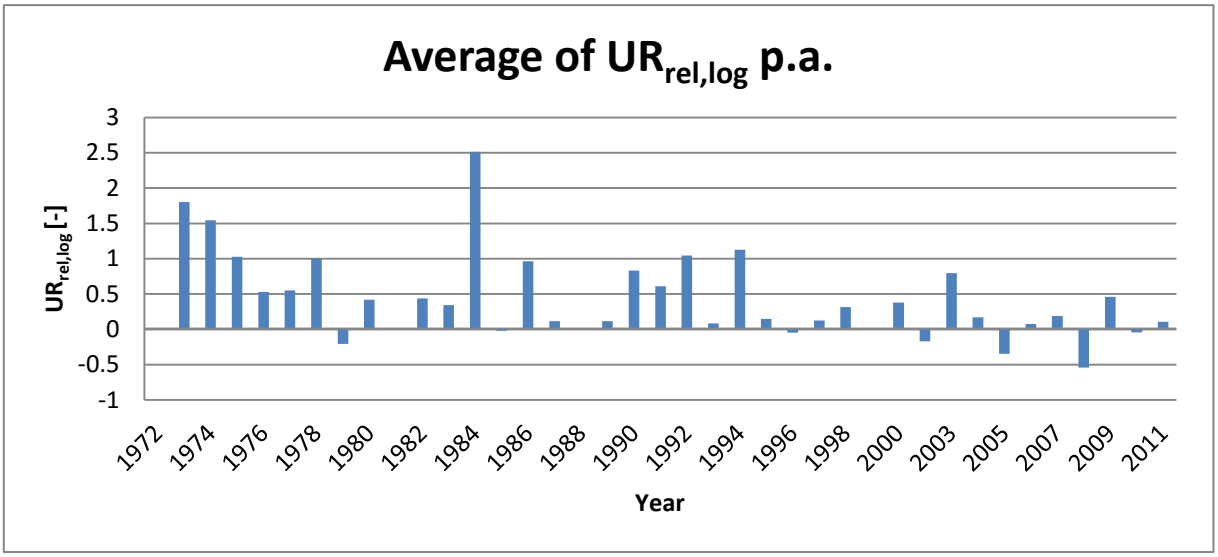

Figure 23: Average of $UR_{rel,\ log}$ per year.

3.3.2 Open-hole tests versus cased-hole tests

To compare the ability of GIIP prediction of CHTs and OHTs, the parameter $UR_{rel,log}$ is plotted in various forms. For all successful tests, the average of this parameter is plotted in Figure 24. For both, OHT and CHT, the average is greater than zero, meaning that in average the tests underestimate the reservoirs' extents. Although this does not tell us anything about the relative size of these reservoirs, it is a measure of the exactness of the prediction. Furthermore Figure 24 suggests that there is a significant difference between the predictability of reservoirs, depending highly on the type of test.

For a better understanding of the data the next step is to define various intervals for ultimate recovery. The dataset is split into very small reservoirs (up to 5 MMscm), small to medium reservoirs (5 to 25 MMscm) and medium to large reservoirs (above 25 MMscm). The average of parameter $UR_{rel,log}$ is plotted per test species and per interval.

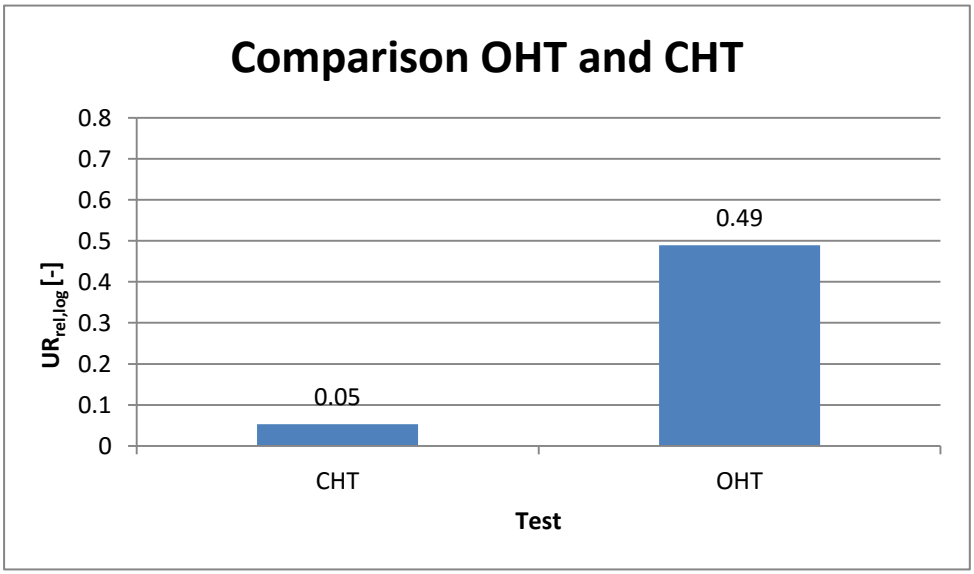

Figure 24: Comparison OHT and CHT

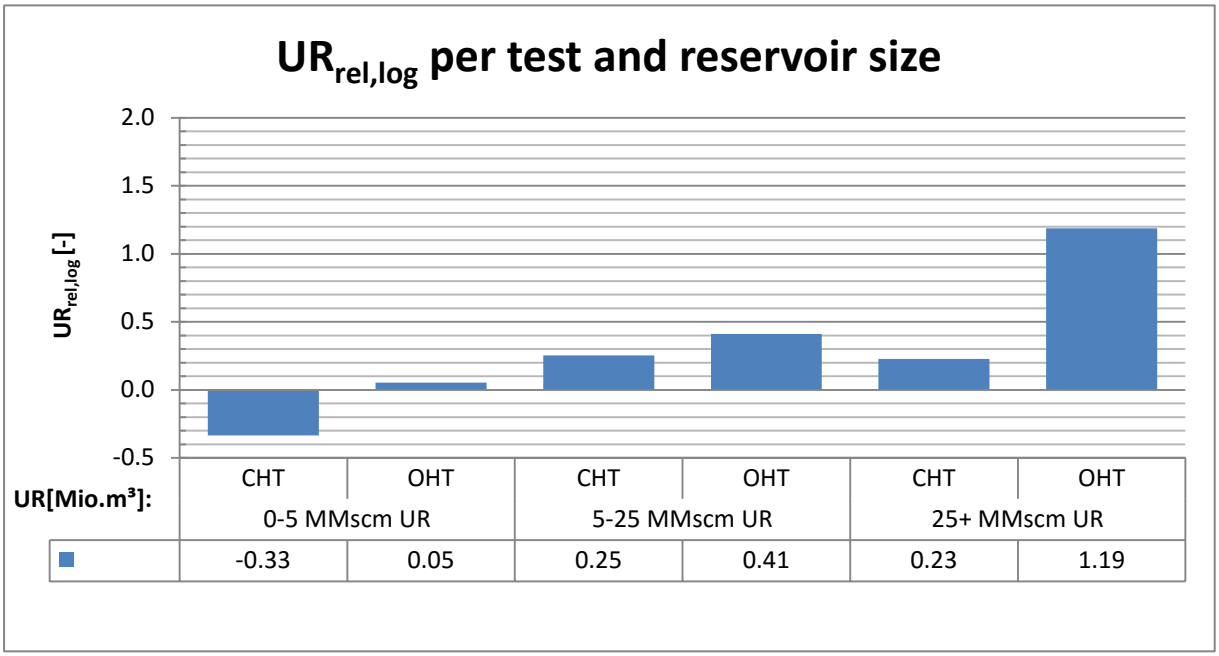

Figure 25: $UR_{rel,log}$ per test and reservoir size

Figure 25 shows that in all ranges, OHT shows a higher underestimation of reserves compared to the CHT. Moreover it shows that underestimation of GIIP grows with reservoir size. It is suspected that compartmentalization is a reason for that, as commented a few pages above: Accepting compartmentalization as a common feature in the geological play that is under analysis, it obviously is more likely that a well is not connected to the complete volume if the reservoir is large.

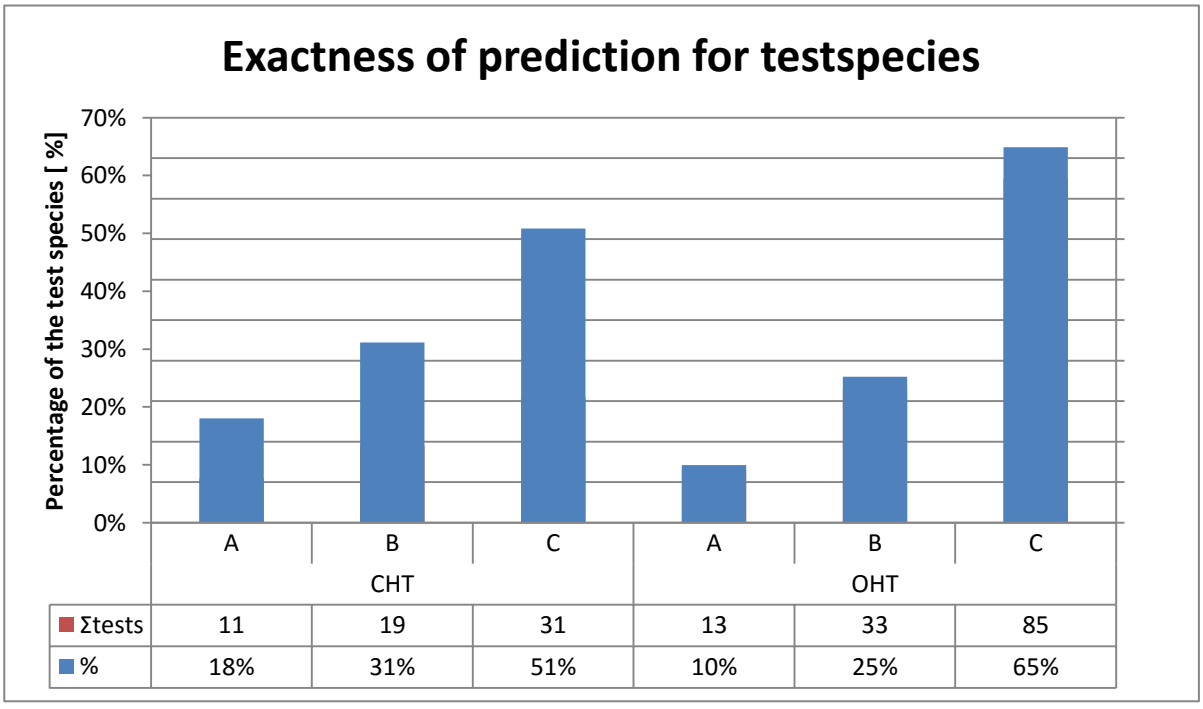

Figure 26: A, B and C are ranges for UR_{rel}: A is for values between 0.75 and 1.25; B is for values below 0.75; C is for values beyond 1.25.

Another insight into the dataset can be gained from Figure 26. UR_{rel} is used to categorize the tests. As explained, values above 1 indicate an underestimation, values below 1 show an overestimation of reserves.

UR_{rel} is categorized: “A” is defined as a value of 0.75 to 1.25, which is a relatively exact estimate, allowing for both an over- and underestimation of 25%. “B” involves all severe underestimates (0.75 and smaller) and “C” includes all overestimates above a value of 1.25. Figure 26 shows that for both test species two trends are obvious: Firstly, very few tests fall into group “A”. Only 18% of CHT fall into the category, but for OHTs the percentage is even smaller. Secondly, far more reservoirs are underestimated than overestimated – 51% of CHTs and 65% of OHTs.

Figure 27 displays the same variable (number of tests falling in respective UR_{rel} ranges), further refined in the ranges of UR (likewise to Figure 25). Very small and small reservoirs show a high overestimation as well as underestimation in reserves. The reason for this result can lie in the problems related with boundary-dominated flow, which leads to exponential behavior in the semi-log plot and can result in either an over- or underestimation in reserves (this example is illustrated in section 4.1.3). Also this figure presents the general trend that almost no test results lie in the “acceptable” range of uncertainty (“A”), with the exception of CHT in large reservoirs. The test duration and possibility to lower the reservoir pressure significantly enough in order to achieve good results is one explanation for this outcome.

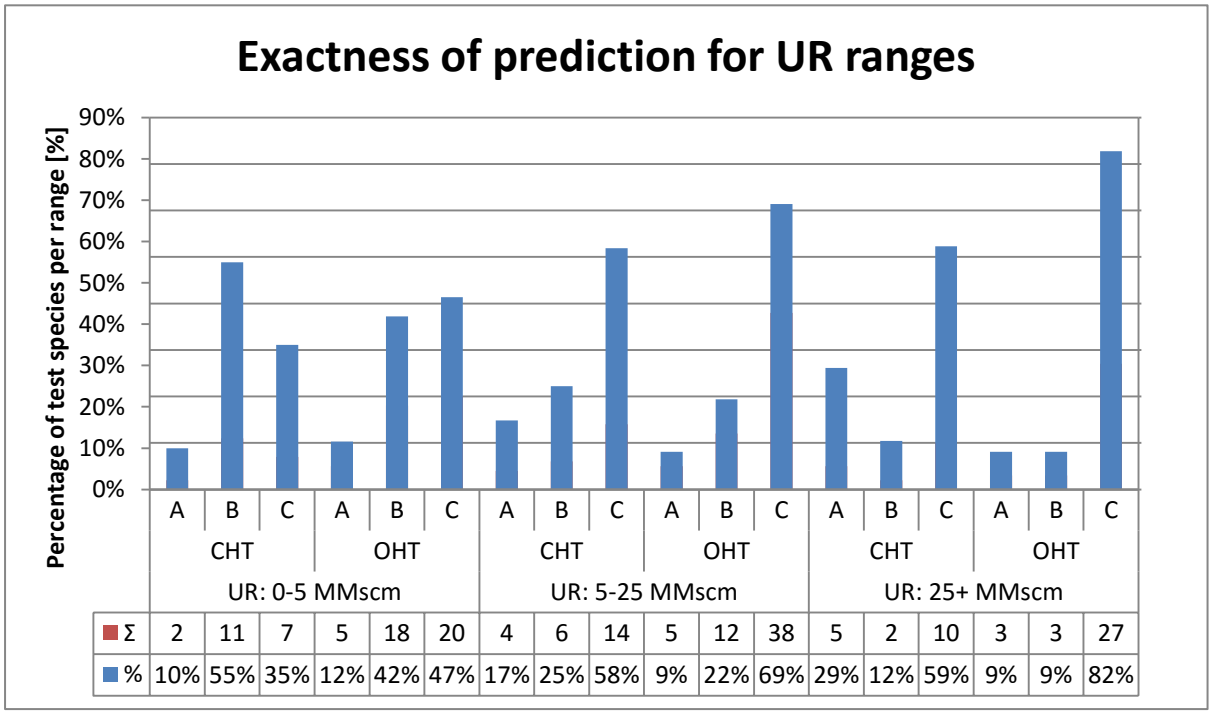

Figure 27: A, B and C are ranges for UR_{rel}: A is for values between 0.75 and 1.25; B is for values below 0.75; C is for values beyond 1.25. A is, therefore, an acceptable prediction, B predicts a higher volume than could ultimately be produced; C predicts a lower volume than ultimately producible.

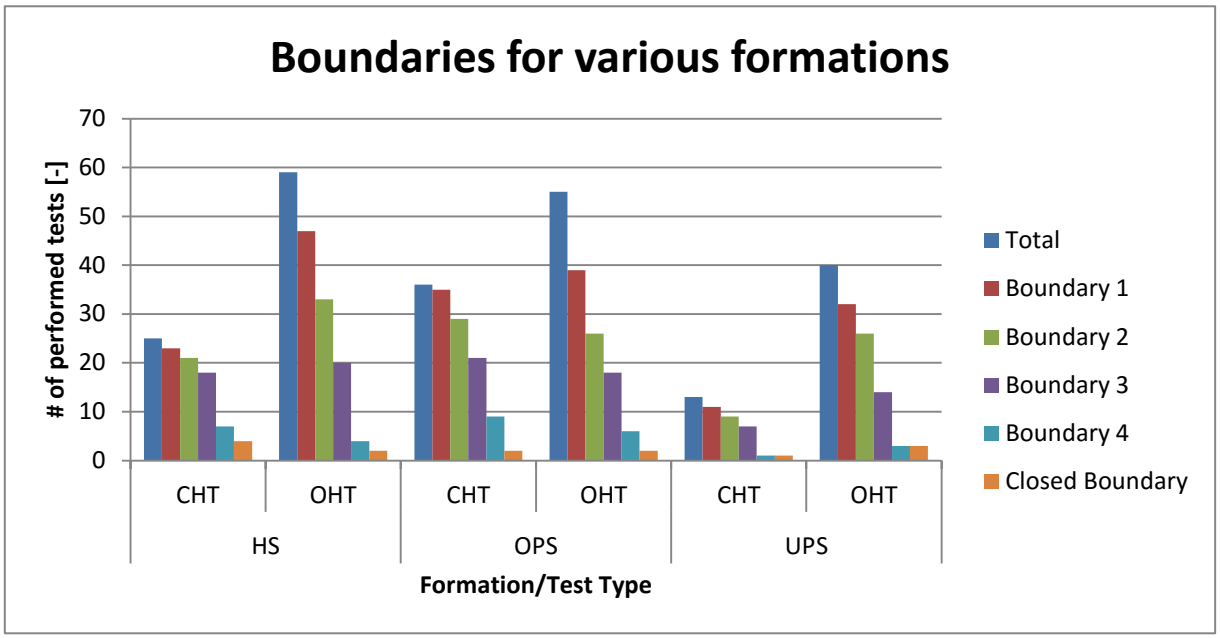

Figure 28: Boundaries for various formations sorted for OHT and CHT.

3.3.3 Boundaries

Figure 28 gives a detailed comparison between the Saphir®-analysed tests and the encountered boundaries. It is illustrated that almost all CHTs discover at least one boundary (blue bar stands for the number of tests, red bar for the number of tests encountering one boundary), compared to a smaller percentage for OHTs. Obviously, due to the limited time for the flow and shut-in periods, and consequently a shorter radius of investigation, OHTs are not always able to reach the limits of a reservoir. Inspecting the data in more detail (Figure 29) the question arises, why OHTs encounter boundaries much closer to the wellbore than CHTs. The dataset used for Figure 29 includes only those tests, where the reservoirs have a

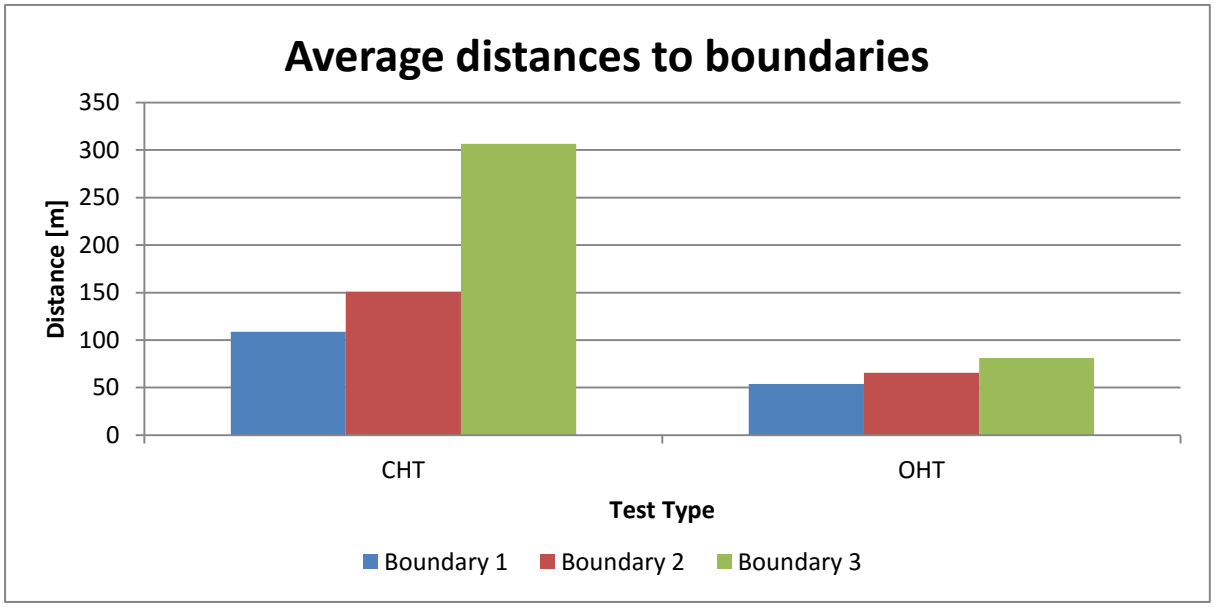

Figure 29: Average Distances to Boundaries.

minimum ultimate recovery (UR) of 3 MMscm, which excludes the assumption that OHTs test more reservoirs with smaller volumes. One explanation for this behavior is the determination of rates, which is less exact in OHTs than in CHTs. So, if the rate in an analysis of an OHT is too high at shut-in due to averaging, the permeability is too high, and the boundaries are projected as being closer to the well.

3.4 Application of neural networks

In sections 3.1 to 3.3 the data gathering and processing is discribed, as well as some statistics are presented, which allow for a first evaluation of the presented dataset. The ultimate goal for the following revision is to find numerical relationships within the data and project it on the estimation of UR.

As already stated in section 2.4, NN should only be used, if conventional methods are too time consuming or prone to fail. According to Mohaghegh, historical databases inherit the ability to solve problems, and have valuable and relevant information, which can be fed into neural networks to find a solution to complex problems [68, p. 68]. A neural network may work better, if the mathematical inter-correlation of parameters is too complex to be solved with mathematical models, as it finds correlations between parameters to model an output. This approach is output oriented rather than a correct mirror of predefined physics and geology.

GIIP calculation in the earliest development phase of a well only takes into account the (visible) depletion according to the extrapolated pressures on the Horner plot (described in section 2.2.3). Unfortunately, this method is not valid for many conditions, especially in boundary dominated flow. The foundation for application of a NN for GIIP calculation builds on the idea that the input of all investigated parameters (discussed in section 3.2) like boundaries and geological sequence additional to the pressures is more able to predict the ultimate recovery, which so often differs from the initial GIIP estimation. In the following section, the dataset is conditioned and the NN is built.

3.4.1 Validation Criteria

Like every real dataset, also in this case outliers and gaps exist. Concerning outliers, neural networks are able to handle them – which makes them so popular and powerful. Gaps in the information, however, are an issue. This is illustrated in Figure 30. The input data in columns

	A	B	C	D	E	F	G
1	#	Input1	Input2	Input3	Output	vc:F:FC (e1)	vc:OD:output
2	1	3	2	3	8	L	8
3	2	2	2	3	7	L	7
4	3	4	5	2	11	L	11
5	4	3	3	0	6	L	6
6	5	1	4	4	9	T	9
7	6	2	8	2		F	12
8	6	6	0	7	13	V	13
9	7	1	3	3	7	L	7
10	8	2	4	2	8	V	8
11	9			3	3		
12	10		2		2		
13							

Figure 30: Data read-in procedure for neural network application with cVision®.

B, C and D is added up to achieve the output data in column E. The neural network is fed with the input data, and the output data is also presented to the network for the training dataset (but is not a necessary input for each dataset). The neural network creates its internal connections in such a way that it is able to find the output itself for datasets, which miss an output (like set #7: 2+8+2=12). But the point is that even if the calculation procedure is the same in the datasets #9 and #10, the datasets are ignored because of gaps in the input data.

In the OHT and CHT dataset gaps exist due to various reasons:

- Missing values:

Some values are missing, because a test was performed differently (only one shut-in phase), some are not reported and lost. Every effort is taken to find a replacement, where none can be found, the data-set has to be ommitted by the network.

- GIIP calculation:

If the second extrapolated pressure is not lower than the first, the procedure explained in Section 3.2 can not be used for GIIP calculation. There is no simple solution to these missing values. If the GIIP is used as a network input, the tests are ignored by the NN.

- Boundaries:

LTR reactions in a derivative plot can have many reasons. In order to be able to set up a NN, the reactions are combined in boundary values. They can be classified as one per cardinal direction or can be radial, which resembles equal distance to each direction. A boundary in each direction results in a closed system. Obviously, in many cases the test will not see the boundaries of a reservoir, depending on the duration, reservoir properties and the distance to the boundary. Therefore some datasets “miss” these inputs. Another issue is that for several tests, no derivative analysis could be done because the pressures are not digitized. These tests, therefore, do not have values for boundaries, even if they were present. The solution to these gaps is proposed in two ways: For the first issue, if only one or two directions encounter boundaries, the other values are filled with the “radius of investigation” from Saphir® (the calculation procedure is explained in section 3.2). This approach is chosen, because boundaries at or beyond the distance of radius of investigation to the measurement point are limiting the reservoir, but do not change the derivative curve and the interpretation of extrapolated pressures. For the second problem, either the datasets have to be ignored, or the same approach is chosen. Choosing the approach of “filling” the missing values one has to be careful, as in reality the boundaries could be completely different.

- Perforation interval:

cVision® provides an error norm, which is error insensitive and outlier resistant [72]. Nevertheless, a certain category of outliers has to be removed from the dataset manually: If

a horizon is tested in a different interval than produced, the data cannot be accepted. This happens, if several intervals are additionally opened to production, but the reservoir identifier within the RAG data systems stayed the same. These tests, therefore, do not resemble the later-on produced horizons. All tests with this characteristic are excluded for the usage of neural networks.

3.4.2 Analysis

Different setups are chosen in terms of input parameters, the details are explained in the Appendix. The NN configuration is the same for all simulations. The architecture is explained in section 2.4.1, containing from 0 up to 10 neurons. The error norm is insensitive, allowing for outliners. The basic setup from cVision® is generally retained. It has been found that the natural logarithm of the final ultimate recovery as output is more comprehensive for the NN in the matching process.

Average errors for the simulations are presented in the Appendix. But not only the average values are important, also a visual depiction helps in categorizing the final solutions: On the one hand, the average error of the validation dataset to the provided output is calculated, on the other hand the same chart as in Figure 21 is created calculating the ratio of UR to the NN output, instead of UR_{est}.

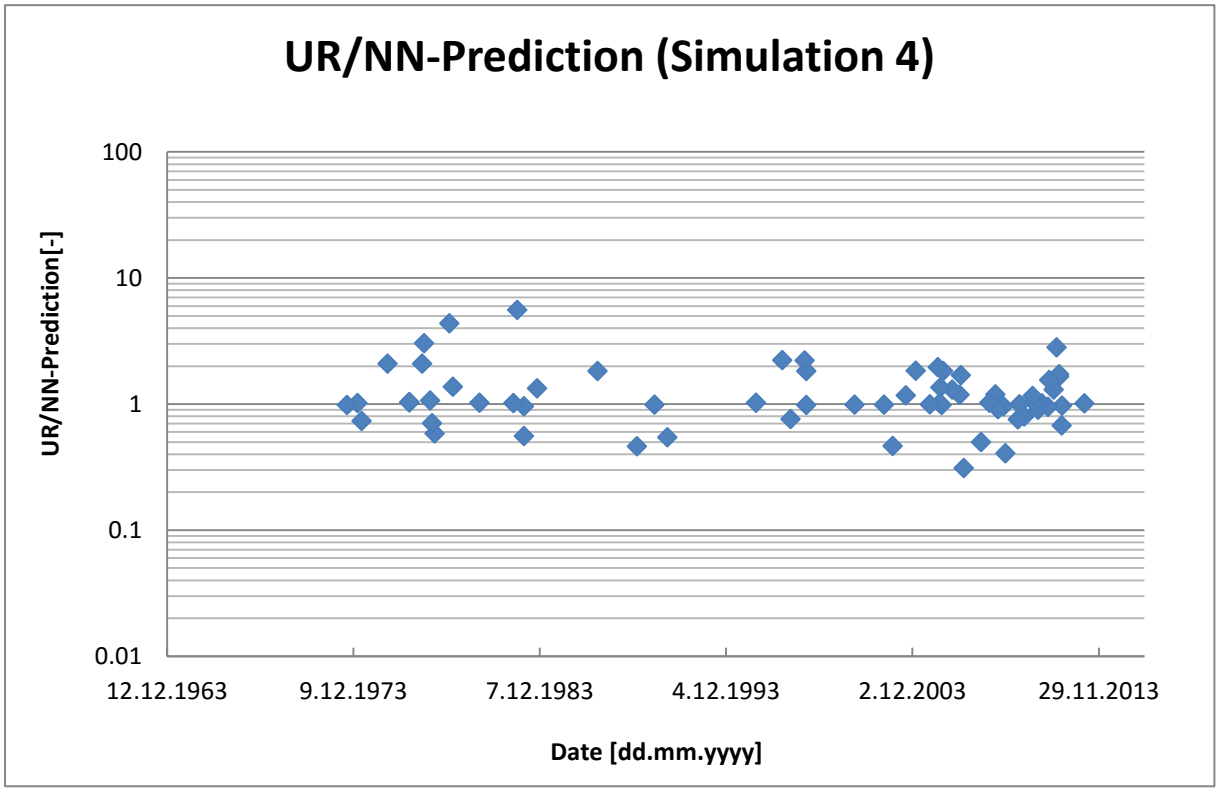

Figure 31: Visual outcome of simulation 4.

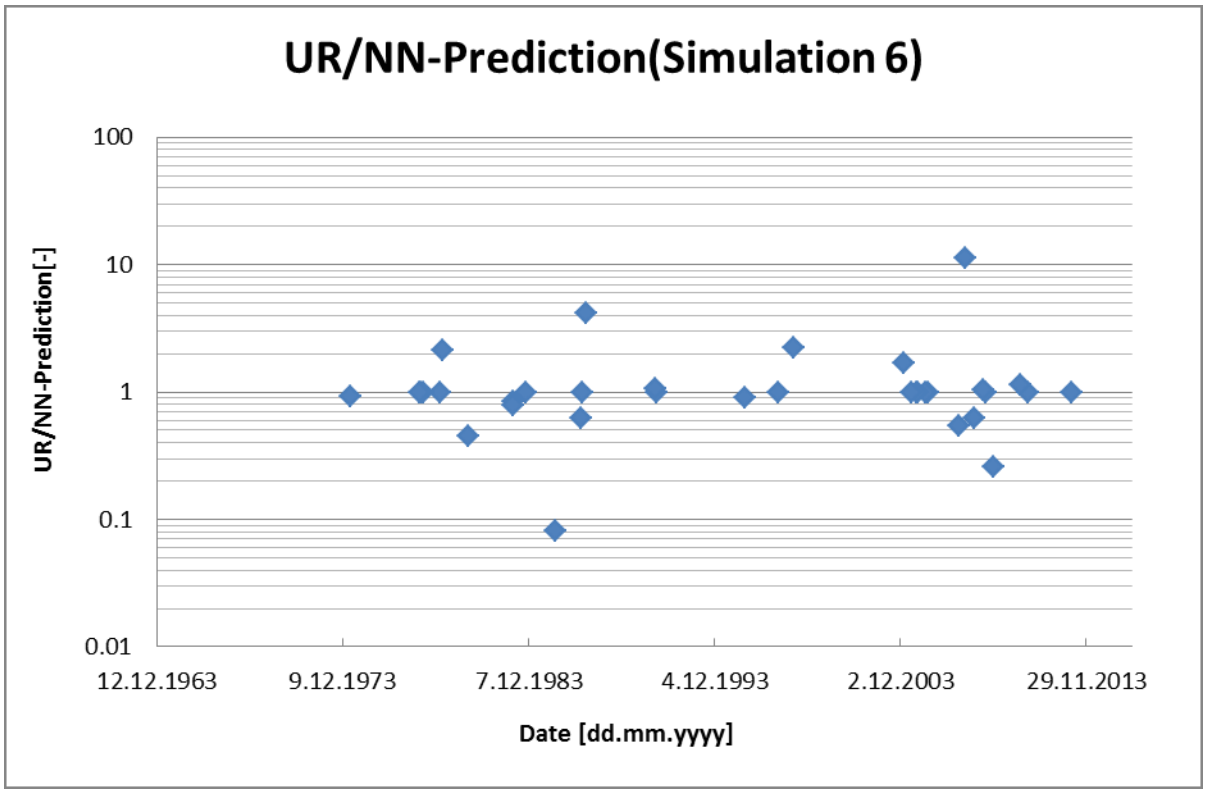

Figure 32: Visual outcome of simulation 6.

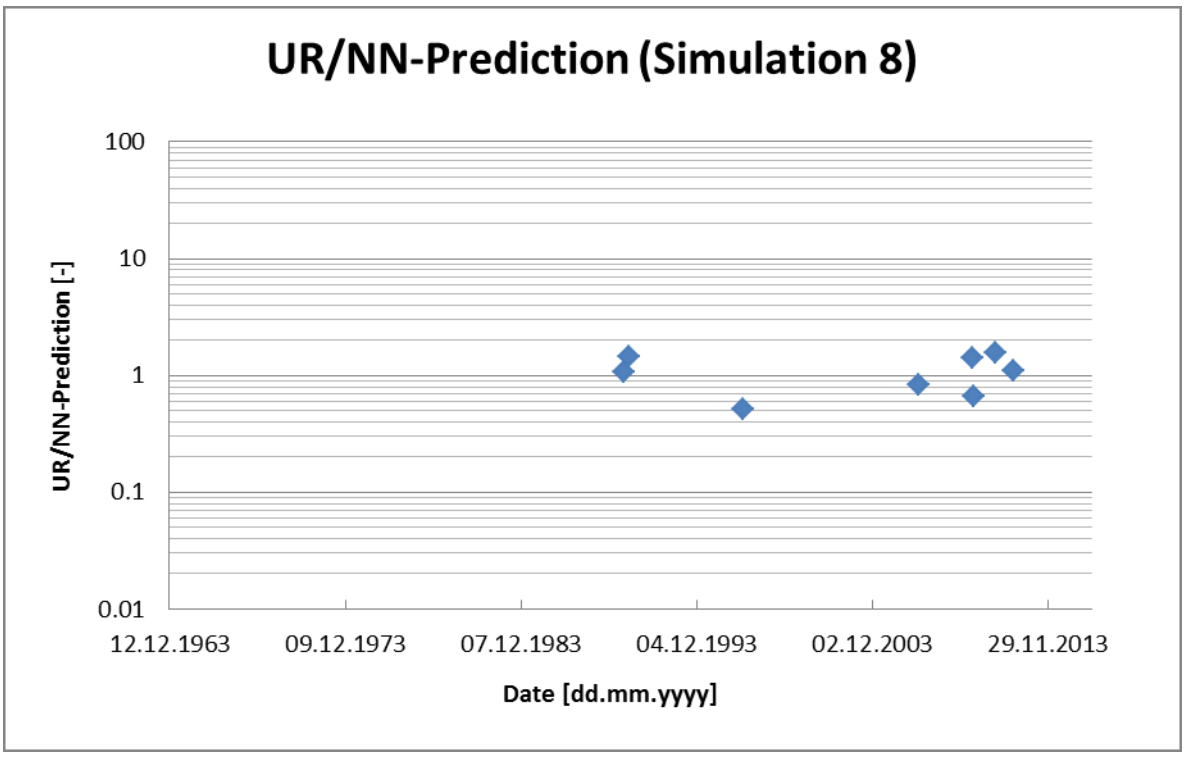

Figure 33: Visual outcome of simulation 8.

The sample size ranges from 13 to 294. The setups vary in boundary inclusion, formation, UR range and date of conduction. Boundaries have shown to improve the results, and all simulations, but “1”, include them. Most NN setups show unsatisfying results. The only three exceptions are the numbers “4”, “6” and “8”. Compared to Figure 21 the outcomes of the NN are much more exact than the GIIP calculation using MB.

In simulation 4, only the reservoirs which show an UR of more than 5 MMscm are included. It seems that these reservoirs are very similar in terms of GIIP calculation versus production, and the characteristics can be compared very well (Figure 31).

Simulations 6 and 8 only include the datasets of the same formations. “6” is relating the Hall formation reservoirs (Figure 32), “8” models the imbricated Molasse reservoirs (Figure 33). Simulation for other formations showed very poor numerical relations, but these two show the highest potential.

3.4.3 Results

A NN is per definition able to find numerical relationships between the input data and the output data. In the best case, the NN could be able to improve and meet all outcomes, finding various connections for the different situations. In our case, a success would prerequisite the provided input data (including reservoir parameters, the production and pressure conditions during the test and the production period and surface pressures) and the output (UR) to be related in very similar manners.

This would require that the same, optimum conditions prevail in the test and the production period. The changes in the test procedures are discussed in section 3.2 and 3.3. Outcomes of the OHTs vary a lot in terms of the usability of this data. Missing boundaries for many tests limit the included datasets to numbers, which are actually not acceptable for the NN configuration with such a high number on inputs. The values of UR are questionable, because the forecasts are included and involve uncertainties as well.

But not only can these details be stumble stones for a NN to work properly. The results for the different formations show that some can be numerically related, others cannot. It could be suspected that CHTs can be better interrelated than OHTs, but results show, that even CHTs are very poorly connected.

The reason for the poor relatedness even in optimum conditions is non-uniqueness and its consequences on the GIIP, as discussed in detail in section 2.2.3. The addition of further datasets will create more assurance, both in the well-working and malfunctioning cases.

4 Numerical modelling of well tests

Although a range of analytical models are available in commercial PTA software, realistic modelling is still restricted and the result of an analytical model lacks in terms of vividness. An example is a simple shale-out with decreasing permeability. This cannot be modelled analytically - the only approximation is a radial-composite reservoir, offering to model a variation in mobility. A pinch-out, which resembles a gradual decrease in reservoir thickness, cannot be integrated in an analytical model. Another important consideration is the ability to model the pressure history of a test, considering the complete sequence and not only the matched build-up. Analytical models often fail to deliver acceptable matches in terms of pressure depletion.

To address the challenges of PTA pointed out in section 2.2.3, the usage of numerical models is the method of choice. Numerical modelling in conjunction with analytical modelling has been widely used to confirm geological features and detect sub-seismic faults [17, p. 4]. Others have used WT results to adjust the geostatistically generated geological model [10], or vice-versa – used the simulation model and geological or geophysical input to interpret a well test [13, 15, 16].

For this thesis different models are created in Petrel® and Eclipse100®, as well as in Saphir® for different purposes and are presented in various examples.

A numerical model in Petrel®, simulated with Eclipse 100®, illustrates non-uniqueness and its consequences on GIIP determination using the extrapolation of pressures on the Horner plot. The simulation outcomes will also be used for the NN in chapter 4.1.4.

Saphir® from the Ecrin®-suite is the standard program for WT interpretation in RAG. Along with the traditional interpretation techniques, the software provides a numerical simulation tool. The functionality is presented, and a workflow for future usage is provided.

A discussion on the advantages and challenges for the different tools is also provided.

4.1 Numerical modelling with Petrel®

4.1.1 Simulation setup

For simulation purposes, a very simple numerical model is created with Petrel®. First of all, the model has to be large enough to allow for boundary variations. Secondly, the wellbore-grid-block has to be small enough to reach equilibrium conditions within short time-steps. Using a Cartesian grid, these two requirements result in a vast amount of grid cells. To realize short simulation times, therefore, a tartan grid is chosen. As can be seen in Figure 34, this tartan grid has small grid cells in the centre of the model, with grid cell dimensions increasing logarithmically away from the wellbore. Table 3 provides an overview of the fundamental parameters for the grid.

Table 3: Parameters for the simulation grid setup.

Parameter	**Value**
Number of grid cells in x-, y-, z-direction	81 x 81 x 10
Grid size [m]	10000 x 10000 x 10
Gas gravity, γ_g [-]	0.565
Irreducible water saturation, S_{wi} [-]	0.30
Initial pressure, p_i [bara]	100
Temperature, T [°K]	213.15
Porosity, Φ [-]	0.12
Vertical permeability [mD]	40
Horizontal permeability [mD]	4
Skin factor, S [-]	0

As an OHT as well as CHT is limited in terms of time, variations in the durations of flow- and shut-in-period are simulated to resemble realistic test procedures (Table 4).

Table 4: Test procedures.

	Test Type	
Parameter	**OHT**	**CHT**
Gas flow-rate, q_g [Sm³/day]	105000	105000
Duration of production, t_p [hr]	4	8
Total gas production, G_p [m³]	17500	35000
Time of shut-in, t_{si} [hr]	6	304

In total, more than 200 simulations are performed. The aim is to simulate a variety of different geometries and boundary conditions for the different tests. The simulation outcomes are then loaded into Saphir® to visualize the resulting derivative plot and perform a linear pressure extrapolation. The findings are presented in this section, a NN application is explained in section 4.1.4.

The geometries under inspection are those, which exhibit a certain boundary effect encountered very often in RAG reservoirs. This effect is visible in the derivative curve as a steep slope in the LTR. The origins of such a behaviour are discussed in section 2.2.3. According to the proposed geological model (section 2.3), the suggested analytical solution is often a two- or three-sided channel [49, p. 2, 73], or even meandering channels [9, p. 5]. Therefore, the geometries in Figure 34 are the fundamental setups for the simulations. The colors in this figure indicate different permeabilities.

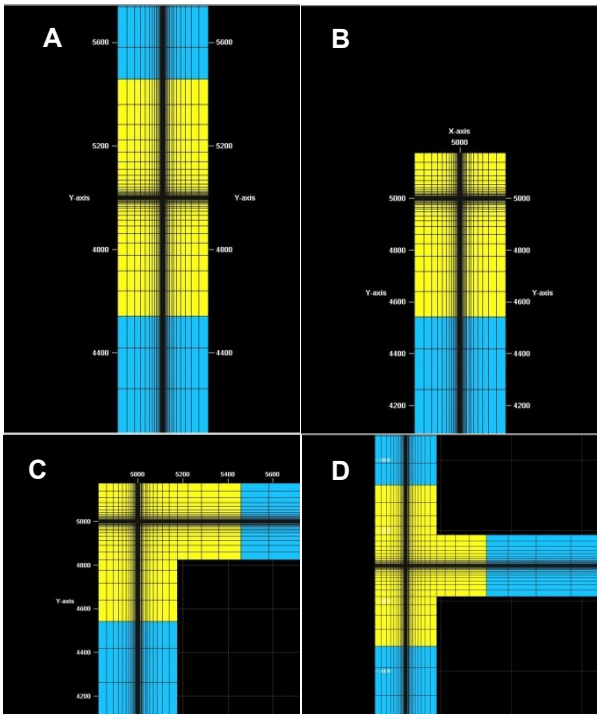

Figure 34: Different geometries as input for simulations

Table 5 gives an overview of the different geometries and volumes of the reservoirs. In order to be able to compare the GIIP from the pressure extrapolation with the real GIIP, G_{model}, the value has to be calculated using the volumetric approach defined in **eq**. 20 (metric units):

$$G_{model} = \frac{A * h * \Phi * (1 - S_{wi})}{B_{gi}} \tag{20}$$

G_{model}… gas in place in the model [MMscm]

A…areal extent of the reservoir [m²]

h…reservoir height [m]

S_{wi}… initial water saturation [-]

B_{gi}…gas formation volume factor $\left[\frac{Rm^3}{Sm^3}\right]$

The volumes are not randomly chosen, but adjusted to the average producible volumes of RAG reservoirs. From the statistics it is found that the tested formations show an average UR_{final} of 36.71 MMscm giving a GIIP of about 44 MMscm assuming a recovery factor of 85%.

Table 5: Geometries and volumes.

	A	**B**	**C**	**D**
Channel Width [m]	319.13	319.13	319.13	319.13
Channel Length [m]	10000	5159.57	5159.57	10000
Volume, G_{model} [MMscm]	29.59	15.32	29.59	43.86

4.1.2 Workflow

The test procedure, as well as the geometries of the reservoirs is explained in section 4.1.1. For the different simulations, changes in the geometries are also accompanied with changes in the permeability at several distances to resemble a shale-out. Figure 34 shows a change in permeability at a distance of approximately 400 m from the wellbore. Furthermore, faults are inserted at varying distances.

Eclipse® is used for simulation purposes and the outputs are extracted from the .RSM-files. For the MB calculation, the following values are reported with 6-minute time steps:

- Gas production rates and total gas production
- Field pressure of the model and bottom-hole pressures of the well

Field pressures are calculated by the simulator through MB, and resemble the real average drainage volume pressures. They are used to verify the volumes calculated with **eq**. 14 and justify the MBE. Initial pressure and final output of this field pressure, as well as the total produced volume, are inserted in **eq**. 14 (Section 3.2).

The bottom-hole pressures show a transient build-up behavior, because of the small grid cell size. The main difference to a real pressure measurement is the recording frequency: Whereas modern pressure gauges are able to record pressures every few seconds, the reporting frequency of the simulation is ten per hour. This interval is chosen, because the focus lies on the LTR of the derivative curve. As the plot is logarithmic, the large time intervals still produce acceptable results. For the shut-in period, the pressure is extrapolated to p* and used in **eq**. 14 to calculate the discovered GIIP, G_{disc}, in MMscm.

4.1.3 Results and conclusions

Numerous different simulation cases can be reviewed with relative simple changes. The most important findings are presented in the following scenarios.

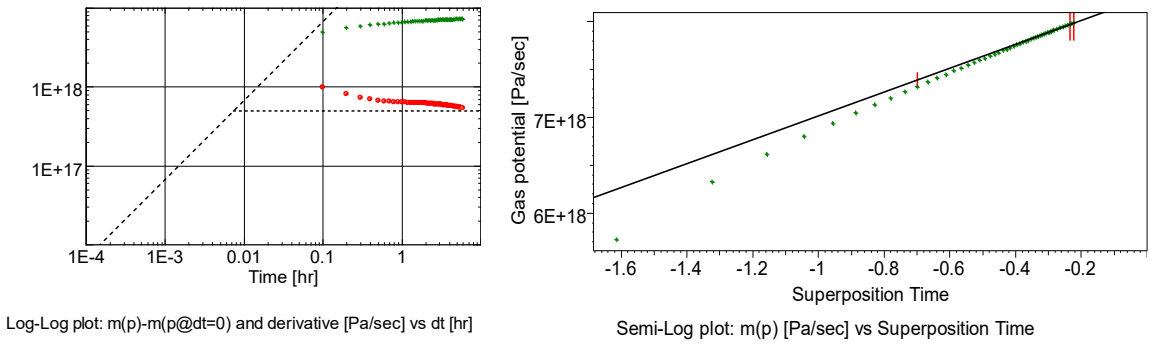

Figure 35: OHT simulation in geometry A.

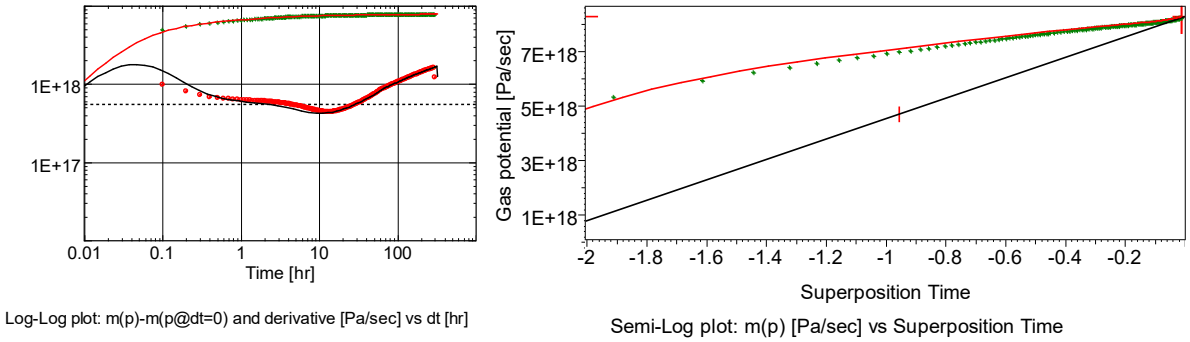

Figure 36: CHT simulation of geometry A.

Illustration 1 – Comparison of OHT and CHT

As explained, the simulated reservoirs resemble average reservoirs in terms of size and geological features. The main difference in the outcomes for the simulated OHT and CHT is that the boundaries cannot be seen on the derivative of the OHT at all. The reason is a shorter duration, hence a smaller radius of investigation.

As an example, Figure 35 and Figure 36 show the different log-log and semi-log plots for OHT and CHT in the reservoir geometry A. Performing the approach explained above clearly shows that a usual test duration in the standard geometries will not be able to yield G_{model}. The percentage of GIIP that can be seen through the extrapolation of pressures is given in Table 6.

Reviewing the results in Table 6, an interesting discovery becomes obvious: Although the duration of the final shut-in of a CHT is 304 hours and, therefore, 50-times the duration of an OHT, the outcomes are not so much more precise. In fact, only 35 – 40% of G_{model} can be discovered, the OHT discovers between 20-27% of the volume. The short radius of investigation, and the consequence of a restricted possibility of a build-up test to reach equilibrium is the downfall of reserves estimation.

Table 6: Percentage of detected GIIP vs. real GIIP.

	OHT	**CHT**
G_{model} for geometry A [MMscm]	29.59	29.59
G_{disc} for geometry A [MMMscm]	6.26	11.49
G_{disc}/G_{model} for geometry A	21.25%	38.86%
G_{model} for geometry B [MMscm]	15.32	15.32
G_{disc} for geometry B [MMscm]	4.22	5.39
G_{disc}/G_{model} for geometry B	27.61%	35.20%
G_{model} for geometry C [MMscm]	29.59	29.59
G_{disc} for geometry C [MMscm]	6.19	11.83
G_{disc}/G_{model} for geometry C	20.94%	39.99%

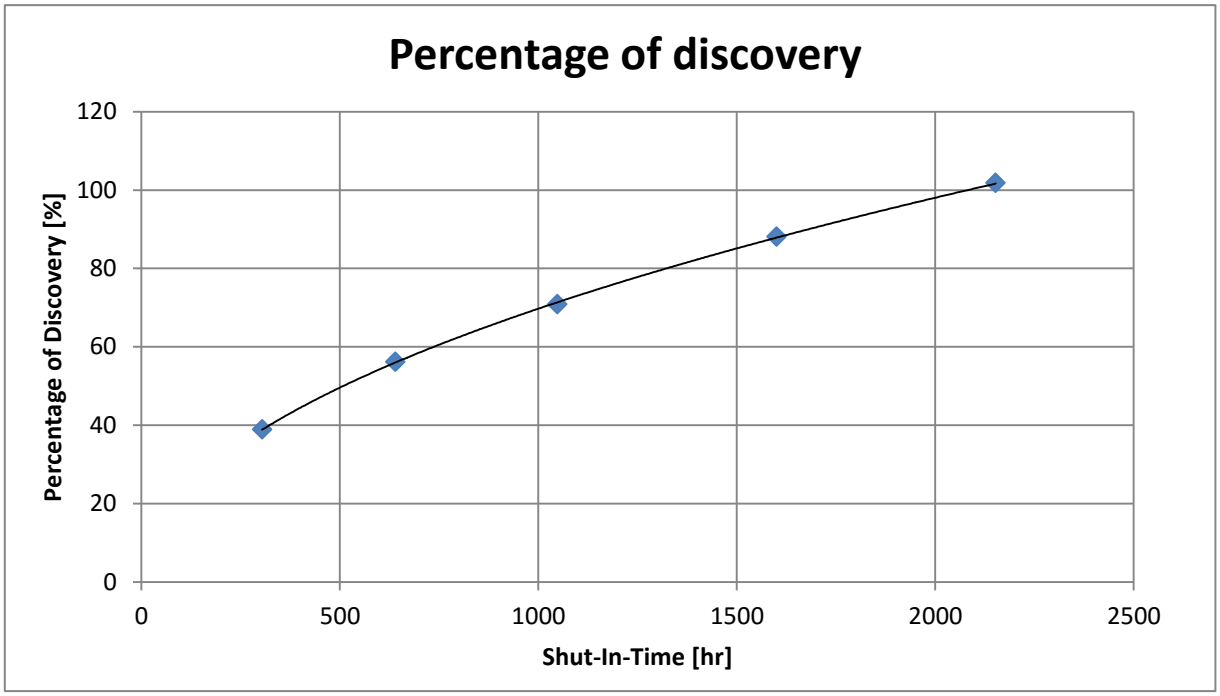

Figure 37: Percentage of discovery for CHT with different shut-in times.

Illustration 2 – Time dependency of a CHT

As the detected volumes for a standard CHT with 304 hours of pressure build-up are not satisfying, further CHTs are performed, investigating the duration needed for the shut-in to deliver 100% of the real GIIP for geometry A. Figure 37 shows the simulation outcomes for various durations. The percentage of discovery is plotted, and a trend-line can be inserted. At around 2200 hours, the extrapolation of pressures would yield an approximately correct GIIP, at longer shut-ins, the result is inverted, and an overestimation of reserves will occur. One explanation for this trend is the exponential behavior of the last part of the curve on the semi-log plot, which if extrapolated with a linear trendline leads to an under- and overestimation of GIIP depending on the duration of shut-in.

This illustration clearly shows that the requirement for a shut-in duration in an average reservoir with boundaries is very long, in order to be able to calculate the reservoir volumes.

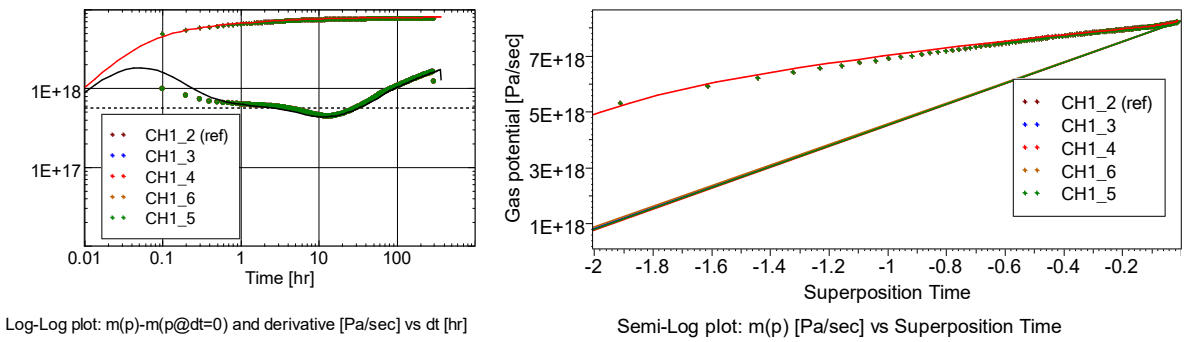

Figure 38: Pressure response in various reservoirs with different extent.

Illustration 3 – Change in GIIP and the consequences

The principle of non-uniqueness, explained in detail in section 2.2.3, says that different reservoirs can yield exactly the same derivative response. Without an underlying geological model, the pure look at the derivative and calculation of GIIP cannot tell the reservoir engineer anything about the real GIIP. Taking a look at Figure 38 it seems that only one response is visible. But the legend shows that actually the responses of six different reservoirs are plotted, yielding exactly the same log-log and semi-log pressure behavior.

The outcomes in Table 7 show the problems occurring due to pressure extrapolation in boundary dominated flow: As usual, a linear pressure extrapolation on the Horner plot is performed. The issue is, as already mentioned, that this linear extrapolation is simply wrong in boundary dominated flow, because it is unknown, whether the pressure will keep on building up, or not. Assuming a continuity in a pressure build-up will therefore lead to either an overestimation of reserves (for small reservoirs, almost approaching the final reservoir boundaries) or an underestimation (for larger reservoirs).

Table 7: Outcomes for different geometries.

	Simulation					
Parameter	**1**	**2**	**3**	**4**	**5**	**6**
G_{model} [MMscm]	29.59	23.30	18.34	14.44	11.37	8.95
G_{disc} [MMscm]	11.50	11.50	11.45	11.55	11.48	11.33
G_{disc}/G_{model}	38.86%	49.36%	62.43%	79.96%	101.01%	126.58%

4.1.4 Neural network for gas-initially-in-place prediction

Neural networks in well testing

AI and NN are widely used in PTA to support the interpreter in the correct choice of the model and are also able to estimate reservoir parameters. The foundations for the involvement of AI in PTA are laid in 1988, when a rule-based approach is invented as a pattern recognition tool, refined in 1989 to a knowledge-based system [18, 20]. The first approach for the combined usage of NN and PTA is proposed in 1993, eliminating the need for pre-processing and definition of rules [19]. Many improvements have been achieved since then, by today, all commercial software packages offer a NN tool to assist the interpreter.

The workflow of building such a NN usually starts with the collection of representative datasets using the most common reservoir models. There are different algorithms available, but in general they follow the same rules. The aim is to capture all behaviors of the pressure response, which can be linked to prevailing conditions and arrive at a model proposal. The output of the NN is then a clear categorization [21, p. 1].

But even in 2015 the subject of model identification is still under investigation, mainly because the available software tools have noise-handling issues and show weaknesses in distinguishing between models and offering too many choices [21, p. 5].

Although cooperated and evaluated in various studies and papers since now almost three decades, NN in PTA have an issue to perform clear distinctions between the different cases, suffering under the issue of non-uniqueness. The following approach tries to capture the workflow of building a NN from simulation results, not with the aim of model identification, but improving the reserves prediction capabilities of well tests. The output is not a categorization but a numerical estimation of the observable reserves from such a well test. Although it is tempting to use this method to predict actual GIIP, this cannot work due to the non-uniqueness of buildup curves when this is to be the sole input to the NN.

Workflow and results

The numerical model created with Petrel® gives the opportunity to simulate various geometries and summarize the outcomes. For the respective NN the geometries from Figure 34 are chosen to be simulated, using the parameters from Table 3 as input values, but changing the distance to the boundaries (Table 8). The simulations also vary in terms of boundary species, which could either be a permeability contrast or slightly permeable faults. In order to find the correct boundary transmissibility and the permeability contrast, trials are performed and the shape of the derivative is reviewed. The criterion for the inclusion of a sample into the training set of the NN is a strongly upwards turning derivative in the LTR. Hence, from the pool of 200 performed simulations 70 are included in the NN.

Table 8: Input parameters NN.

Parameter	Value
Boundary transmissibility coefficient [-]	0.1
Permeability contrast original/altered [-]	10
Shortest boundary distance from well [m]	93.78
Farthest boundary distance from well [m]	782.65

In section 4.1.3 OHTs and CHTs are simulated and it is shown that OHTs do not show any boundaries, if simulated in the prevailing conditions of a (multi-armed) channel. As the method of pressure extrapolation was to be reviewed in boundary dominated flow, it is decided to simulate a CHT with 8 hours of flow and 304 hours of shut-in.

The pressure outputs are normalized according to **eq**. 21:

$$p_n(t) = \frac{p(t) - p_{wf}}{p_{si} - p_{wf}} \tag{21}$$

$p_n(t)$… normalized pressure at time t [-]

p(t)…pressure at time t [bara]

p_{wf}… well-flowing pressure before shut-in [bara]

p_{si}…last recorded shut-in pressure [bara]

The normalized values are extracted at certain time steps, i. e. at 0.5, 1, 2, 5, 10, 20, 50, 100 and 200 hours of shut-in time. The nine time steps act as channels and are the input nodes for the NN. The output of the neural network is the percentage of GIIP that is observed by the method of pressure extrapolation of the last slope in the Horner plot of simulated results. To achieve the outcomes, each simulation is run with the outputs as described in section 4.1.2 and loaded into Saphir®. Depending mainly on the boundary distance as the variable, the range of the observed volume varies from 11.52% to 70.04% of the actual GIIP.

The same NN setup with the default settings and the same allocation of 60% learning, 20% validation and 20% testing datasets is simulated. The only difference is the error norm, because it is decided that the NN is trained with a sensitive Euclidean error function, given in **eq**. 22:

$$E = \frac{1}{2}\sum_{k=1}^{n} |y_k - d_k|^2 \tag{22}$$

E…Euclidean Error function

k… counting index

n…number of samples

y_k… output of the NN

d_k… desired output

In Figure 39, the output of the NN is compared to the desired output. The exactness of predictability is good and the highest error is 6.25%. The equations for the average error and standard deviation are presented in **eq**. 23 and **eq**. 24 [74, pp. 54, 72, 316]. The average errors for the dataset are presented in Table 9.

$$\bar{x} = \frac{1}{n}\sum_{k=1}^{n} x_k \tag{23}$$

$\bar{x}$…average of the differences between the output of the NN and the desired output [%]
x_k…absolute difference between the output of the NN and the desired output [%]

$$\sigma = \sqrt{\frac{1}{n-1}\sum_{k=1}^{n}(x_k - \bar{x})^2} \tag{24}$$

σ…corrected sample standard deviation [%]

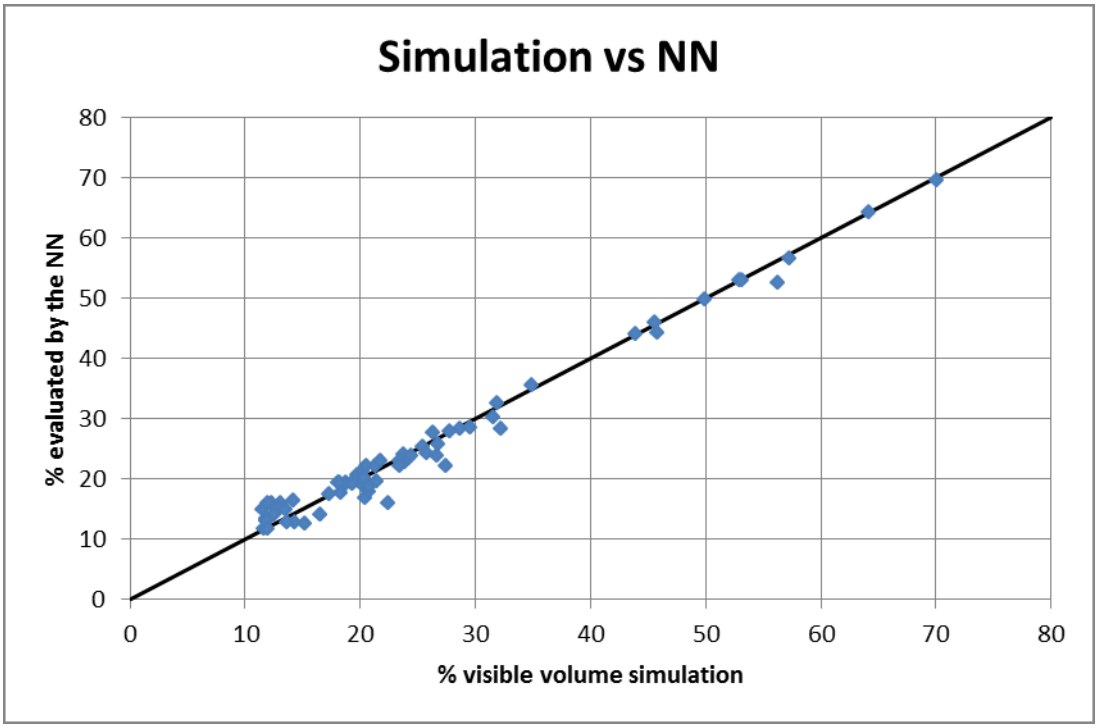

Figure 39: Comparison of simulations outcome and NN prediction.

Table 9: Average errors and standard deviation of the different datasets.

	Average Error, $\bar{x}$ [%]	**Standard Deviation, σ [%]**
Learning	1.02	1.02
Validation	1.75	1.51
Testing	2.49	1.45
Complete dataset	1.45	1.33

The example shows that the outputs of the models can be numerically related, despite their distinction in two sections: Underlying geometry (Figure 34) and type of boundary. In these simulations, the aspect of the distances to the channel boundary and the reservoir extent is held constant.

Extending this project to a greater dimension, including parameter variations, requires the automation of the modelling, simulation and analysis procedures in order to be realizable. If any variation is added, i. e. the ratio of channel boundary to reservoir boundary, an additional input channel for the neural network is recommended. This is due to the fact that of course the concept of non-uniqueness is applicable, which has been discussed into depth in several parts of this thesis. If differences in data cannot be quantified in a separate input channel (i.e. because it is simply not known, like the size of a connected tight layer, or the transmissibility of a fault), the numerical relationship between the data is not explicit and a NN is prone to fail.

4.2 Numerical modelling with Saphir®

4.2.1 Overview

In comparison to building a model in Petrel® and performing a simulation with Eclipse®, numerical modelling in Saphir® is relatively simply and can be performed quite straight-forward. This 2D simulation is easy to set up and modify. It allows not only to introduce permeability variations, but also thickness variations (pinch-out) and porosity maps. This software feature has been used in some publications (i.e. [12]), but has not been performed in the standard PTA within RAG yet.

The advantage of the numerical simulation is that the outcomes can be vividly demonstrated, the test analysis is enriched with an illustration helping to demonstrate one possible form of the reservoir, as seen by the test. To demonstrate this feature, examples are shown, followed by the definition of a simple workflow.

4.2.2 Examples

Obviously, the geological definition of a reservoir becomes more exact, the longer the horizon is on production. Nevertheless, in already drilled horizons, some geological features are available (i.e. gas-water-contact, faults). OHTs are generally too short to see very far into the reservoir, and can therefore hardly describe a formation very exactly. But a CHT has the ability to give the interpreter a relatively exact idea on geological features and reservoir extent. In the following, four examples of RAG tests are chosen to be modeled. The achieved outcomes are compared to the analytical models performed by reservoir engineers.

As a starting point, the geological maps from the horizons are used to model the tests. Boundaries, thickness and permeability are adjusted accordingly to history match the derivative curve and the pressure history of the well.

Example 1

Example 1 (E-001) is a well in a horizon, which has already been drilled and some wells are on production. This well, indicated in Figure 41 by the green dot, is the last wellbore drilled in this area, but the geological model was very sophisticated at the time it was successfully

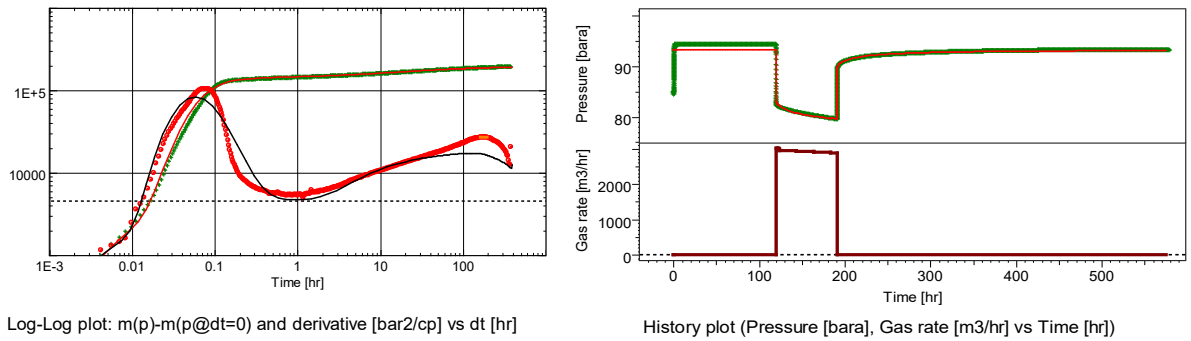

Log-Log plot: m(p)-m(p@dt=0) and derivative [bar2/cp] vs dt [hr]

History plot (Pressure [bara], Gas rate [m3/hr] vs Time [hr])

Figure 40: Original analysis E-001.

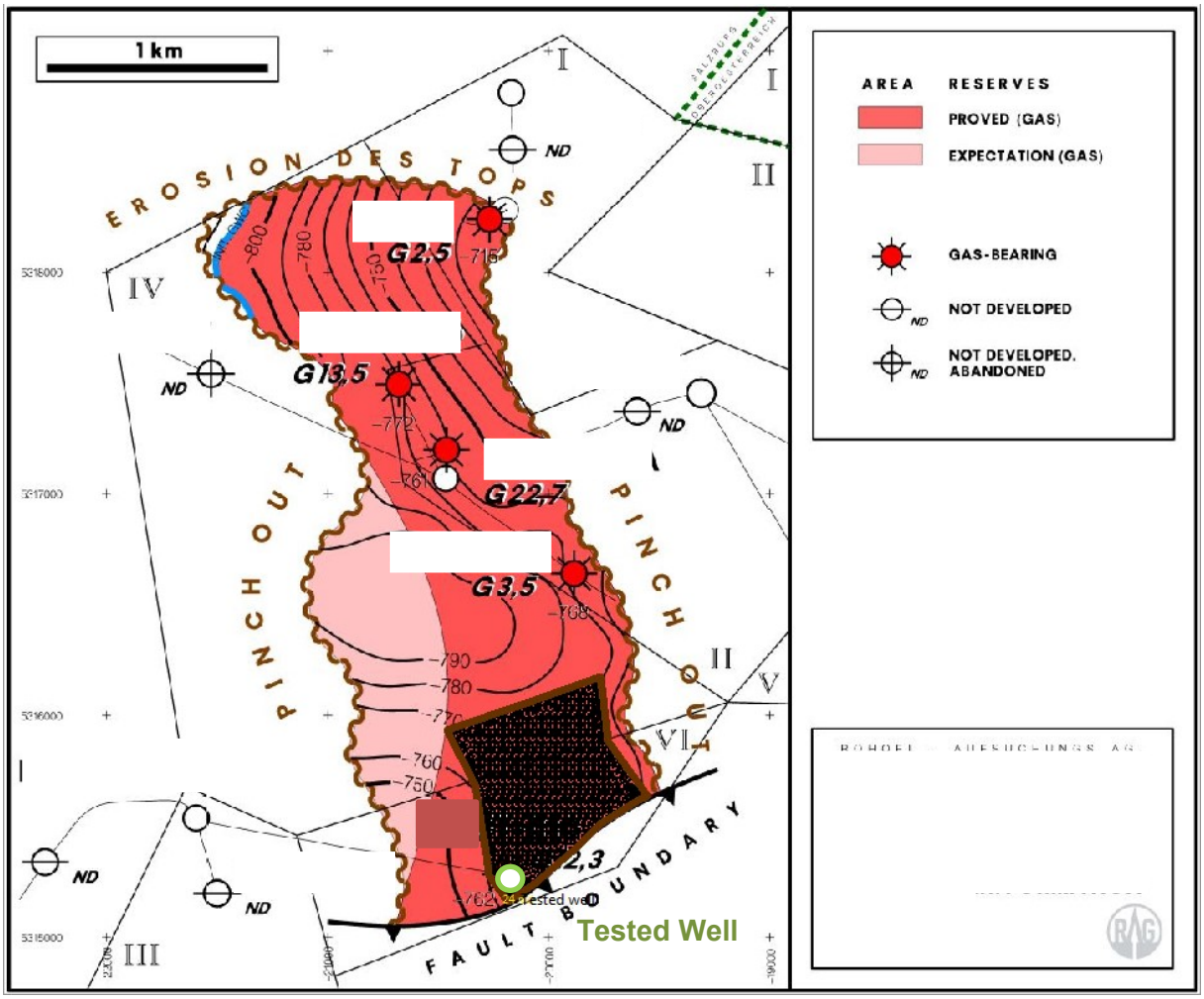

Figure 41: Geological map of horizon with E-001.

finished. The map on Figure 41 shows that on two directions from the well the horizon is limited by a pinch out, on one side by a fault.

The reservoir engineer in charge for the analysis (Figure 40) interprets the reservoir as homogenous being a rectangle with two boundaries at 57.8 m distance south and east, and two boundaries with 924 m distance north and west.

The derivative in Figure 40 is not perfectly matched in the LTR, and the history plot of the

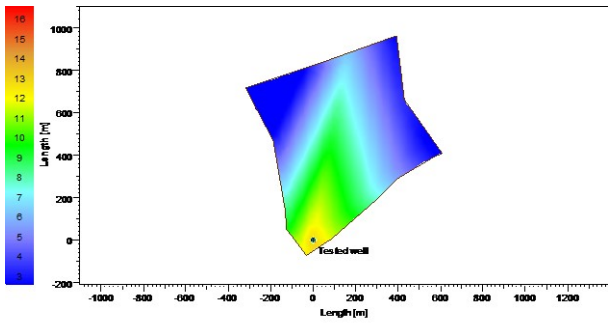

Thickness [m], Length [m] vs Length [m]

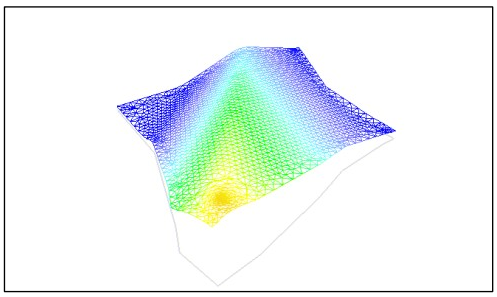

Pseudo 3D geometry plot

Figure 42: Thickness map of horizon with E-001.

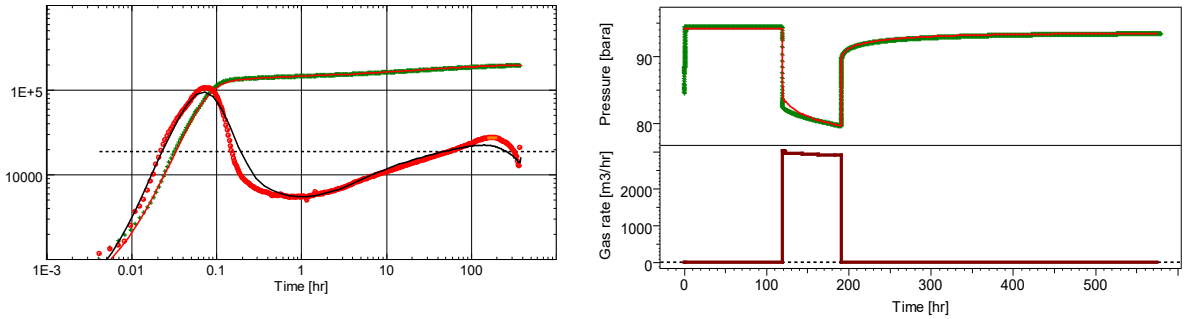

Log-Log plot: m(p)-m(p@dt=0) and derivative [bar2/cp] vs dt [hr]

History plot (Pressure [bara], Gas rate [m3/hr] vs Time [hr])

Figure 43: Numerical analysis E-001.

pressure shows a higher depletion in the test than in the match.

In order to improve the interpretation, the map is used as a reference. The original match and the boundaries of the system are chosen as a starting point, before iterating the distances. The final area is depicted in Figure 41 with a brown line and the grid-cells in between. A thickness map is also included, resulting in a horizon with the shape shown in Figure 42.

The effort of this numerical model, including the thickness map as well as orienting the boundaries on the geological model is rewarded with a better match in both plots (Figure 43).

Figure 42 shows that the horizon is of a great thickness at the position of the well. In conventional analysis, it is not possible to include a thickness variation. Therefore, the total volumes are too large, and the pressure history match, which is oriented on the MB of the system, is wrong (Figure 40). This opportunity of thickness modelling offers an easy realization with a very realistic outcome.

Example 2

The next example (E-002) is a CHT in a horizon which was already tested with an OHT and determined as relatively small, but the decision was to perform a CHT to get more reliable reserves. The CHT produced more than 1 MMscm of gas and was shut-in for the usual period of two weeks.

The test is originally matched with a two layer model, and a rectangular boundary, on the

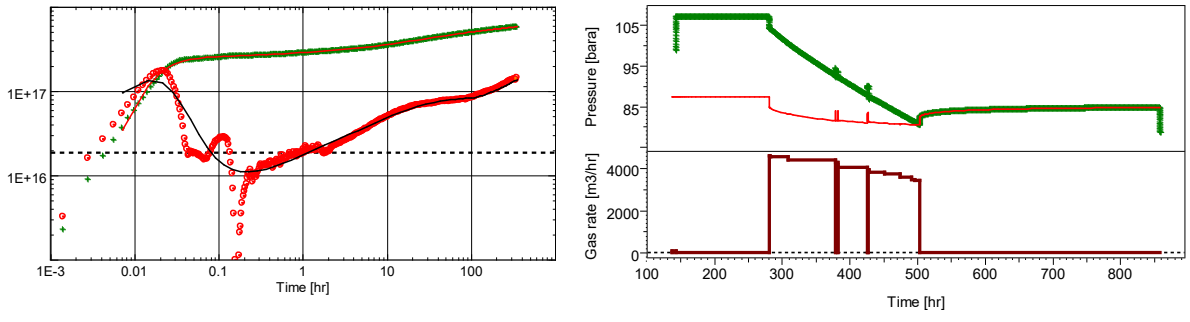

Log-Log plot: m(p)-m(p@dt=0) and derivative [Pa/sec] vs dt [hr]

History plot (Pressure [bara], Gas Rate [m3/hr] vs Time [hr])

Figure 44: Original analysis E-002.

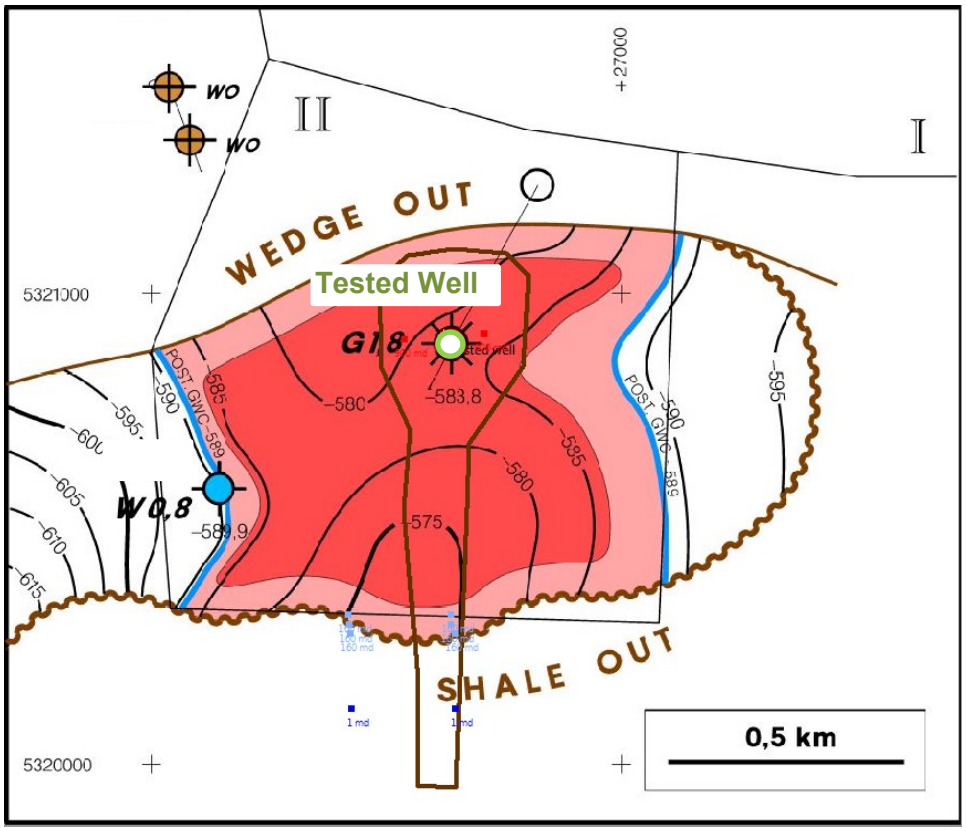

Figure 45: Geological map of horizon with E-002.

distances 233 m, 1866 m, 92 m and 4165 m (clockwise starting north). A two layer model is relatively complicated in terms of parameters, involving two different skin factors and three parameters Omega, Lambda and Kappa to define the relationship between the horizons. The match of the derivative is almost perfect with this structure, but the pressure history plot (Figure 44) is not matched at all.

As the logs do not imply a two layer system, the author took the decision to match the analysis with one layer but vary the permeability with offset. Again, the horizon map is taken as a reference (Figure 45).

First trials were not successful, because the permeability near the wellbore is extremely high

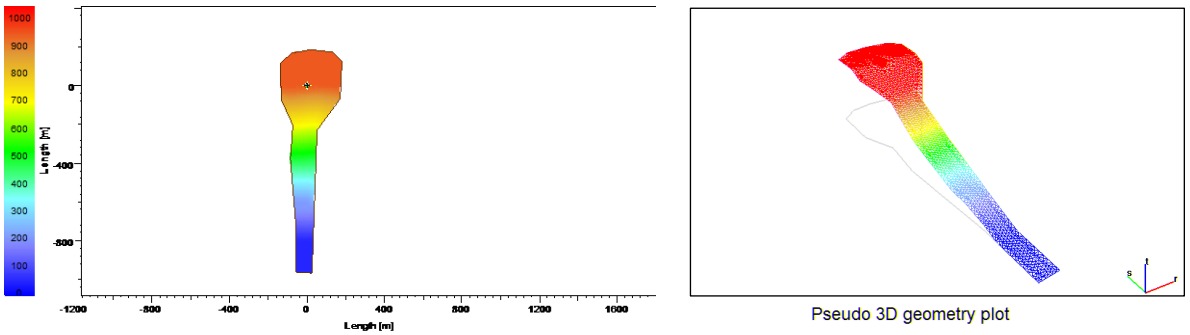

Figure 46: Permeability map of horizon with E-002.

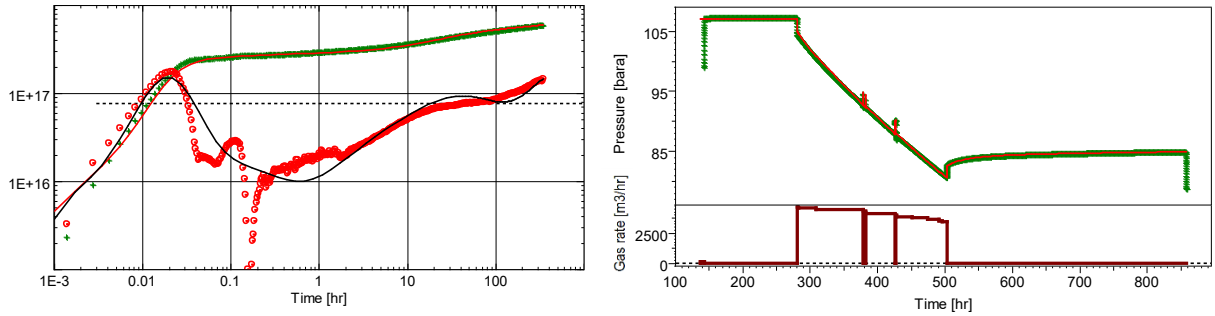

Log-Log plot: m(p)-m(p@dt=0) and derivative [Pa/sec] vs dt [hr]

History plot (Pressure [bara], Gas rate [m3/hr] vs Time [hr])

Figure 47: Numerical analysis E-002.

(600 md) causing the derivative to show a closed boundary system, if the boundaries as implicated by the geological map, are chosen. Figure 45 shows the location of the well and the final geometry of the boundary. A permeability variation is introduced and shown in Figure 46. The boundaries seem very close, but they are designed so that the derivative is matched. The reduced volume of the reservoir is necessary to arrive at a realistic history match of the pressure (Figure 47).

The derivative match is acceptable, but the pressure match of the history is a vast improvement in comparison to the original analysis (Figure 44). The reason for this is that in the original analysis the permeability was the same in the total reservoir. Therefore, the boundaries are located at very far distances from the well, but the volumetric relationship is not fulfilled (Figure 44).

In this example, the permeability variation is very helpful in modelling a realistic reservoir and illustrating the connected reservoir volume.

Example 3

The derivative of the following well is originally matched with a special model, a “two porosity slab”. Furthermore, two intersecting boundaries, one no-flow boundary at the distance of 37 m and one constant pressure boundary at 79 m is used for the pressure match.

The two-porosity model assumes two different regions in terms of permeability and porosity,

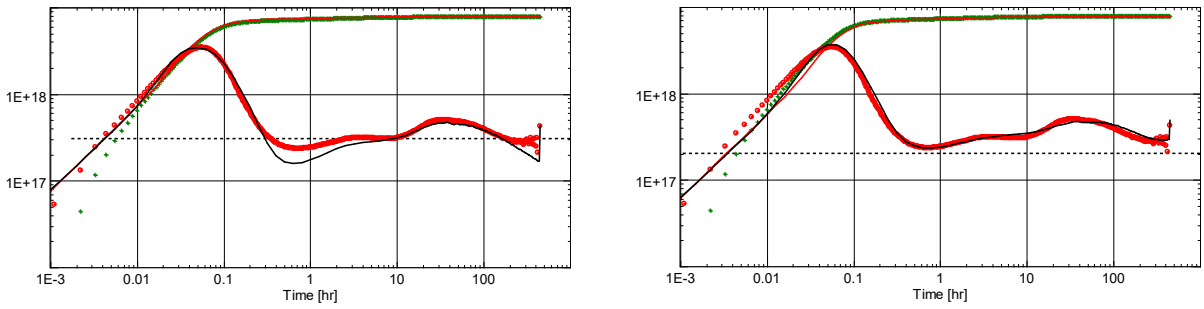

Log-Log plot: m(p)-m(p@dt=0) and derivative [Pa/sec] vs dt [hr]

Log-Log plot: m(p)-m(p@dt=0) and derivative [Pa/sec] vs dt [hr]

Figure 48: Original analysis (left) and numerical analysis (right) of E-003.

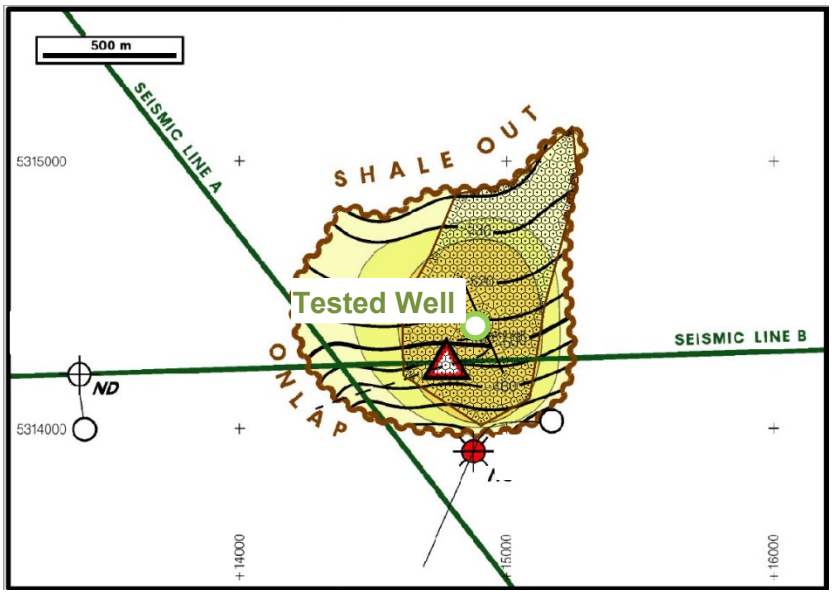

Figure 49: Geological map of horizon with E-003.

whereas one of the regions is directly connected to the wellbore and exhibits a first homogeneous flow, before the other region delivers reservoir fluids into the more permeable region and is found as another “radial infinite” flow behavior on the derivative plot. The concept applicable to this model is a fissured reservoir [46, p. 550].

The author modeled the reservoir without the usage of a two-porosity model, but with two boundaries at 13 m and 56 m distance to the well (Figure 49). Furthermore, the LTR boundary behavior, which is exhibited by a downturn of the derivative (Figure 48), is modeled with reservoir boundaries, oriented on the geological map (Figure 49). Using numerical modelling the boundaries and probable reservoir shape are illustrated more simplified, then the analytical match.

Example 4

The last example is again matched with four no-flow boundaries, one at 72 m distance, the other three at 540 m (Figure 50). The derivative match works fine, but, the pressure depletion during the test is not matched with this model and the boundaries contradict the map.

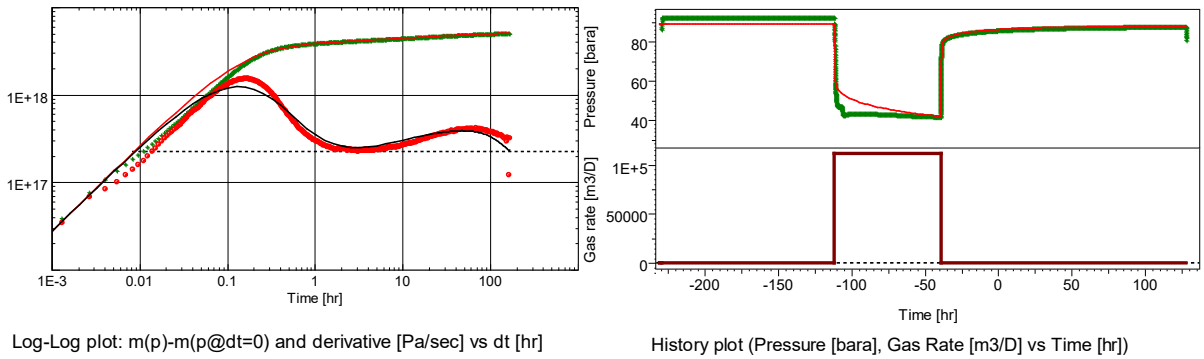

Log-Log plot: m(p)-m(p@dt=0) and derivative [Pa/sec] vs dt [hr]

History plot (Pressure [bara], Gas Rate [m3/D] vs Time [hr])

Figure 50: Original analysis E-004.

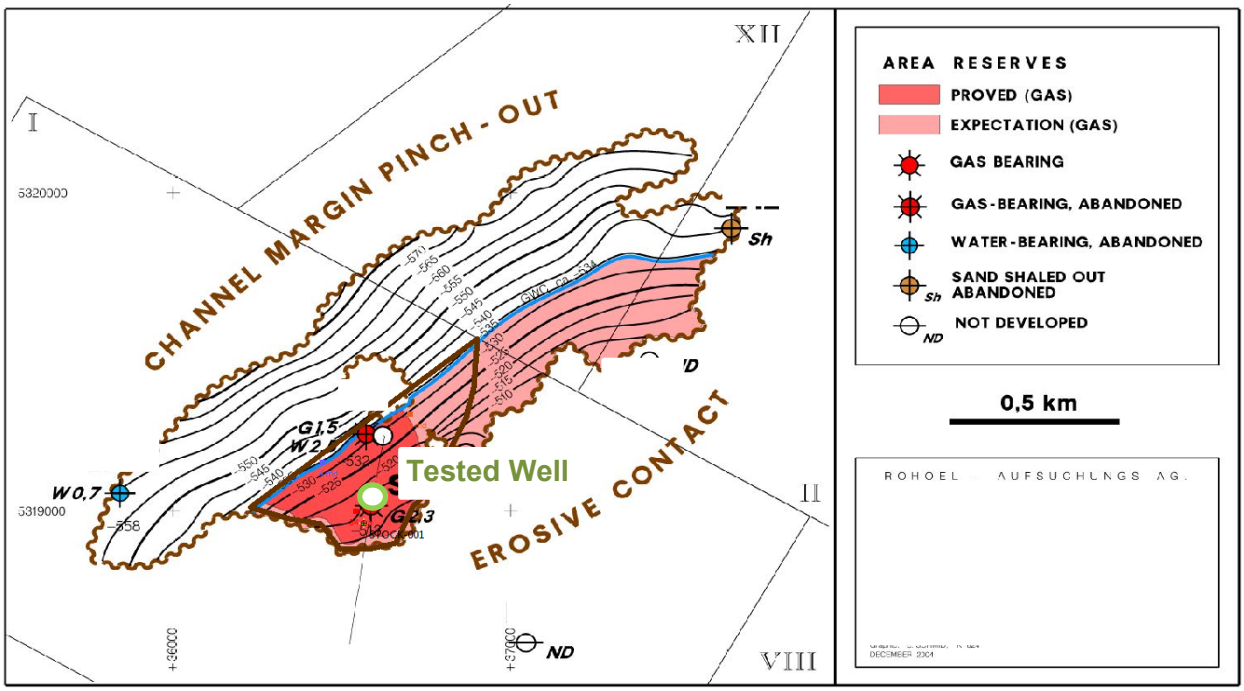

Figure 51: Geological map of horizon with E-004.

For this well, a very well defined geological map is available, because the gas-water-contact is already introduced for the layer. The contact is included as a boundary in the map, as well as the erosive contact to the other direction (Figure 51). The map is once more a good orientation for the reservoir's shape and extent. Also, a permeability variation shows a great match. The pressure history could not be matched with the conventional analysis, but is matched with the numerical model (Figure 53).

Example 4 is a great demonstration of the inclusion of well-known parameters like the gas-water-contact in the numerical model. The proved gas area is tested by the CHT, and the pressure history plot shows a much better match than the analytical plot.

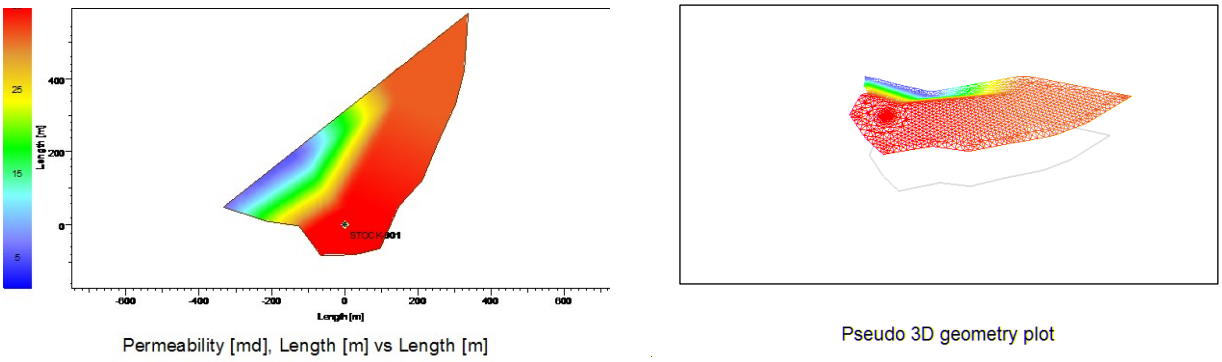

Figure 52: Permeability map of horizon with E-004.

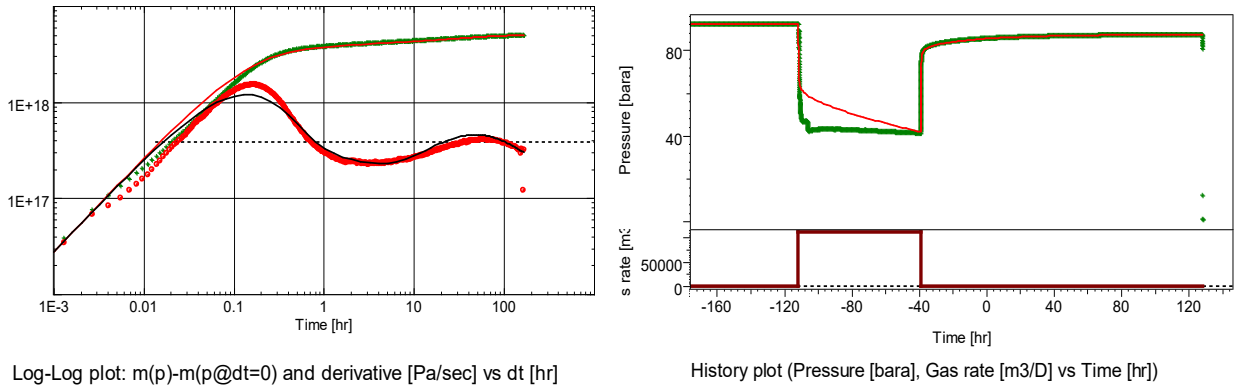

Log-Log plot: m(p)-m(p@dt=0) and derivative [Pa/sec] vs dt [hr]

History plot (Pressure [bara], Gas rate [m3/D] vs Time [hr])

Figure 53: Numerical analysis of E-004.

4.2.3 Workflow

In order to achieve the presented results, the following workflow is used:

1. Perform a usual PTA, in order to determine basic parameters:
    a. Wellbore model and coefficients: well-storage coefficient, ratio of changing well-storage coefficient; time to change in wellbore storage and skin factor;
    b. Well model: Vertical, slanted and horizontal well.
    c. Reservoir model: k*h-product
    d. Boundary model: Define boundaries at chosen k*h-product
2. Import a 2D map illustrating the respective tested horizon and well location.
3. Set the scale and draw the contours for the suggested proved gas area to create a grid, take into account thickness variations on the provided 2D map.
4. Change the analytical model to a numerical model – the basic parameters as defined in the first step are automatically used for the numerical model.
5. Compare the model with the historic data on the log-log plot as well as on the history plot. The LTR in the log-log plot will show the boundaries of the grid and the permeability distribution, the pressure depletion on the history plot is a simple MB.
6. Iteratively change the model parameters and include or exclude porosity, permeability and thickness models as they are adapted.
7. As soon as the depletion match is acceptable, as well as the LTR, the pore volume, PV, in m^3, can be found in the results section of the log-log plot in Saphir®. PV resembles $h*A*\Phi$ in **eq.** 20. Equation 20 can now be used to calculate the GIIP, which changes the usual workflow of pressure extrapolation and calculation with **eq.** 14.

4.3 Discussion

Different examples have been introduced, illustrating the advantages of numerical modelling.

Using Petrel® and Eclipse® for the simulations is helpful, if methods and procedures are reviewed, as well as to illustrate the effects of various conditions. Reservoir compartmentalization and transmissible faults can be included in an attempt to create a more realistic model. Refined conclusions can be made from these illustrations. But, the total workflow of modelling to simulation to interpretation involves several programs (Petrel®, Eclipse®, Saphir®) and is relatively complicated, making it unsuitable as a tool for quick-look well test interpretation. Also, the variability of the basic setup is quite restricted. Another issue is the grid itself. The reasons for the choice of a tartan grid are explained, but it has the limitation to restrict complex geologies for the model.

The examples for successful usage of the numerical modelling tool in Saphir® clearly show the advantages of the application. The tool is very simple, boundaries and faults are easily modified and the iterative approach works fine. Having a visual aid in the interpretation can lead to an interdisciplinary dialog about the reasonableness of the suggested outcome, and the implications for other disciplines. Nevertheless, the involvement of parameter variations results in a long iterative matching process, which is only shortened by experience. The problem of non-uniqueness cannot be circumvented. On the contrary, the ability to use spatial variation of thickness and permeability will match almost anything, but it helps to build a plausible model that honors both shape of the buildup and material balance, even within the constraints of additional information like the geological map and theory of the depositional environment, for example.

Modelling and simulating a test in Petrel® and Eclipse® and interpreting the test in Saphir® gives a lot of insight in the ability of the method of pressure extrapolation to predict reserves. On the other hand, the exclusive use of the numerical modelling tool of Saphir® has the restriction that impermeable zones or faults restrict the size of the reservoir, which is why the volume is not replicating the complete volume. Therefore, the program is not able to detect or account for impermeable zones able to recharge the reservoir, or a faulted horizon, i.e. reservoir compartmentalization.

The NN is a great approach to capture a variety of different setups. The issue of non-uniqueness can be described as multi-dimensional, involving: The first dimension, which is the basic reservoir geometry, the second, which is the quantification of boundaries, and the third dimension, which is the actual size and extent of a reservoir. Excluding the first two reasons by stating that the boundaries and reservoir model are varied, the last dimension of non-uniqueness, which is the extent, is still prevailing, leading to equiprobable solutions of different settings. This fact sets a strong limitation to the application of the method for GIIP prediction.

The issue of non-uniqueness is present in both methods, analytical and numerical analysis. Nevertheless, it leads to different reactions: In analytical modelling the results can be very

much decoupled from geological principles, because of the lack of vividness. Simulations with Saphir® as well as Petrel® face the issue of non-uniqueness. In both applications, it is advised to involve every detail and the learnings from past reservoirs.

5 Conclusion

The data of all OHTs and CHTs performed by RAG is analyzed and shows interesting trends. It has been shown that the majority of reservoirs in Upper Austria is characterized by boundary-dominated flow. Examples in this thesis as well as several studies come to the conclusion that extrapolated pressures of these boundary-dominated reservoirs in the Horner plot are severely erroneous. The usage of material balance therefore mostly leads either to an underestimation in reserves or an overestimation. Being able to predict reservoir volumes within a reasonable uncertainty is not assured. The method of pressure extrapolation for average pressure determination in the drainage area may seem as an acceptable approach ("better than nothing"), but is certainly misleading in many cases and needs to be performed carefully with these restrictions in mind.

Other methods for estimating average reservoir pressures need correctly predefined geometries, shapes and probable extent of the reservoir, as presented in section 2.2.4. Obviously, these methods are very much depending on the initial guess and the provided geometries, and therefore cannot provide an improvement to the reservoir pressure estimation in boundary-dominated flow regimes unless the reservoir geometry is known. Of course, if it were known, that knowledge would also improve a PTA model using the standard approach.

Another interesting fact from the analysis is the underestimation of ultimate recovery for all reservoir sizes from tests, which is presented in chapter 3. The presented figures mirror uncertainties arising from operational restrictions and the extrapolation of pressures in boundary dominated flow regimes, which is not able to account for the size of reservoir units poorly connected to the tested block or drainage area (reservoir compartmentalization). According to geological investigations, reservoirs in the Molasse basin qualify for the phenomenon of reservoir compartmentalization and the low exactness in predicted volumes supports this assumption. In order to evaluate the range of uncertainty, reservoir models with severe reservoir compartmentalization and high volumes of "late gas" are simulated and the results clearly demonstrate the limited predictability of volumes-in-place. This fact has also been shown on a p/Z plot in section 2.1.2. The p/Z-plot is unable to project and predict the total reserves of the combined reservoirs.

The trial to use the collected data for an implementation in a NN, which shall be able to predict the correct reserves, points at the high variations in possible solutions for pressure responses and analysis results. Some setups are able to show better correlations than others, but an overall prediction involving all formations and test types is not possible. The reason can be found in the great variety in data and simple unpredictability in outcomes. Also, due to non-uniqueness, which has the consequence that the same derivative can indicate very different volumes, it is very hard to find common ground and to identify a connection in the dataset. If a relationship is present, it means that the reservoir geometries must be very similar. Due to this knowledge it is possible to say that Hall Formation

reservoirs seem to have more features in common and are more easily relatable than Puchkirchen Formation reservoirs.

Another NN is designed to assist in the prediction of reserves, not from well test interpretation results but from parameterized pressure build-up curves. But again, similar to the presented average reservoir pressure calculation procedures in section 2.2.4, the method highly depends on the predefined parameter of reservoir extent. If this parameter is approximately available, the NN is able to help in the more exact definition of volumes.

The numerical modelling tool in Saphir® offers a great opportunity to simulate reservoir shapes and features, which cannot be included in analytical models, and to visualize the reservoir. A workflow is implemented to simplify the approach. The usage of numerical modelling with Petrel® and Eclipse® in the daily routine of a reservoir engineer is greatly constrained due to a time issue. Simulation of newly drilled reservoirs with a traditional simulator also involves too many obstacles (e.i. unavailable data about geometry, spatial variations of reservoir parameters), and is not recommended for interpretation purposes.

The review of more than one hundred WT analyses with a PTA software shows great differences in the chosen interpretation approaches. Disregarding parameters (i.e. water saturation) and questionable geological concepts can result in mismatches and lead the reservoir engineer in a “blind alley”. Formulation of a concept for a WTI “focal point” within the reservoir engineering team is highly advisable. The focal point can lay a great foundation of general understanding and knowledge about WT and will be able to build on these fundaments, becoming accompanied with the available numerical modelling tools. With broad knowledge, the person can act as a bridge to other reservoir engineers within RAG and give great advice.

An overall solution to the issue of reservoir compartmentalization (“late gas”) combined with boundary effects and an underestimation of reservoirs cannot be found, mainly because the prevailing conditions can vary. The general underestimation in reserves with the applied methods sheds a light on the fact that small reservoirs are able to perform better than expected.

Outlook

As explained in section 3.1, it was not possible in terms of time restrictions to completely digitize the pressure data from well tests. This excludes the usage of derivative analysis, which is important for the quantification of reservoir responses like boundaries. Having a greater subset of data could improve the NN for this dataset and show new relations.

It is also possible to extend the simulation database for the NN prediction. The downfall in this case is still the lack of previous geological knowledge, but it is unfortunately almost impossible to arrive at an approximation of the extent of the hydrocarbon accumulation, because of the sub-seismicity of most of the reservoirs.

The NN as a tool to predict reservoir response is tested further in an upcoming Master thesis and project. There are also other opportunities in reservoir engineering, which should be reviewed. The powerful tool may not have succeeded 100% with the presented approaches due to insurmountable constraints, but is nevertheless a promising development.

6 References

[1] Mitsubishi Heavy Industries, Ltd., “History of Fossil Fuel Usage since the Industrial Revolution,” 31 March 2010. [Online]. Available: https://www.mhi-global.com/discover/earth/issue/history/history.html. [Accessed 16 10 2015].

[2] Statistik Austria, “Energie und Umwelt,” 17 November 2015. [Online]. Available: http://www.statistik.at/web_de/statistiken/energie_umwelt_innovation_mobilitaet/energie_und_umwelt/index.html. [Accessed 24 November 2015].

[3] Eurostat, “Erneuerbare Energien in der EU,” 10 März 2015. [Online]. Available: http://ec.europa.eu/eurostat/documents/2995521/6734517/8-10032015-AP-DE.pdf. [Accessed 24 November 2015].

[4] “Strategieplattform Power To Gas,” Deutsche Energie Agentur, [Online]. Available: http://www.powertogas.info/english/introduction-to-power-to-gas/. [Accessed 21 January 2016].

[5] B. Howard, Petroleum Engineering Handbook, Richardson, TX, U.S.A.: Society of Petroleum Engineers, 1987.

[6] R. C. Earlougher, Advances in Well Test Analysis, Dallas: Society of Petroleum Engineers of AIME, 1977.

[7] S.-Y. Zheng and P. Corbett, "Well Testing Best Practice," in *SPE Europec/EAGE Annual Conference*, Madrid, Spain, 2005.

[8] M. T. Halbouty, “Synergy is Essential to Maximum Recovery,” *Journal of Petroleum Technology,* pp. 750-754, July 1977.

[9] K. I. Idigbe and P. P. Obeahon, *Semi-Infinite Channel Sands: The Signature and Effects of Wedge Angles,* 34th Annual SPE International Conference and Exhibition held in Tinapa - Calabar, Nigeria: SPE 140747, 2010.

[10] M. M. Kamal, Y. Pan, J. L. Landa and O. O. Thomas, *Numerical Well Testing - A Method To Use Transient Testing Results in Reservoir Simulation,* SPE Annual Technical Conference and Exhibition Dallas, TX, U.S.: SPE 95905, 2005.

[11] P. K. Neog and N. M. Borah, “Reservoir Characterization Through Well Test Analysis Assists in Reservoir Simulation - A Case Study,” in *SPE Asia Pacific Oil and Gas Conference and Exhibition*, Brisbane, Australia, 2000.

[12] M. Nnadi and M. Onyekonwu, *Numerical Welltest Analysis,* 28th Annual SPE International Technical Conference and Exhibition in Abuja, Nigeria: SPE 88876, 2004.

[13] R. Raghavan, T. N. Dixon, V. Q. Phan and S. W. Robinson, *Integration of Geology, Geophysics, and Numerival Simulation in the Interpretation of a Well Test in a Fluvial Reservoir,* SPE Annual Technical Conference and Exhibition Dallas, TX, U.S.: SPE 72097, 2001.

[14] T. Chen, J.-C. Noirot, A. Khandelwal, G. Xue, M. D. Barton and F. O. Alpak, *Estimating Stratigraphic Parameters from Well Test Data in Turbidite Reservoirs,* SPE Annual Technical Conference and Exhibition, San Antonio, Texas, U.S.: SPE 159090, 2012.

[15] R. Labourdette, M. C. Devilliers and T. Bui, *History Match of a DST Using Turbidite Elementary Channels Modelling Technique, Deep Offshore Congo,* SPE Reservoi Characterisation and Simulation Conference and Exhibition in Abu Shabi, UAE: SPE 166006, 2013.

[16] R. Tovar and C. Ehlig-Economides, *Improves Reservoir Description from Pressure Transients,* SPE Annual Technical Conference and Exhibition in Amsterdam, The Netherlands: SPE 170719, 2014.

[17] M. Noman, M. N. Khan, B. Amjad and J. Afsar, *Attempting To Quantify Subsurface Uncertainties With Dynamic Data - A Reservoir Management Case Study,* PAPG/SPE Pakistan section Annual Technical Conference in Islamabad, Pakistan: SPE 174715, 2014.

[18] O. F. Allain and R. N. Horne, “Use of Artificial Intelligence in Well Test Interpretation,” *Journal of Petroleum Technology,* pp. 342-349, March 1990.

[19] A.-A. U. Al-Kaabi and W. J. Lee, “Using Artificial Neural Nets to Identify the Well-Test Interpretation Model,” *SPE Formation Evaluation,* pp. 233-242, September 1993.

[20] G. Stewart and K. Du, *Feature Selection and Extraction for Well Test Interpretation Model Selection by an Artificial Intelligence Approach,* SPE Annual Technical Conference and Exhibizion, San Antonio: SPE 18920, 1989.

[21] A. M. AlMaraghi and A. El-Bandi, *Antomatic Reservoir Model Identification using Artificial Neural Networks in Pressure Transient Analysis,* SPE North Africa Technological Conference and Exhibition in Cairo, Egypt: SPE 175850, 2015.

[22] SPE, AAPG, WPC and SPEE, *Petroleum Resource Management System,* 2007.

[23] L. Mullins, “Reserves Uncertainty Quantification – An Executive Perspective,” Stochastic Simulation Ltd., 9 June 2014. [Online]. Available:

https://www.linkedin.com/pulse/20140609221345-3401550-reserves-uncertainty-quantification-an-executive-perspective. [Accessed 6 November 2015].

[24] T. Ahmed, Reservoir Engineering Handbook 2nd Edition, Houston, Texas: Gulf Publishing Company, 2001.

[25] L. P. Dake, The Practice of Reservoir Engineering (Revised Version), Amsterdam, The Netherlands: Elsevier, 2001.

[26] J. S. Archer and C. G. Wall, Petroleum Engineering Principles and Practice, London, UK: Graham and Trotman Ltd., 1986.

[27] D. R. Harrell, J. E. Hodgin and T. Wagenhofer, “Oil and Gas Reserves Estimated: Recurring Mistakes and Errors,” in *SPE Annual Technical Conference and Exhibition*, Houston, Texas, 2004.

[28] D. W. Harville and M. F. Hawkins, “Rock Compressibility and Failure as Reservoir Mechanisms in Geopressured Gas Reservoirs,” *JPT,* pp. 1528-1530, December 1969.

[29] J. O. Duggan, “The Anderson 'L' - An Abnormally Pressured Gas Reservoir in South Texas,” *JPT,* pp. 132-138, February 1972.

[30] R. V. Smith, Practical Natural Gas Engineering, Tulsa, Oklahoma: PennWell Publishing Company, 1990.

[31] S. J. Jolley, Q. J. Fisher, R. B. Ainsworth, P. J. Vroluk and S. Delisle, Reservoir Compartmentalization, London: Geological Society, 2010.

[32] T. L. Hower and R. E. Collins, “Detecting Compartmentalization in Gas Reservoirs Through Production Performance,” in *64th Annual Technical Conference and Exhibition of SPE*, San Antonio, TX, U.S., 1989.

[33] G. T. Cervantes, “Reservoir Compartmentalisation in the Roma Area,” in *SPE Asia Pacific Oil and Gas Conference*, Adelaide, South Australia, Australia, 1996.

[34] P. Diamond and J. Ovens, “Practical Aspects of Gas Material Balance: Theory and Application,” in *SPE Europe/EAGE Annual Conference and Exhibition*, Vienna, Austria, 2011.

[35] F. Ross, *What happened to all my Gas? p/Z plots in Layered Reservoirs,* Doha, Qatar: IPTC, 2014.

[36] M. F. Tugan, *Selection of Best Reserves Estimation Methodology to Quantify and Reduce the Uncertainty - Accompanied By Cayirderem Gas Field Case Study,* Manama,

Bahrein: SPE 172590, 2015.

[37] J. Lee and R. Sidle, *Gas-Reserves Estimation in Resource Plays,* Unconventional Gas Conference, Pittsburgh, Pennsylcania, U.S.: SPE 130102, 2010.

[38] D. Bourdet, Well Test Analysis: The Use of Advanced Interpretation Models; Handbook of Petroleum Exploration and Production, 3, Amsterdam, The Netherlands: Elsevier Science B. V., 2002.

[39] M. A. Sabet, Well Test Analysis, Houston, TX, U.S.: Gulf Publishing Company, 1991.

[40] J. C. Erdle, *Current Drillstem Testi8ng Practices: Design, Conduct & Interpretation,* Dallas, TX, U.S.: SPE, 1984.

[41] A. U. Chaudhry, Gas Well Testing Handbook, Burlington, UK: Elsevier Science, 2003.

[42] C. S. Matthews and D. G. Russel, Pressure Build Up and Flow Tests in Wells, Dallas: Society of Petroleum Engineers of AIME, 1967.

[43] D. R. Horner, “Pressure build up in wells,” in *Protocoll of the 3rd WPC II*, 1951.

[44] R. Al-Hussainy, H. J. Ramey and P. B. Crawford, “The Flow of Real Gases through Porous Media,” *Trans. of AIME, 237,* 1966.

[45] T. Ahmed, Advanced Reservoir Engineering, Oxford, UK: Elsevier Inc., 2005.

[46] A. C. Gringarten, “Interpretation of Tests in Fissured and Multilayerd Reservoirs With Double-Porosity Behavior: Theory and Practice,” *Journal of Petroleum Technology,* pp. 549 - 564, 1984.

[47] SPE, “PetroWiki,” [Online]. Available: http://petrowiki.org/Diagnostic_plots. [Accessed 24 January 2000].

[48] J. Lee, Well Testing, Dallas, TX, U.S.: Society of Petroleum Engineers of AIME, 1982.

[49] D. J. Pridie, *Gas-Well Testing: Changing Requirements, Changing Perspective,* SPE/CERI gas Technology Symposium in Calgary, Alberta, Canada: SPE 59744, 2000.

[50] C. Ehlig-Economides, “Use of the Pressure Derivative for Diagnosing Pressure-Transient Behavior,” *Journal of Petroleum Technology,* pp. 1280-1282, October 1988.

[51] A. H. Al-Ghamdi and M. B. Issaka, “Uncertainties and Challenges of Modern Well Test Interpretation,” in *SPE Annual Technical Conference and Exhibition*, New Orleans,

Lousiana, U.S., 2001.

[52] I. Ershaghi and J. J. Woodbury, “Examples of Pitfalls in Well Test Analysis,” *Journal of Petroleum Technology,* pp. 335 - 341, 1985.

[53] C.-C. Chen, W.-C. Chu and S. Soleiman, “Pressure-Transient Testing of Gas Reservoirs With Edge-Waterdrive,” *SPE Formation Evaluation,* pp. 251-256, December 1996.

[54] A. Shayan and D. Wong, “Well Testing Information and its Use in Shallow Reservoir Development,” *The Journal of Canadian Petroleum Technology, Vol. 37, No. 3,* pp. 55-62, 1998.

[55] G. J. Massonnat and D. Bandiziol, *Interdepedence Between Geology and Well Test Interpretation,* 68th Annual Technical Conference and Exhibition of the Society of Petroleum Engineers in Dallas, TX, U.S.: SPE 22740, 1991.

[56] C. S. Matthews, F. Brons and P. Hazebroek, “A method for determination of average pressure in a bounded reservoir,” *Trans. AIME, 201,* pp. 182-191, 1954.

[57] H. Ramey and W. Cobb, “A General Buildup Theory for a Well Located in a Closed Drainage Boundary,” *Journal of Petroleum Technology,* pp. 1493-1505, December 1971.

[58] D. N. Dietz, “Determination of Average Reservoir Pressure from Buildup Surveys,” *Journal of Petroleum Technology,* pp. 955-959, August 1965.

[59] M. J. De Ruig, “Deep Marine Sedimentation and Gas Reservoir Distribution in Upper Austria,” *Oil Gas European Magazine,* pp. 64-73, May 2003.

[60] P. Ziegler, Geological atlas of western and central Europe, Shell Internationale Petroleum Maatschappij: Amsterdam,: Elsevier, 1982.

[61] C. Rupp, M. Linner and G. W. Mandl, Geologie der österreichischen Bundesländer, Oberösterreich, Wien: Geologische Bundesanstalt, 2011.

[62] S. M. Hubbard and M. J. de Ruig, *Seismic Stratigraphy, Sedimentology and Reservoir Geology of the Puchkirchen Formation, Upper Austria.*

[63] J. Zweigel, T. Aigner and H. Luterbacher, “Eustatic versus tectonic controls on Alpine foreland basin fill: Sequence stratigraphy and subsidence analysis in the SE German Molasse,” in *A. Mascle, C. Puigdefabregas, H. P. Luterbacher, and M. Fernandez, eds., Cenozoic foreland basins of western Europe*, London, Geological Society (London) Special Publication 134, 1998, pp. 299-323.

[64] M. J. De Ruig and S. M. Hubbard, “Seismic fascies and reservoir characteristics of a deep-marine channel belt in the Molasse forland basin, Puchkirchen Fornmation, Austria,” *AAPG Bulletin, v.90, No. 5,* pp. 735-752, May 2006.

[65] G. Braswell, “Artificial Intelligence Comes of Age in Oil and Gas,” *Journal of Petroleum Technology,* pp. 50-57, January 2013.

[66] R. B. Gharbi and G. A. Mansoori, “An introduction to artificial intelligence applications in petroleum exploration and production,” *Journal of Petroleum Science and Engineering 49,* pp. 93-96, 2005.

[67] C. Bravo, L. Saputelli, F. Rivas, A. G. Pérez, M. Nikolaou, G. Zangl, N. de Guzmán, S. Mohaghegh and G. Nunez, “State of the Art of Artificial Intelligence and Predictive Analytics in the E&P Industry: A Technology Survey,” *SPE Journal,* pp. 547-563, August 2014.

[68] S. Mohaghegh, “Virtual-Intelligence Applications in Petroleum Engineering: Part 1 - Artificial Neural Networks,” *Journal of Petroleum Technology,* pp. 64-72, September 2000.

[69] S. Mohaghegh, “Virtual-Intelligence Applications in Petroleum Engineering: Part 2- Evolutionary Computing,” *Journal of Petroleum Technology,* pp. 40-46, October 2000.

[70] Y. Freund and R. E. Schapire, “Large Margin Classification Using the Perceptron Algorithm,” *Machine Learning 37 (3),* pp. 277-296, 1999.

[71] C. Li, X. Chen and Z. Du, “A New Relationship of Rock Compressibility with Porosity,” in *SPE Asia Pacific Oiol and Gas Conference and Exhibition*, Perth, Australia, 2004.

[72] Fruhwirth, R. NGS, *cVision Help.*

[73] J. Zambrano, R. Zimmerman and A. Gringarten, *Influence of Geological Features on Well Test Behavior,* SPE Asia Pacific Conference on integrated Modelling for Asset Management in Yokohama, Japan: SPE 59398, 2000.

[74] A. Büchter and H.-W. Henn, Elementare Stochastik, Berlin Heidelberg: Springer Verlag Berlin Heidelberg, 205.

[75] M. B. Standing, Volumetric and Phase Behavior of Oil Field Hydrocarbon Systems, Dallas, U.S: Society of Petroleum Engineers of AIME, 1977.

[76] A. Toeffler, The Third Wave, New York City, U.S.A.: Bantam Books, 1991.

[77] IHS Inc., “Material Balance Analysis Theory,” 2014. [Online]. Available: http://www.fekete.com/SAN/WebHelp/FeketeHarmony/Harmony_WebHelp/Content/HTML_Files/Reference_Material/Analysis_Method_Theory/Material_Balance_Theory.htm. [Accessed 03 11 2015].

[78] D. Bourdet, J. Ayoub and Y. M. Pirard, “Use of Pressure Derivative in Well Test Interpretation,” in *SPE California Regional Meeting*, Long Beach, CA, U.S., 1984.

Appendices

Appendix A

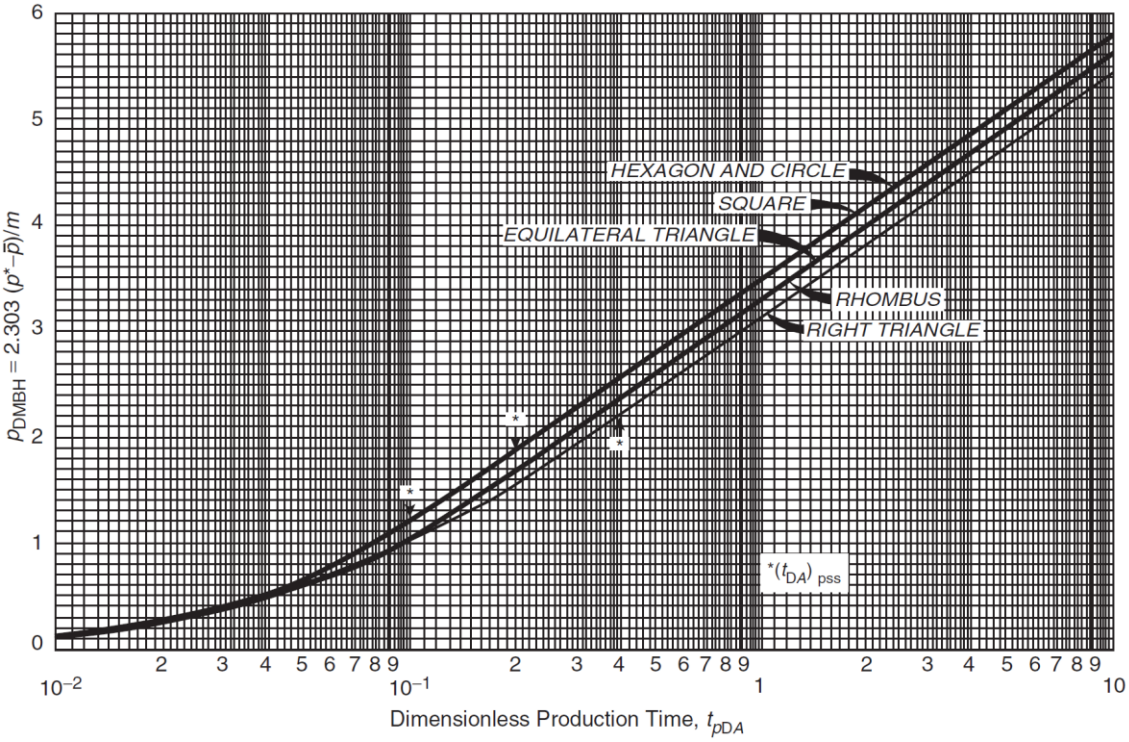

Figure 54: MBH dimensionless pressure chart, used for wellbores, which are in the center of the presented boundary areas [45, p. 1/60, 6, p. 61]

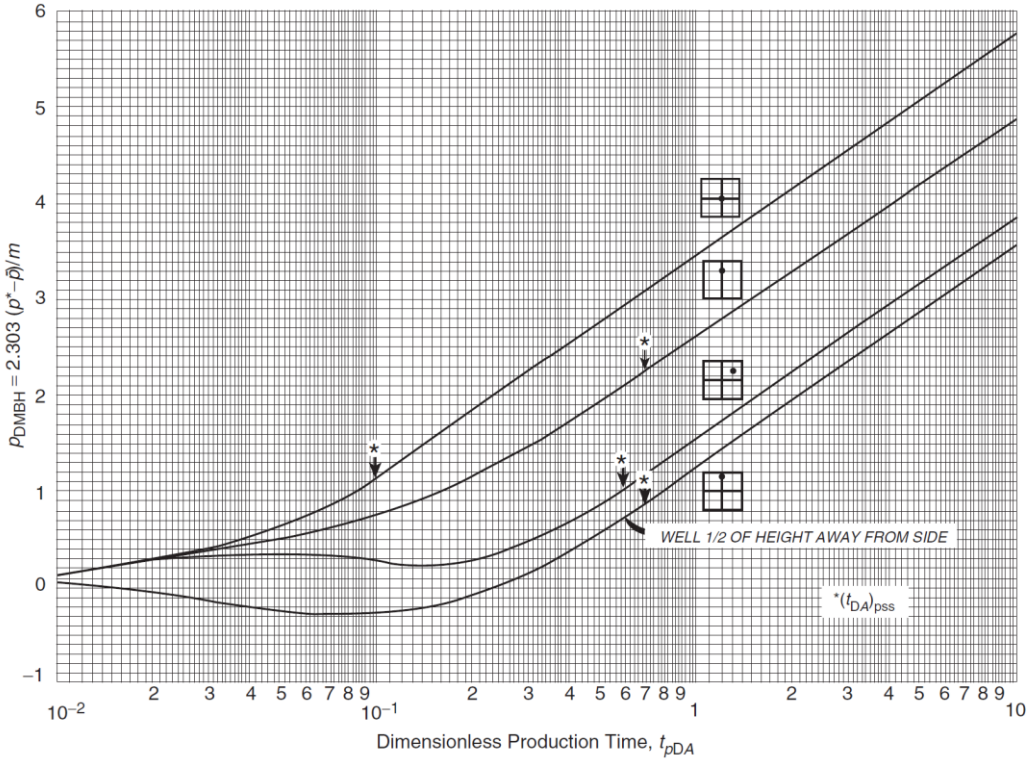

Figure 55: MBH dimensionless pressure chart, used for wellbores being located in specific square drainage area [45, p. 1/60, 6, p. 62]

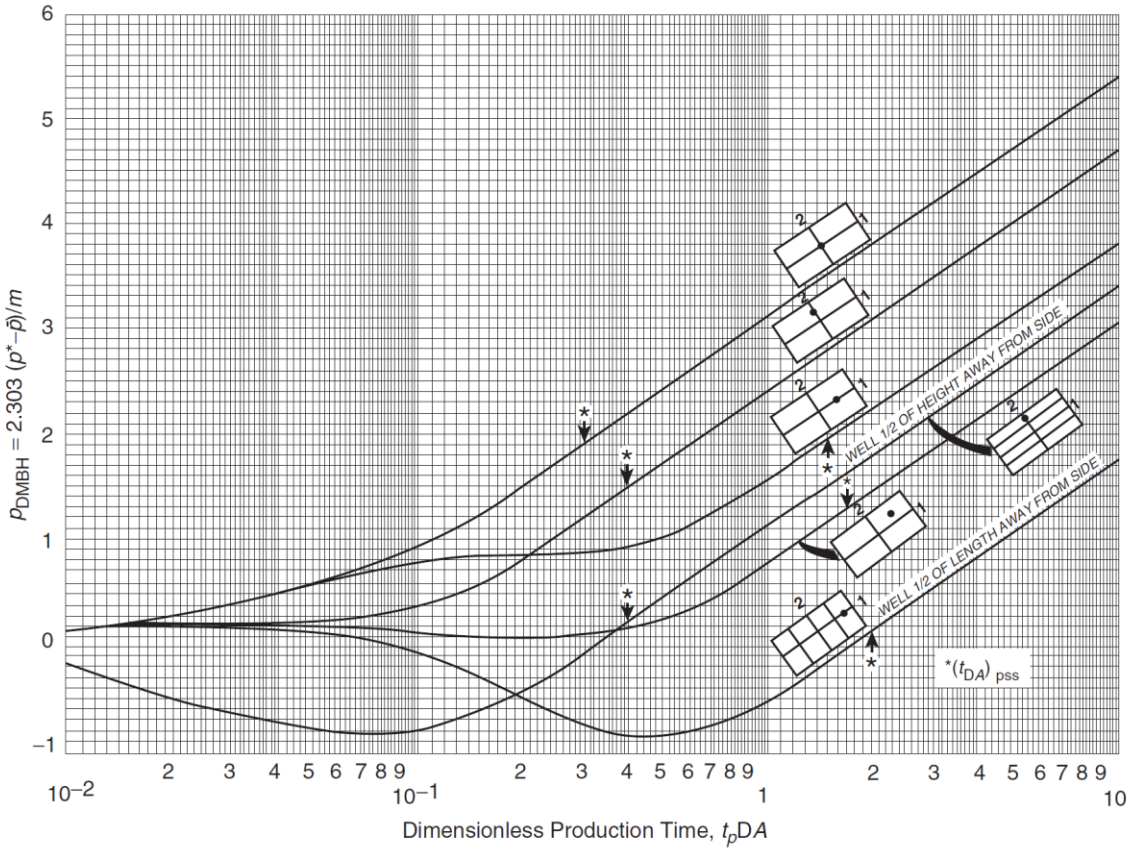

Figure 56: MBH dimensionless pressure chart, used for wellbores being located in specific 2:1 rectangular drainage area [45, p. 1/61, 6, p. 63]

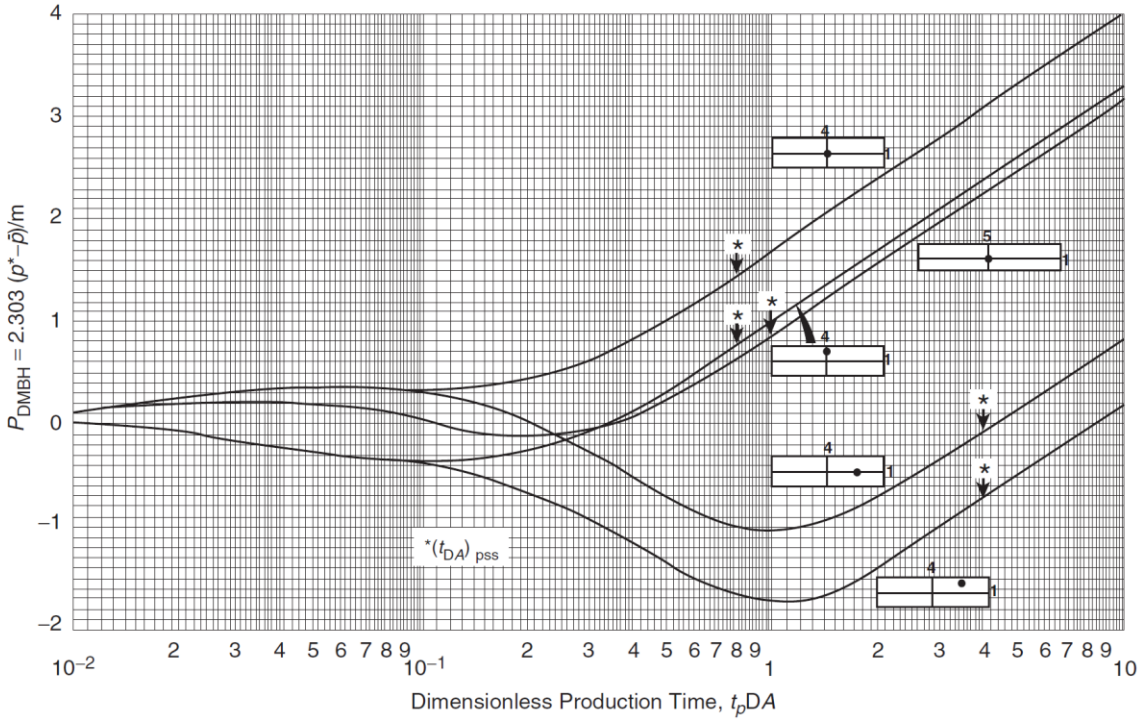

Figure 57: MBH dimensionless pressure chart, used for wellbores being located in specific 4:1 rectangular drainage area [45, p. 1/61, 6, p. 64]

Table 10: Shape factors and other parameters for different reservoirs [45, p. 1/34, 6, p. 203f]

In bounded reservoirs	C_A	$\ln C_A$	$\frac{1}{2}\ln\left(\frac{2.2458}{C_A}\right)$	*Exact for* $t_{DA} >$	*Less than 1% error for* $t_{DA} >$	*Use infinite system solution with less than 1% error for* $t_{DA} >$
	31.62	3.4538	−1.3224	0.1	0.06	0.10
	31.6	3.4532	−1.3220	0.1	0.06	0.10
	27.6	3.3178	−1.2544	0.2	0.07	0.09
	27.1	3.2995	−1.2452	0.2	0.07	0.09
	21.9	3.0865	−1.1387	0.4	0.12	0.08
	0.098	−2.3227	+1.5659	0.9	0.60	0.015
	30.8828	3.4302	−1.3106	0.1	0.05	0.09
	12.9851	2.5638	−0.8774	0.7	0.25	0.03
	10132	1.5070	−0.3490	0.6	0.30 0.25	0.025 0.01
	3.3351	1.2045	−0.1977	0.7		
	21.8369	3.0836	−1.1373	0.3	0.15	0.025
	10.8374	2.3830	−0.7870	0.4	0.15	0.025
	10141	1.5072	−0.3491	1.5	0.50	0.06
	2.0769	0.7309	−0.0391	1.7	0.50	0.02
	3.1573	1.1497	−0.1703	0.4	0.15	0.005
	0.5813	−0.5425	+0.6758	2.0	0.60	0.02
	0.1109	−2.1991	+1.5041	3.0	0.60	0.005
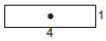	5.3790	1.6825	−0.4367	0.8	0.30	0.01
	2.6896	0.9894	−0.0902	0.8	0.30	0.01
	0.2318	−1.4619	+1.1355	4.0	2.00	0.03
	0.1155	−2.1585	+1.4838	4.0	2.00	0.01
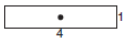	2.3606	0.8589	−0.0249	1.0	0.40	0.025
	In vertically fractured reservoirs use $(x_e/x_f)^2$ in place of A/r_w^2, for fractured systems					
	2.6541	0.9761	−0.0835	0.175	0.08	cannot use
	2.0348	0.7104	+0.0493	0.175	0.09	cannot use
	1.9986	0.6924	+0.0583	0.175	0.09	cannot use
	1.6620	0.5080	+0.1505	0.175	0.09	cannot use
	1.3127	0.2721	+0.2685	0.175	0.09	cannot use
	In water-drive reservoirs					
	0.7887	−0.2374	+0.5232	0.175	0.09	cannot use
	19.1	2.95	−1.07	–	–	–
	In reservoirs of unknown production character					
	25.0	3.22	−1.20	–	–	–

Appendix B.1

Table 11: Parameters included in the datasheet for OHTs and CHTs in RAG.

Feature	Sign	Unit	Source
Well name	-	-	Report
Test type	-	-	Report
Date	-	-	Report
Height	h	m	Well log (petrophysicist)
Duration (2nd flow period)	t_{flow}	hr	Raw data
Duration (2nd shut-in period)	t_{si}	hr	Raw data
Temperature	T	°C	Raw data; report
Rate at shut-in	q	scm/hr	Raw data (rates) – PVSS; report
Well-flowing pressure	p_{wf}	bara	Raw data; report
Porosity	Φ	-	Well log (petrophysicist); report
Water saturation	S_w	-	Well log (petrophysicist); report
Permeability*Height product	kh	mD*m	Horner plot; log-log plot
Permeability	k	mD	calculated
Skin	S	-	Horner plot; log-log plot
Boundaries	-	m	Derivative (log-log plot)
Radius of Investigation (r_{inv})	r_{inv}	m	KAPPA; calculation (for calculation procedure see chapter 3)
Quantity of produced gas – 1st and 2nd flow period, total	Q_1, Q_2	m^3	Raw data
Reservoir depth in measured depth (MD), total vertical depth (TVD) and total vertical depth sub-sea-level(TVDSS)	MD_{res}, TVD_{res}, $TVDSS_{res}$	m	Report; Well data port (Ragweb)
Depth of Mesurement in MD, TVD and TVDSS	MD_{meas}, TVD_{meas}, $TVDSS_{meas}$	m	Report; Well data port (Ragweb)
Extrapolated pressures	p_1^*, p_2^*	bara	Horner plot
Gas Initially in Place and estimated ultimate recovery	GIIP and UR_{est}	MMscm	RAG employee; calculated (for calculation procedures see chapter 3)
Total Production and Forecast	UR_{final}	MMscm	RAG database in OFM®
Abandonment pressure	p_{ab}	bara	Backpressure from RAG database

Appendix B.2

For numerical simplification purposes, the well-known Standing compressibility chart is translated into the following equations, published by Brill and Beggs resulting in accurate compressibility values and, therefore, used for Z-factor calculations in Section 3.2. p in bara and T in K [75, p. 121]

$$Z = a + \frac{(1-a)}{e^{b}} + c{p_{pr}}^{d}$$

$$a = 1.39(T_{pr} - 0.92)^{0.5} - 0.36T_{pr} - 0.101$$

$$b = \left(0.62 - 0.23T_{pr}\right)p_{pr} + \left(\frac{0.066}{\left(T_{pr} - 0.86\right)} - 0.037\right){p_{pr}}^{2} + \frac{0.32}{10^{9(T_{pr}-1)}}{p_{pr}}^{6}$$

$$c = (0.132 - 0.32logT_{pr})$$

$$d = 10\text{^}(0.3106 - 0.49T_{pr} + 0.1824{T_{pr}}^{2})$$

$$p_{pr} = \frac{p}{p_{pc}}$$

$$T_{pr} = \frac{T}{T_{pc}}$$

T_{pr}… pseudo-reduced temperature [-]

p_{pr}… pseudo-reduced pressure [-]

T_{pc}… pseudo-critical temperature [K]

p_{pc}… pseudo-critical pressure [bara]

Appendix C

Table 12: Input parameters and output exactness for NNs.

	Simulation Setups						
Input	**1(1)**	**2 (4)**	**3(5)**	**4 (6)**	**5 (7)**	**6 (9)**	**7 (12)**
Date	All	All	1997-	All	-1997	All	All
t_{flow}	Yes	Yes	Yes	Yes	Yes	Yes	Yes
Formation	All	All	All	All	All	HS	OPS
T	Yes	Yes	Yes	Yes	Yes	Yes	Yes
Type	All	All	All	All	All	All	All
Boundaries	None	1-3	1-3	1-3	None	1-3	1-3
h	Yes	Yes	Yes	Yes	Yes	Yes	Yes
kh	Yes	Yes	Yes	Yes	Yes	Yes	Yes
Q_{1+2}	Yes	Yes	Yes	Yes	Yes	Yes	Yes
Q_2/Q_{1+2}	Yes	Yes	Yes	Yes	Yes	Yes	Yes
p_1*	Yes	Yes	Yes	Yes	Yes	Yes	Yes
p_2*	Yes	Yes	Yes	Yes	Yes	Yes	Yes
Φ	Yes	Yes	Yes	Yes	Yes	Yes	Yes
p_{wf}	Yes	Yes	Yes	Yes	Yes	Yes	Yes
q	Yes	Yes	Yes	Yes	Yes	Yes	Yes
r_{inv}	Yes	Yes	Yes	Yes	Yes	Yes	Yes
t_{si}	Yes	Yes	Yes	Yes	Yes	Yes	Yes
S	Yes	Yes	Yes	Yes	Yes	Yes	Yes
S_{wi}	Yes	Yes	Yes	Yes	Yes	Yes	Yes
TVD_{res}	Yes	Yes	Yes	Yes	Yes	Yes	Yes
TVD_{meas}	Yes	Yes	Yes	Yes	Yes	Yes	Yes
UR_{est}	Yes	Yes	Yes	Yes	Yes	Yes	Yes
UR_{final}	All	All	All	5+ MMscm	All	All	All
Samples	294	186	102	68	190	53	74
Error 1: Val.	1.23	0.89	0.67	0.17	1.70	0.26	0.77
Error 2: Learn.	1.32	1.99	1.25	0.35	2.46	0.12	2.22
Error 3: Test.	1.18	1.40	1.37	0.57	1.88	1.24	1.97

The symbols are described in Appendix B.1, except for the following:

- Type: OHT or CHT
- Formation: HS, UPS, OPS, IM
- Boundaries: Depicted boundaries (only the tests with derivative). Empty fields filled with radius of investigation
- Errors 1, 2 and 3: Validation set average error, testing and training set errors

Table 13: Input parameters and output exactness for NNs.

	Simulation Setups			
Input	**8 (13)**	**9 (14)**	**10(15)**	**11 (16)**
Date	All	All	All	All
t_{flow}	Yes	Yes	Yes	Yes
Formation	I_PS	UPS	All	All
T	Yes	Yes	Yes	Yes
Type	All	All	CHT	OHT
Boundaries	1-3	1-3	1-3	1-3
h	Yes	Yes	Yes	Yes
kh	Yes	Yes	Yes	Yes
Q_{1+2}	Yes	Yes	Yes	Yes
Q_2/Q_{1+2}	Yes	Yes	Yes	Yes
p_1*	Yes	Yes	Yes	Yes
p_2*	Yes	Yes	Yes	Yes
Φ	Yes	Yes	Yes	Yes
p_{wf}	Yes	Yes	Yes	Yes
q	Yes	Yes	Yes	Yes
r_{inv}	Yes	Yes	Yes	Yes
t_{si}	Yes	Yes	Yes	Yes
S	Yes	Yes	Yes	Yes
S_{wi}	Yes	Yes	Yes	Yes
TVD_{res}	Yes	Yes	Yes	Yes
TVD_{meas}	Yes	Yes	Yes	Yes
UR_{est}	Yes	Yes	Yes	Yes
UR_{final}	All	All	All	All
Samples	13	34	79	107
Error 1: Val.	0.52	0.07	1.10	1.09
Error 2: Learn.	0.17	1.34	0.54	1.87
Error 3: Test.	0.43	1.55	1.54	1.68